THE UNIVERSITY OF MICHIGAN

INDUSTRY PROGRAM OF THE COLLEGE OF ENGINEERING

SOME ASPECTS OF THERMAL NEUTRON DETECTORS

George R. Dalton

A dissertation submitted in partial fulfillment
of the requirements for the degree of
Doctor of Philosophy in the
University of Michigan
1960

May, 1960

IP-431

Doctoral Committee:

Professor Richard K. Osborn, Chairman
Assistant Professor Bernard A. Galler
Professor Henry J. Gomberg
Professor William Kerr
Associate Professor Paul F. Zweifel

ACKNOWLEDGMENTS

The writer wishes to express his sincere gratitude to the following persons:

To Professors Richard K. Osborn, Chairman and Bernard A. Galler for their advice and interest in this thesis.

To the staff of the Computer Center of the University of Michigan.

To my wife for her assistance and patience in preparing this and other manuscripts.

To the Industry Program of the College of Engineering at the University of Michigan for considerable assistance in the reproduction of this dissertation.

TABLE OF CONTENTS

TABLE

LIST OF FIGURES

LIST OF FIGURES (CON'T)

LIST OF FIGURES (CON'T)

LIST OF FIGURES (CON'T)

NOMENCLATURE

$\underline{r}$	A vector indicating a position in space.
$\underline{\Lambda}_{\underline{r}}$	A vector of unit length with the direction of $\underline{r}$.
$\underline{\Omega}$	A unit vector indicating the direction of motion of a neutron.
v	The average speed of a neutron population in thermal equilibrium with its surrounding.
$N(\underline{r}, \underline{\Omega})\, d\underline{r}d\underline{\Omega}$	The number of neutrons in a volume $d\underline{r}$ about point $\underline{r}$ with directions of motion in solid angle $d\underline{\Omega}$ about $\underline{\Omega}$ before the detector is put in place.
$N'(\underline{r}, \underline{\Omega})\, d\underline{r}d\underline{\Omega}$	The number of neutrons in a volume $d\underline{r}$ about point $\underline{r}$ with directions of motion in solid angle $d\underline{\Omega}$ about $\underline{\Omega}$ after the detector is put in place.
$\Phi(\underline{r}, \underline{\Omega}) = vN(\underline{r}, \underline{\Omega})$	This quantity will be called the angular flux, or simply flux, before the detector is put in place.
$\Phi'(\underline{r}, \underline{\Omega}) = vN'(\underline{r}, \underline{\Omega})$	This quantity will be called the angular flux, or simply flux, after the detector is put in place.
$\Psi(\underline{r}, \underline{\Omega}) = \Phi(\underline{r}, \underline{\Omega}) - \Phi'(\underline{r}, \underline{\Omega})$	This quantity will be called the angular difference flux, or simply the difference flux.
$\varphi(\underline{r}) = \int_{\underline{\Omega}} \Phi(\underline{r}, \underline{\Omega})\, d\underline{\Omega}$	This quantity will be called the scalar flux before the detector is put in place.
$\varphi'(\underline{r}) = \int_{\underline{\Omega}} \Phi'(\underline{r}, \underline{\Omega})\, d\underline{\Omega}$	This quantity will be called the scalar flux after the detector is put in place.
$\psi(\underline{r}) = \varphi(\underline{r}) - \varphi'(\underline{r})$	This quantity will be called the scalar difference flux.
i =	D when the detector is considered. 0 or not present when the surrounding medium is considered.
Σ_a^i	The probability of an absorption collision per centimeter of path length, for small paths.
Σ_s^i	The probability of a scattering collision per centimeter of path length, for small paths.

Σ_t^i — The probability of any type of a collision occurring per centimeter of path length, for small paths.

$S(\underline{r}, \underline{\Omega})\, d\underline{r}d\underline{\Omega}$ — The number of neutrons being supplied to volume element $d\underline{r}$ about $\underline{r}$ with direction of motion in solid angle $d\underline{\Omega}$ about $\underline{\Omega}$ due to scattering from higher energies per second

$\sigma_s(\underline{\omega} \rightarrow \underline{\Omega})\, d\underline{\Omega}$ — The probability per centimeter per nucleus per square cubic centimeter that a neutron having suffered a scattering collision while traveling in direction $\underline{\omega}$ will be scattered into solid angle $d\underline{\Omega}$ about $\underline{\Omega}$.

$\Sigma_s(\underline{\omega} \rightarrow \underline{\Omega}) = \sigma_s(\underline{\omega} \rightarrow \underline{\Omega})x$ — Atomic density.

The following Green's functions denoted by G are all for an infinite homogeneous scattering and absorbing medium.

$G(\underline{r}', \underline{\Omega}' \rightarrow \underline{r}, \underline{\Omega})\, d\underline{r}d\underline{\Omega}$ — The speed v times the number of neutrons in $d\underline{r}$ about $\underline{r}$ with directions of motion in $d\underline{\Omega}$ about $\underline{\Omega}$ due to a source of neutrons of speed v at point $\underline{r}'$ which emits one neutron per second in direction $\underline{\Omega}'$.

$$G(\underline{r}' \rightarrow \underline{r}, \underline{\Omega}) = \int_{\underline{\Omega}'} G(\underline{r}', \underline{\Omega} \rightarrow \underline{r}, \underline{\Omega})\, d\underline{\Omega}'$$

The speed v times the number of neutrons in $d\underline{r}$ about $\underline{r}$ with direction of motion in $d\underline{\Omega}$ about $\underline{\Omega}$ due to a source of neutrons of speed v at point $\underline{r}'$ isotropically emitting 4π neutrons per second.

$$G(\underline{r}', \underline{\Omega}' \rightarrow \underline{r}) = \int_{\underline{\Omega}} G(\underline{r}', \underline{\Omega}' \rightarrow \underline{r}, \underline{\Omega})\, d\underline{\Omega}$$

The speed v times the number of neutrons in $d\underline{r}$ about $\underline{r}$ due to a source of neutrons of speed v at point $\underline{r}'$ emitting one neutron per second in direction $\underline{\Omega}'$.

$$G(\underline{r}' \rightarrow \underline{r}) = \int G(\underline{r}', \underline{\Omega}' \rightarrow \underline{r}, \underline{\Omega})\, d\underline{\Omega}' d\underline{\Omega}$$

The speed v times the number of neutrons in $d\underline{r}$ about $\underline{r}$ due to a source of 4π isotropic neutrons of speed v per second at point $\underline{r}'$.

The following, denoted by a script $\mathcal{G}$, is the Green's function for an infinite homogeneous medium where all collisions result in removal from the population.

$\mathcal{G}(\underline{r}', \underline{\Omega}' \rightarrow \underline{r}, \underline{\Omega})d\underline{r}d\underline{\Omega}$ — The neutron speed v times the number of neutrons in $d\underline{r}$ with directions of motion in $d\underline{\Omega}$ about $\underline{\Omega}$ due to a source emitting one neutron per second at point $\underline{r}'$ in direction $\underline{\Omega}'$ in an infinite purely absorbing medium.

$F(a;b|c|Z)$ — The Hypergeometric function, discussed Appendix I, Part 2.

$$F_a(K, \Sigma_t) = \int_{x=0}^{\infty} e^{-\Sigma_t x} j_a(Kx)\,dx$$

A special function discussed in Appendix I, Part 2.

$j_a(Z)$ — The spherical Bessel function, discussed in Appendix I, Part 3.

$Y_a^b(\underline{\Omega})$ — The spherical harmonic function, discussed in Appendix I, Part 4.

INTRODUCTION

When a thermal neutron absorber is used to measure a thermal neutron density, the extent to which the detector disturbs the neutron density must be considered. One method for investigating this problem is to derive an analytical expression which relates the neutron population which exists when a detector is present to the population when a detector is not present. Then the effect on this expression of such quantities as detector composition, detector geometry, composition of the surrounding medium, and many others may be investigated.

In deriving the expression relating the steady state detector absorption and the unperturbed neutron population there are no restrictive assumptions. In adapting the problem for a numerical solution the number of assumptions has been kept as small as possible while still allowing the problem to be handled on a large digital computer. There are two general restrictive assumptions which are made throughout this paper. First, the neutron energy spectrum in and around the detector is assumed to be independent of position and to be the same energy spectrum that exists when the detector is not present. Second, it is assumed that the detector is located in a large homogeneous medium. Further, the detector is assumed to be several mean free paths from any boundaries of the medium.

There are several features which are built into the analytical relationship between the detector activation and the unperturbed neutron density. These features which are investigated for the first time are:

1. The initial unperturbed neutron density is allowed to be non-isotropic in angular distribution. This implies that the initial neutron density is non-uniform in space.

2. The scatter of thermal neutrons is allowed to be non-isotropic in the laboratory coordinate system.

3. The detector may have up to three independent dimensions and it may be of any arbitrary size and shape.

4. Isotropic scatter in the laboratory coordinate system of thermal neutrons by the detector is allowed.

5. The neutron density at points inside and outside the detector is available as a result of the calculation.

CHAPTER I

FORMULATION OF THE PROBLEM

The time independent neutron transport equation is assumed to be applicable to the neutron population both before and after the neutron detector is in place. It will be assumed that the thermal neutron energy spectrum is independent of position both before and after the detector is put in place. The energy dependence of the transport equation can now be integrated out and all cross-sections will be average cross sections, averaged over the neutron spectrum.

Define $N(\underline{r}, \underline{\Omega})d\underline{r}d\underline{\Omega}$ = number of neutrons in unit volume $d\underline{r}$ about $\underline{r}$ with directions of motion in $d\underline{\Omega}$ about $\underline{\Omega}$. Let v = average thermal neutron speed in centimeters per second. Define $\Phi(\underline{r}, \underline{\Omega}) = v\, N(\underline{r}, \underline{\Omega})$ and call it angular flux or simply flux.

Let the neutron flux before the detector is put in place be called $\Phi(\underline{r}, \underline{\Omega})$ and the neutron flux after the detector is put in place be called $\Phi'(\underline{r}, \underline{\Omega})$. Finally define a difference flux as

$$\Psi(\underline{r}, \underline{\Omega}) = \Phi(\underline{r}, \underline{\Omega}) - \Phi'(\underline{r}, \underline{\Omega})$$

This difference flux is not necessarily small compared to $\Phi(\underline{r}, \underline{\Omega})$. The transport equation which $\Phi(\underline{r}, \underline{\Omega})$ must satisfy before the detector is put in place is:

$$\underline{\Omega} \cdot \nabla \Phi(\underline{r}, \underline{\Omega}) + \Sigma_t \Phi(\underline{r}, \underline{\Omega}) - \int_{\underline{\omega}} \Phi(\underline{r}, \underline{\omega})\, \Sigma_s(\underline{\omega} \to \underline{\Omega})\, d\underline{\omega} = S(\underline{r}, \underline{\Omega}) \qquad (1)$$

$\mathbf{S}$ $(\underline{r}, \underline{\Omega})$ = source of thermal neutrons due to slowing down of neutrons.

The transport equation which $\Phi'(\underline{r}, \underline{\Omega})$ must satisfy after the detector is present is:

$$\underline{\Omega} \cdot \nabla \Phi'(\underline{r}, \underline{\Omega}) + \left[\Sigma_t - \Delta(\Sigma_t - \Sigma_t^D)\right] \Phi'(\underline{r}, \underline{\Omega}) - \tag{2}$$

$$\int_{\underline{\omega}} \Phi'(\underline{r}, \underline{\omega}) \left[\Sigma_s(\underline{\omega} \to \underline{\Omega}) - \Delta\left\{\Sigma_s(\underline{\omega} \to \underline{\Omega}) - \Sigma_s^D(\underline{\omega} \to \underline{\Omega})\right\}\right] d\underline{\omega}$$

$$= S(\underline{r}, \underline{\Omega}) - \Delta\left[S(\underline{r}, \underline{\Omega}) - S^D(\underline{r}, \underline{\Omega})\right]$$

Where the superscript D indicates detector and no superscript indicates surrounding medium.

$$\Delta = \begin{cases} 0 & \text{when } \underline{r} \text{ is outside Detector} \\ 1 & \text{when } \underline{r} \text{ is inside Detector} \end{cases}$$

By subtracting one transport equation from the other and introducing the difference flux notation one obtains:

$$\underline{\Omega} \cdot \nabla \Psi(\underline{r}, \underline{\Omega}) + \Sigma_t \Psi(\underline{r}, \underline{\Omega}) - \int_{\underline{\omega}} \Psi(\underline{r}, \underline{\Omega}) \Sigma_s(\underline{\omega} \to \underline{\Omega}) \, d\underline{\omega}$$

$$= \Delta(\Sigma_t - \Sigma_t^D) \Psi(\underline{r}, \underline{\Omega}) - \Delta(\Sigma - \Sigma_t^D) \Phi(\underline{r}, \underline{\Omega}) - \tag{3}$$

$$- \Delta \int_{\underline{\omega}} \Phi(\underline{r}, \underline{\omega}) \left[\Sigma_s(\underline{\omega} \to \underline{\Omega}) - \Sigma_s^D(\underline{\omega} \to \underline{\Omega})\right] d\underline{\omega} -$$

$$- \Delta \int_{\underline{\omega}} \Psi\ (\underline{r},\ \underline{\omega}) \left[\Sigma_s(\underline{\omega} \rightarrow \underline{\Omega}) - \Sigma_s^D(\underline{\omega} \rightarrow \underline{\Omega}) \right] d\underline{\omega} -$$

$$- \Delta \left[S\ (\underline{r},\ \underline{\Omega}) - S^D\ (\underline{r},\ \underline{\Omega}) \right]$$

Now define the Green's function $G(r',\ \Omega' \rightarrow \underline{r},\ \underline{\Omega})$ as the solution to Equation (4).

$$\underline{\Omega} \cdot \nabla\ G(\underline{r}',\ \underline{\Omega}' \rightarrow \underline{r},\ \underline{\Omega}) + \Sigma_t\ G(\underline{r}',\ \underline{\Omega}' \rightarrow \underline{r},\ \underline{\Omega}) -$$

$$- \int_{\underline{\omega}} G(\underline{r}',\ \underline{\Omega}' \rightarrow \underline{r},\ \underline{\omega})\ \Sigma_s\ (\underline{\omega} \rightarrow \underline{\Omega})\ d\underline{\omega} = \delta(\underline{r}'-\underline{r})\ \delta(\underline{\Omega}'-\underline{\Omega}) \qquad (4)$$

Where δ is the Dirac delta function.

The function $G(\underline{r}',\ \underline{\Omega}' \rightarrow \underline{r},\ \underline{\Omega})$ can be given a physical meaning. $G(\underline{r}',\ \underline{\Omega}' \rightarrow \underline{r},\ \underline{\Omega})\ d\underline{r}d\underline{\Omega}$ is the number of neutrons in $d\underline{r}$ about $\underline{r}$ with directions of motion in $d\underline{\Omega}$ about $\underline{\Omega}$ times the average speed v, due to a source located at point $\underline{r}'$ emitting one neutron per second in direction $\underline{\Omega}'$ into an infinite homogeneous medium of total cross-section Σ_t and scattering cross-section $\Sigma_s(\underline{\omega} \rightarrow \underline{\Omega})\ d\underline{\Omega}$. Where $\sigma_s(\underline{\omega} \rightarrow \underline{\Omega})\ d\underline{\Omega}$ is the differential scattering cross-section in the laboratory system and $\Sigma_s(\underline{\omega} \rightarrow \underline{\Omega}) = \sigma_s(\underline{\omega} \rightarrow \underline{\Omega})$ x the atomic density.

Using the general properties of Green's functions Equation (2) can be converted into an integral equation:

$$\Psi\ (\underline{r},\ \underline{\Omega}) = (\Sigma_t^D - \Sigma_t) \int_{\underline{r}',\underline{\Omega}'} \Phi\ (\underline{r}',\ \underline{\Omega}')\ G\ (\underline{r}',\ \underline{\Omega}' \rightarrow \underline{r},\ \underline{\Omega})\ d\underline{r}'d\underline{\Omega}' \qquad (5)$$

$$+ (\Sigma_t - \Sigma_t^D) \int_{\underline{r}',\underline{\Omega}'} \Psi\ (\underline{r}',\ \underline{\Omega}')\ G\ (\underline{r}',\ \underline{\Omega}' \rightarrow \underline{r},\ \underline{\Omega})\ d\underline{r}'d\underline{\Omega}' +$$

$$+\int_{\underline{r}',\underline{\Omega}'} G\,(\underline{r}',\ \underline{\Omega}' \rightarrow \underline{r},\ \underline{\Omega}) \int_{\underline{\omega}} \Phi\,(\underline{r}',\ \underline{\omega}) \left[\Sigma_s\,(\underline{\omega} \rightarrow \underline{\Omega}') - \Sigma_s^D\,(\underline{\omega} \rightarrow \underline{\Omega}')\right] d\underline{\omega}\, d\underline{r}'\, d\underline{\Omega}'$$

$$-\int_{\underline{r}',\underline{\Omega}'} G(\underline{r}',\ \underline{\Omega}' \rightarrow \underline{r},\ \underline{\Omega}) \int_{\underline{\omega}} \Psi\,(\underline{r}',\underline{\omega}) \left[\Sigma_s(\underline{\omega} \rightarrow \underline{\Omega}') - \Sigma_s^D\,(\underline{\omega} \rightarrow \underline{\Omega}')\right] d\underline{\omega}\, d\underline{r}'\, d\underline{\Omega}'$$

$$+\int_{\underline{r}',\underline{\Omega}'} G\,(\underline{r}',\ \underline{\Omega}' \rightarrow \underline{r},\ \underline{\Omega}) \left[S(\underline{r}',\ \underline{\Omega}') - S^D(\underline{r}',\ \underline{\Omega}')\right] d\underline{r}'\, d\underline{\Omega}'$$

From this point on it will be understood that all spatial integrations over vectors $\underline{r}$, $\underline{r}'$ etc. are limited to integration over the detecor volume.

Conversion of the differential-integral Equation (2) to the integral Equation 5 by means of the Green's function has effectively separated the problem into two separate problems. The first problem is that of formulating the Green's function in some useable form. The second problem is that of carrying out the spatial integrations over the detector volume.

Equation 5 will now be converted to an iterative equation by merely appending subscripts to the $\Psi\,(\underline{r},\ \underline{\Omega})$ terms.

$$\Psi_n\,(\underline{r},\ \underline{\Omega}) = (\Sigma_t^D - \Sigma_t) \int_{\underline{r}',\ \underline{\Omega}'} \Phi(\underline{r}',\ \underline{\Omega}') G(\underline{r}',\ \underline{\Omega}' \rightarrow \underline{r},\ \underline{\Omega})\, d\underline{r}'\, d\underline{\Omega} \qquad (6)$$

$$+ (\Sigma_t - \Sigma_t^D) \int_{\underline{r}',\underline{\Omega}'} \Psi_{n-1}(\underline{r}',\ \underline{\Omega}')\ G\,(\underline{r}',\ \underline{\Omega}' \rightarrow \underline{r},\ \underline{\Omega})\, d\underline{r}'\, d\underline{\Omega}' +$$

$$\int_{\underline{r}',\underline{\Omega}'} G(\underline{r}', \underline{\Omega}' \rightarrow \underline{r}, \underline{\Omega}) \int_{\underline{\omega}} \Phi(\underline{r}', \underline{\omega}) \left[\Sigma_s (\underline{\omega} \rightarrow \underline{\Omega}) - \Sigma_s^D (\underline{\omega} \rightarrow \underline{\Omega}) \right] d\underline{\omega} d\underline{r}' d\underline{\Omega}'$$

$$- \int_{\underline{r}',\underline{\Omega}'} G(\underline{r}', \underline{\Omega}' \rightarrow \underline{r}, \underline{\Omega}) \int_{\underline{\omega}} \Psi_{n-1}(\underline{r}', \underline{\omega}) \left[\Sigma_s (\underline{\omega} \rightarrow \underline{\Omega}) - \Sigma_s^D (\underline{\omega} \rightarrow \underline{\Omega}) \right] d\underline{\omega} d\underline{r}' d\underline{\Omega}'$$

$$+ \int_{\underline{r}',\underline{\Omega}'} G(\underline{r}', \underline{\Omega}' \rightarrow \underline{r}, \underline{\Omega}) \left[S(\underline{r}', \underline{\Omega}') - S^D(\underline{r}', \underline{\Omega}') \right] d\underline{r}' d\underline{\Omega}'$$

Any initial guess for $\Psi_0(\underline{r}, \underline{\Omega})$ can be used in Equation (6) to generate a series of functions $\Psi_n(\underline{r}, \underline{\Omega})$ for $n > 0$. Furtner, as n goes to infinity $\Psi_n(\underline{r}, \underline{\Omega})$ will approach $\Psi(\underline{r}, \underline{\Omega})$ the solution of Equation (5). The proof of this convergence is discussed in Appendix III.

Apparently no analytic expression for the Green's function $G(\underline{r}', \underline{\Omega}' \rightarrow \underline{r}, \underline{\Omega})$ is known, however the somewhat less complex Green's function $G(\underline{r}' \rightarrow \underline{r}, \underline{\Omega})$ has been expressed in analytical form. Where

$$G(\underline{r}' \rightarrow \underline{r}, \underline{\Omega}) = \int_{\underline{\Omega}'} G(\underline{r}', \underline{\Omega}' \rightarrow \underline{r}, \underline{\Omega}) \, d\underline{\Omega}' \tag{7}$$

$G(\underline{r}' \rightarrow \underline{r}, \underline{\Omega})$ satisfies the equation which is obtained by integrating Equation (4) over all $\underline{\Omega}$.

In appendix I it is shown that $G(\underline{r}' \rightarrow \underline{r}, \underline{\Omega})$ can be expressed as

$$G(\underline{r}' \rightarrow \underline{r}, \underline{\Omega}) = \sum_{\substack{a=0 \\ b=-a}}^{\substack{a=\infty \\ b=a}} \overline{G}_a (|\underline{r} - \underline{r}'|) \, Y_a^b (\underline{r} - \underline{r}') \, Y_a^{b*} (\underline{\Omega}) \tag{8}$$

$$\bar{G}_a(|R|) = \frac{\int_0^\infty j_a(Kx)\, e^{-\Sigma_t x}\, dx}{\frac{2}{\pi}\int_{K=0}^{\infty} \frac{j_a(KR)\; x=o}{1 \pm \frac{\Sigma_s}{K} \tan^{-1}\frac{K}{\Sigma_t}}\, K^2\, dK} \qquad (9)$$

The function $\bar{G}_a(|R|)$ will clearly depend upon $|R|$ and upon the properties of the external medium. Except for the assymptotic limits the function $\bar{G}_a(|R|)$ has not been expressed in a simple analytical form, however a numerical evaluation is coded for the IBM 704. Details of the numerical evaluation are given in Appendix I. Thus $\bar{G}_a(|R|)$ may be considered a known function of R once the external medium has been specified.

Using the reciprocity theorem it is easily shown that

$$G(\underline{r}', \underline{\Omega}' \to \underline{r}) = G(\underline{r} \to \underline{r}', -\underline{\Omega}') = \qquad (10)$$

$$= \sum_{a,b} \bar{G}_a(|\underline{r} - \underline{r}'|)\, Y_a^b(\underline{r} \overset{\Lambda}{-} \underline{r}')\, Y_a^{*b}(\underline{\Omega}')$$

Due to the fact that only the Green's function $G(\underline{r}', \underline{\Omega}' \to \underline{r})$ is available rather than the complete $G(\underline{r}', \underline{\Omega}' \to \underline{r}, \underline{\Omega})$ only a few iterations can be carried out using Equation (6). Thus it is desirable to use the best possible guess for $\Psi_o(\underline{r}, \underline{\Omega})$ the starting function in the series $\Psi_n(\underline{r}, \underline{\Omega})$.

In order to obtain a good starting guess for $\Psi_o(\underline{r}, \underline{\Omega})$ expand

$$\Psi(\underline{r}, \underline{\Omega}) = \sum_{a,b} \Psi_a^b(\underline{r})\, Y_a^b(\underline{\Omega}) \qquad (11)$$

Assume that all $\Psi_a^b(\underline{r})$ for any $\underline{r}$ and for "a" > 0 are small compared to $\Psi_o^o(\underline{r})$ and thus can be neglected. This is equivalent to assuming that the difference flux is nearly isotropic. Similarly expand

$$\Phi(\underline{r}, \underline{\Omega}) = \sum_{a,b} \Phi_a^b(\underline{r})\, Y_a^b(\underline{\Omega})$$

$$S(\underline{r}, \underline{\Omega}) = \sum_{a,b} S_a^b(\underline{r})\, Y_a^b(\underline{\Omega}) \qquad (12)$$

$$S^D(\underline{r}, \underline{\Omega}) = \sum_{a,b} S^D{}_a^b(\underline{r})\, Y_a^b(\underline{\Omega})$$

and assume that all terms for "a" > 0 are small compared to the corresponding "a" = 0 term.

Now combine Equations (6), (11), and (12), and integrate over all $\underline{\Omega}$ and $\underline{\Omega}'$ to obtain:

$$\psi(\underline{r}) = \frac{\Sigma_a^D - \Sigma_a}{4\pi} \int_{\underline{r}'} \varphi(\underline{r}')\, \bar{G}_o(|\underline{r} - \underline{r}'|)\, d\underline{r}'$$

$$+ \frac{\Sigma_a - \Sigma_a^D}{4\pi} \int_{\underline{r}'} \psi(\underline{r}')\, \bar{G}_o(|\underline{r} - \underline{r}'|)\, d\underline{r}' \qquad (13)$$

$$+ \frac{1}{4\pi} \int_{\underline{r}'} \bar{G}_o(|\underline{r} - \underline{r}'|) \left[\mathcal{S}(\underline{r}') - \mathcal{S}^D(\underline{r}') \right] d\underline{r}'$$

Where

$$\varphi(\underline{r}) = \int_{\underline{\Omega}} \Phi(\underline{r}, \underline{\Omega})\, d\underline{\Omega} = \sqrt{4\pi}\, \Phi_o^o(\underline{r})$$

$$\mathcal{S}(\underline{r}) = \int_{\underline{\Omega}} S(\underline{r}, \underline{\Omega})\, d\underline{\Omega} = \sqrt{4\pi}\, S_o^o(\underline{r}) \qquad (14)$$

$$\psi(\underline{r}) = \int_{\underline{\Omega}} \Psi(\underline{r}, \underline{\Omega})\, d\underline{\Omega} = \sqrt{4\pi}\, \Psi_o^o(\underline{r})$$

If it is assumed that the sperical harmonic expansions for

$$\Psi(\underline{r}, \underline{\Omega}),\ \Phi(\underline{r}, \underline{\Omega}),\ S(\underline{r}, \underline{\Omega}) \text{ and } S^D(\underline{r}, \underline{\Omega})$$

can resonably be cut off after "a" = 0 then

$$\int_{\underline{\Omega}} \Psi(\underline{r}, \underline{\Omega})\, d\underline{\Omega} = \psi(\underline{r})$$

In the sense that $\Psi(\underline{r}, \underline{\Omega})$ is a separable function of $\underline{r}$ and $\underline{\Omega}$ and is isotropic in $\underline{\Omega}$ then $\psi(\underline{r})$ gives an approximation to the spatial form of $\Psi(\underline{r}, \underline{\Omega})$.

An iterative form of Equation (13) can be written as

$$\psi_n(\underline{r}) = \frac{\Sigma_a^D - \Sigma_a}{4\pi} \int_{\underline{r}'} \varphi(\underline{r}')\, \bar{G}_o(|\underline{r} - \underline{r}'|)\, d\underline{r}'$$

$$+ \frac{\Sigma_a - \Sigma_a^D}{4\pi} \int_{\underline{r}'} \psi_{n-1}(\underline{r}') \, \bar{G}_o \, (|\underline{r}' - \underline{r}|) \, d\underline{r}' \qquad (15)$$

$$+ \frac{1}{4\pi} \int_{\underline{r}'} \bar{G}_o \, (|\underline{r} - \underline{r}'|) \left[\delta \, (\underline{r}') - \delta^D(\underline{r}') \right] d\underline{r}'$$

In Appendix III it is shown that the series of functions $\psi_n \, (\underline{r})$ generated by Equation (15) converges to $\psi \, (\underline{r})$ the solution of Equation (13) as n goes to infinity. Since the function $\bar{G}_o \, (|\underline{r} - \underline{r}'|)$ is completely known as many iterations of Equation (15) as are necessary may be carried out. The integrations and iterations of Equation (15) are actually carried out on a digital computer. The details of this numerical work are presented in Appendix V. Now that $\psi \, (\underline{r})$ has been calculated it may be used for the initial guess $\Psi_o \, (\underline{r}, \, \Omega)$ in Equation (6).

CHAPTER II

UNIFORM, ISOTROPIC INITIAL FLUX

The effects outlined earlier will be considered one at a time. The first case considered is that of an initial flux which is uniform in space and isotropic in angular distribution. First $\psi(\underline{r})$ the solution of Equation (13) will be obtained by the iterative solution of Equation (15). This function $\psi(\underline{r})$ will then be used as an initial guess in Equation (6) and $\Psi_1(\underline{r}, \underline{\Omega})$ will be calculated using Equation (6). Integration of the equation for $\Psi_1(\underline{r}, \underline{\Omega})$ over $\underline{\Omega}$ will show that

$$\psi(\underline{r}) = \int_{\underline{\Omega}} \Psi_1(\underline{r}, \underline{\Omega})\, d\underline{\Omega}$$

if it is assumed that the source due to slowing-down of neutrons in the detector is zero and that the source due to slowing-down of neutrons in the surrounding medium

$$S(\underline{r}, \underline{\Omega}) = \frac{\Sigma_a}{4\pi} \int_{\underline{\Omega}} \Phi(\underline{r}, \underline{\Omega})\, d\underline{\Omega}$$

Thus it is seen that the first iteration of Equation (6) produces angular information about $\Psi(\underline{r}, \underline{\Omega})$. The function $\Psi_1(\underline{r}, \underline{\Omega})$ is not calculated explicitly but it is implicit in the expression for $\Psi_2(\underline{r}, \underline{\Omega})$. Although the function $\Psi_1(\underline{r}, \underline{\Omega})$ is not explicitly evaluated numerically this calculation could be carried out to give the detailed $\underline{r}$ and $\underline{\Omega}$ dependence of $\Psi_1(\underline{r}, \underline{\Omega})$. Equation (6) is applied a second time to produce a function $\Psi_2(\underline{r}, \underline{\Omega})$ from $\Psi_1(\underline{r}, \underline{\Omega})$. Examination of this equation for $\Psi_2(\underline{r}, \underline{\Omega})$

$$\psi(\underline{r}) = \int_{\underline{\Omega}} \Psi_1(\underline{r}, \underline{\Omega})\, d\underline{\Omega} \quad \text{identically,}$$

will show that it contains the Green's function $G(\underline{r}', \underline{\Omega} \rightarrow \underline{r}, \underline{\Omega})$ which is not available. Since the absorption rate is related to $\int_{\underline{\Omega}} \Psi(\underline{r}, \underline{\Omega})\, d\underline{\Omega}$ the detailed dependence of $\Psi(\underline{r}, \underline{\Omega})$ upon $\underline{\Omega}$ is not necessary in order to calculate absorption rate. Thus the equation for $\Psi_2(\underline{r}, \underline{\Omega})$ may be integrated over to produce:

$$\begin{aligned}
\int_{\underline{\Omega}} \Psi_2(\underline{r}, \underline{\Omega})\, d\underline{\Omega} &= \Sigma_a^D \Phi \int_{\underline{r}', \underline{\Omega}'} G(\underline{r}', \underline{\Omega}' \rightarrow \underline{r})\, d\underline{r}' d\underline{\Omega}' \\
&+ (\Sigma_t - \Sigma_t^D) \Sigma_a^D \Phi \int_{\underline{r}'', \underline{r}', \underline{\Omega}'} G(\underline{r}'' \rightarrow \underline{r}', \underline{\Omega}')\, G(\underline{r}', \underline{\Omega}' \rightarrow \underline{r})\, d\underline{r}'' d\underline{r}' d\underline{\Omega}' \\
&+ \frac{(\Sigma_s^D - \Sigma_s)}{4\pi} \Sigma_a^D \Phi \int_{\underline{r}'', \underline{r}'} G(\underline{r}'' \rightarrow \underline{r}')\, G(\underline{r}' \rightarrow \underline{r})\, d\underline{r}'' d\underline{r}' - \\
&\frac{(\Sigma_t - \Sigma_t^D)(\Sigma_a^D - \Sigma_a)}{4\pi} \int_{\underline{r}'', \underline{r}', \underline{\Omega}'} \psi(\underline{r}'')\, G(\underline{r}'' \rightarrow \underline{r}', \underline{\Omega}')\, G(\underline{r}', \underline{\Omega}' \rightarrow \underline{r})\, d\underline{r}'' d\underline{r}' d\underline{\Omega}' \\
&- \frac{(\Sigma_s^D - \Sigma_s)(\Sigma_a^D - \Sigma_a)}{(4\pi)^2} \int_{\underline{r}'', \underline{r}'} \psi(\underline{r}'')\, G(\underline{r}'' \rightarrow \underline{r}')\, G(\underline{r}' \rightarrow \underline{r})\, d\underline{r}'' d\underline{r}'
\end{aligned} \tag{16}$$

Note that

$$G(\underline{r}' \rightarrow \underline{r}) = \int_{\underline{\Omega}'} G(\underline{r}', \underline{\Omega}' \rightarrow \underline{r})\, d\underline{\Omega}'$$

It is seen that Equation (16) now contains only the Green's functions of the form $G(\underline{r}', \underline{\Omega}' \rightarrow \underline{r})$ or $G(\underline{r}'' \rightarrow \underline{r}', \underline{\Omega}')$, both of which are known.

The spherical harmonic expansion for $G(\underline{r}', \underline{\Omega}' \rightarrow \underline{r})$ and for

$G\ (\underline{r}'' \rightarrow \underline{r}',\ \underline{\Omega}')$ are now inserted in equation and the integration over $\underline{\Omega}'$ is carried out to produce:

$$\int_{\underline{\Omega}} \Psi_2\ (\underline{r},\ \underline{\Omega})\ d\underline{\Omega} = \Sigma_a^D\ \Phi \int_{\underline{r}'} \bar{G}_o\ (|\underline{r} - \underline{r}'|)\ d\underline{r}' + \tag{17}$$

$$(\Sigma_t - \Sigma_t^D)\ \Sigma_a^D\ \Phi \sum_{a,b} \int_{\underline{r}'',\underline{r}'} \bar{G}_a\ (|\underline{r}' - \underline{r}''|)\ Y_a^{*b}\ (\underline{r}' \overset{\Lambda}{-} \underline{r}'')\ x$$

$$G_a\ (|\underline{r} - \underline{r}'|)\ Y_a^b\ (\underline{r} \overset{\Lambda}{-} \underline{r}')\ d\underline{r}''d\underline{r}' +$$

$$\frac{\Sigma_s^D - \Sigma_s}{(4\pi)} \sum_a^D\ \Phi \int_{\underline{r}'',\ \underline{r}'} \bar{G}_o\ (|\underline{r}' - \underline{r}''|)\ \bar{G}_o\ (|\underline{r} - \underline{r}'|)\ d\underline{r}''d\underline{r}'$$

$$+ \frac{(\Sigma_t^D - \Sigma_t)(\Sigma_a^D - \Sigma_a)}{4\pi} \sum_{a,b} \int_{\underline{r}'',\ \underline{r}'} \psi\ (\underline{r}'')\ \bar{G}_a\ (|\underline{r}' - \underline{r}''|)\ x$$

$$Y_a^{*b}\ (\underline{r}' \overset{\Lambda}{-} \underline{r}'')\ \bar{G}_a\ (|\underline{r} \overset{\Lambda}{-} \underline{r}'|)\ Y_a^b\ (\underline{r} - \underline{r}')\ d\underline{r}''d\underline{r}' +$$

$$\frac{(\Sigma_s^D - \Sigma_s)(\Sigma_a^D - \Sigma_a)}{(4\pi)^2} \int_{\underline{r}'',\ \underline{r}'} \psi\ (\underline{r}'')\ \bar{G}_o\ (|\underline{r}' - \underline{r}''|)\bar{G}_o(|\underline{r} - \underline{r}'|)\ d\underline{r}''d\underline{r}'$$

Due to the complexity of the numerical problem it is not practical to obtain $\int_{\underline{\Omega}} \Psi_2\ (\underline{r},\ \underline{\Omega})\ d\underline{\Omega}$, but $\int_{\underline{r},\ \underline{\Omega}} \Psi_2\ (\underline{r},\ \underline{\Omega})\ d\underline{r}d\underline{\Omega}$ is obtained. This

integral is all that is necessary to calculate detector activation.

Terminating the summation over "a" in Equation (17) at some value A is equivalent to termination of the spherical harmonic expansion for $\Psi(\underline{r}, \underline{\Omega})$ at "a" = A. When $\int_{\underline{r}, \underline{\Omega}} \Psi_2(\underline{r}, \underline{\Omega})\, d\underline{r}d\underline{\Omega}$ is calculated numerically, A will be used as a parameter and varied in order to determine how many terms in the spherical harmonic expansion must be retained in a given case so that the neglected higher order terms will have only small effect upon

$$\int_{\underline{r}, \underline{\Omega}} \Psi_2(\underline{r}, \underline{\Omega})\, d\underline{r}d\underline{\Omega}$$

The results of the numerical calculations show that for small detectors, i.e. thin coins or small diameter wires, the value of $\int_{\underline{r}, \underline{\Omega}} \Psi(\underline{r}, \underline{\Omega}) d\underline{r}d\underline{\Omega}$ calculated from Equation (17) will be independent of the value of A, the cut off point for the spherical harmonic expansions. For detectors of this small size the spherical harmonic expansions may be terminated at the zeroth term, thus in this case

$$\psi(\underline{r})/4\pi = \Psi(\underline{r}, \underline{\Omega}) = \Psi_1(\underline{r}, \underline{\Omega}) = \Psi_2(\underline{r}, \underline{\Omega})$$

When the value of $\int_{\underline{r}, \underline{\Omega}} \Psi_2(\underline{r}, \underline{\Omega})\, d\underline{r}d\underline{\Omega}$ is insensitive to "a" for some "a" $\geq$ A but

$$\int_{\underline{r}} \psi(\underline{r})\, d\underline{r} \neq \int_{\underline{r}, \underline{\Omega}} \Psi_2(\underline{r}, \underline{\Omega})\, d\underline{r}d\underline{\Omega}$$

it is clear that including higher order spherical harmonics will not effect the value of $\int_{\underline{r},\,\underline{\Omega}} \Psi_2\,(\underline{r},\,\underline{\Omega})\,d\underline{\Omega}d\underline{r}$. But since the value of $\int_{\underline{r},\,\underline{\Omega}} \Psi_1\,(\underline{r},\,\underline{\Omega})\,d\underline{r}d\underline{\Omega}$ $\left(\text{which is the same as } \int_{\underline{r}} \psi(\underline{r})d\underline{r}\right)$ may be different from $\int_{\underline{r},\,\underline{\Omega}} \Psi_2\,(\underline{r},\,\underline{\Omega})\,d\underline{r}d\underline{\Omega}$ then the question arises of how much would $\Psi_3\,(\underline{r},\,\underline{\Omega})$ differ from $\Psi_2\,(\underline{r},\,\underline{\Omega})$? Since $\Psi_3\,(\underline{r},\,\underline{\Omega})$ cannot be calculated due to lack of information about $G\,(\underline{r}',\,\underline{\Omega}' \rightarrow \underline{r},\underline{\Omega})$ the magnitude of $\Psi_3\,(\underline{r},\,\underline{\Omega})$ will have to be estimated.

In Appendix I it is shown that

$$\|\Psi_{n+1}(\underline{r},\,\underline{\Omega})-\Psi_n(\underline{r},\,\underline{\Omega})\| < K\|\Psi_n(\underline{r},\,\underline{\Omega})-\Psi_{n-1}(\underline{r},\,\underline{\Omega})\| \tag{18}$$

where $K < 1$

$$\|f(\underline{r},\,\underline{\Omega})\| = \underset{\text{for any } \underline{\Omega}}{\overset{\text{for any } \underline{r}}{\text{Max.}}} \text{ of } |f(\underline{r},\,\underline{\Omega})| \tag{19}$$

For the cases where $\Psi\,(\underline{r},\,\underline{\Omega})$ is not a sharply peaked function of $\underline{r}$ or of $\underline{\Omega}$ the maximum differences may be replaced approximately with differences of averages.

$$\|\Psi_3\,(\underline{r},\,\underline{\Omega}) - \Psi_2\,(\underline{r},\,\underline{\Omega})\| <$$

$$K\left|\int_{\underline{r},\,\underline{\Omega}} \Psi_2\,(\underline{r},\,\underline{\Omega})d\underline{r}d\underline{\Omega} - \int_{\underline{r},\,\underline{\Omega}} \Psi_1\,(\underline{r},\,\underline{\Omega})d\underline{r}d\underline{\Omega}\right| \Big/ \int_{\underline{r},\,\underline{\Omega}} d\underline{r}d\underline{\Omega}$$

For the case of a nearly isotropic $\Psi\,(\underline{r},\,\underline{\Omega})$ it was noted above that Equation (6) reduced to Equation (15) and thus

$$\| \psi_{n+1}(\underline{r}) - \psi_n(\underline{r}) \| < K \| \psi_n(\underline{r}) - \psi_{n-1}(\underline{r}) \|$$

The norms $\| \psi_n(\underline{r}) - \psi_{n-1}(\underline{r}) \|$ for all iterations of Equation (15) are available and can be used to get a good estimate of the value of K. So, given the difference between

$$\int_{\underline{r},\,\underline{\Omega}} \Psi_2\,(\underline{r},\,\underline{\Omega})\,d\underline{r}d\underline{\Omega} \quad \text{and} \quad \int_{\underline{r},\,\underline{\Omega}} \Psi_1\,(\underline{r},\,\underline{\Omega})\,d\underline{r}d\underline{\Omega}$$

which results from the calculations, an estimate of the difference between

$$\int_{\underline{r},\,\underline{\Omega}} \Psi_3\,(\underline{r},\,\underline{\Omega})\,d\underline{r}d\underline{\Omega} \quad \text{and} \quad \int_{\underline{r},\,\underline{\Omega}} \Psi_2\,(\underline{r},\,\underline{\Omega})\,d\underline{r}d\underline{\Omega}$$

can be obtained.

All of the formalism is now set up to evaluate the average neutron flux within the detector compared to the flux which existed before the detector was put in place.

Since all of the above integrations over the detector volume are carried out numerically a completely arbitrary three dimensional detector geometry could be treated. Practical limitations dictated the choice of a right circular cylindrical geometry for consideration here. This cylinder can be in one extreme case a finite length wire or in the other extreme a thin coin, depending upon the dimensions chosen. Thus the effect of finite length of a wire detector and of finite radius of a coin detector are built into this model.

The function $\psi\,(\underline{r})$ will be available as a result of the numerical calculations at a large number of points throughout the detector volume and

at a few select points outside the detector. For those detectors that are small enough so that $\psi(\underline{r})$ and $\int_{\underline{\Omega}} \Psi_2(\underline{r}, \underline{\Omega})d\underline{\Omega}$ are reasonably close to each other the function $\psi(\underline{r})$ will give a good picture of the spatial dependence of $\int_{\underline{\Omega}} \Psi(\underline{r}, \underline{\Omega})d\underline{\Omega}$.

CHAPTER III

NON-ISOTROPIC SCATTER AND NON-ISOTROPIC INITIAL FLUX $\Phi(\underline{r}, \underline{\Omega})$

Consider the problem of a detector placed in a medium which has non-isotropic scatter in the laboratory system. Assume that the initial flux $\Phi(\underline{r}, \underline{\Omega})$ is uniform in space and isotropic in direction. The Green's function $G(\underline{r}', \underline{\Omega}' \rightarrow \underline{r})$ for the case of non-isotropic scattering is available in analytical form which is similar to but more complex than the form of $G(\underline{r}', \underline{\Omega}' \rightarrow \underline{r})$ for the isotropic scattering case. A complete discussion of the derivation of the Green's function for $\bar{\mu} \neq 0$ is given in Appendix II.

Here $\bar{\mu}$ is defined as:

$$\bar{\mu} = \int_{\underline{\Omega}} \Sigma_s (\underline{\omega} \rightarrow \underline{\Omega})\, \underline{\omega} \cdot \underline{\Omega} d\underline{\Omega} \Big/ \int_{\underline{\Omega}} \Sigma_s (\underline{\omega} \rightarrow \underline{\Omega})\, d\underline{\Omega}$$

If it is assumed that terms $\bar{\mu}^2$ can be neglected compared to terms in $\bar{\mu}$ then the zeroth term in the spherical harmonic expansion for the Green's function can be calculated for the case of non-isotropic scatter, i.e.

$$\int_{\underline{\Omega}'} G(\underline{r}', \underline{\Omega}' \rightarrow \underline{r})\, d\underline{\Omega}' = \bar{G}_o (|\underline{r} - \underline{r}'|)_{\bar{\mu}} = \frac{2}{(2\pi)^2} \int_{K=0}^{\infty} \frac{\left[F_o(K, \Sigma_t) + \frac{3\Sigma_s \bar{\mu}}{4\pi} F_1^2 (K, \Sigma_t)\right] j_o (K|\underline{r} - \underline{r}'|)}{1 - \frac{\Sigma_s}{4\pi} F_o(K, \Sigma_t) - \frac{3\Sigma_s^2 \bar{\mu}}{(4\pi)^2} F_1^2 (K, \Sigma_t)} K^2\, dK \qquad (21)$$

This function $\bar{G}_o (R)_{\bar{\mu}}$ is evaluated in a numerical manner very similar to that discussed in Appendix I, Part 4.

Equation (15) may now be rewritten replacing $\bar{G}_o\ (|\underline{r} - \underline{r}'|)$ with $\bar{G}_o\ (|\underline{r} - \underline{r}'|)_{\bar{\mu}}$. The solution to this equation will be called $\psi\ (\underline{r})_{\bar{\mu}}$ to denote the pressence of non-isotropic scatter.

$$\psi\ (\underline{r}) = \frac{\Sigma_a^D - \Sigma_a}{4\pi}\ \varphi \int_{\underline{r}'} \bar{G}_o\ (|\underline{r} - \underline{r}'|)_{\bar{\mu}}\ d\underline{r}' \tag{22}$$

$$+ \frac{\Sigma_a - \Sigma_a^D}{4\pi} \int_{\underline{r}'} \psi\ (\underline{r}')_{\bar{\mu}}\ \bar{G}_o\ (|\underline{r} - \underline{r}'|)_{\bar{\mu}}\ d\underline{r}'$$

$$+ \int_{\underline{r}'} \bar{G}_o\ (|\underline{r} - \underline{r}'|)_{\bar{\mu}} \left[\varphi\ (\underline{r}') - \varphi^D\ (\underline{r}') \right] d\underline{r}'$$

In Chapter II the procedure was discussed for determining how small a detector must be in order that the solution to Equation (13), $\psi\ (\underline{r})$, be essentially the same as the solution to Equation (5), $\Psi\ (\underline{r}, \underline{\Omega})$.

For small detectors Equation (22) can now be evaluated numerically using the non-isotropic $\bar{G}_o\ (|\underline{r} - \underline{r}'|)_{\bar{\mu}}$ and a comparison of $\psi\ (\underline{r})$ with $\psi\ (\underline{r})_{\bar{\mu}}$ will show the effect of non-isotropic scattering in the external medium upon the average flux in the detector.

Next consider the case where scattering is isotropic and the departure of the initial flux $\Phi\ (\underline{r}, \underline{\Omega})$ from isotropy is small enough so that

$$\Phi\ (\underline{r}, \underline{\Omega}) = \sum_{a,\ b}^{1} \Phi_a^b\ (\underline{r})\ Y_a^b\ (\underline{\Omega})$$

Putting this expansion in the transport equation yields the usual diffusion relationship:

$$\frac{-1}{3\Sigma_t} \nabla \int_{\underline{\Omega}} \Phi\ (\underline{r},\ \underline{\Omega})\ d\underline{\Omega} = \int_{\underline{\Omega}} \Phi\ (\underline{r},\ \underline{\Omega})\ \underline{\Omega} d\underline{\Omega} \tag{23}$$

$$\Phi_o^o\ (\underline{r}) = \int_{\underline{\Omega}} \Phi\ (\underline{r},\ \underline{\Omega})\ d\underline{\Omega}\ /\ \sqrt{4\pi} \tag{24}$$

Dividing Equation (23) into rectangular components and evaluating yields:

$$\Phi_1^1\ (\underline{r}) = \left[-\frac{\partial\ \Phi_o^o\ (\underline{r})}{\partial x} + i\ \frac{\partial\ \Phi_o^o\ (\underline{r})}{\partial y} \right] / \left(6\Sigma_t \sqrt{\frac{2\pi}{3}} \right)$$

$$\Phi_1^{-1}\ (\underline{r}) = \left[-\frac{\partial\ \Phi_o^o\ (\underline{r})}{\partial x} - i\ \frac{\partial\ \Phi_o^o\ (\underline{r})}{\partial y} \right] / \left(6\Sigma_t \sqrt{\frac{2\pi}{3}} \right) \tag{25}$$

$$\Phi_1^o\ (\underline{r}) = \left[-\frac{\partial\ \Phi_o^o\ (\underline{r})}{\partial Z} \right] / \left(3\Sigma_t\ \sqrt{4\pi} \right)$$

If the spherical harmonic expansion of the initial flux is terminated at "a" = 1 then all of the coefficients can be calculated as outlined above from $\int_{\underline{\Omega}} \Phi\ (\underline{r},\ \underline{\Omega})\ d\underline{\Omega}$, and the gradient of $\int_{\underline{\Omega}} \Phi\ (\underline{r},\ \underline{\Omega})\ d\underline{\Omega}$, which are assumed specified.

Equation (15) can be solved for this case of a spatially dependent flux. The $\psi(\underline{r})$ which results from this solution will again be used as an initial guess for a single iteration of Equation (6). Carrying out a single iteration and integrating $\Psi_1(\underline{r}, \underline{\Omega})$ over all $\underline{\Omega}$ gives:

$$\int_{\underline{\Omega}} \Psi_1(\underline{r}, \underline{\Omega})\, d\underline{\Omega} = (\Sigma_t^D - \Sigma_t) \int_{\underline{r}', \underline{\Omega}'} \Phi(\underline{r}', \underline{\Omega}') G(\underline{r}', \underline{\Omega}' \to \underline{r})\, d\underline{r}' d\underline{\Omega}'$$

$$+ \frac{(\Sigma_a - \Sigma_a^D)}{4\pi} \int_{\underline{r}', \underline{\Omega}'} \psi(\underline{r}')\, G(\underline{r}', \underline{\Omega}' \to \underline{r})\, d\underline{r}' d\underline{\Omega}' + \qquad (26)$$

$$+ \frac{(\Sigma_s - \Sigma_s^D)}{4\pi} \int_{\underline{r}'} G(\underline{r}' \to \underline{r}) \int_{\underline{\omega}} \Phi(\underline{r}, \underline{\omega})\, d\underline{\omega} d\underline{r}'$$

$$+ \int_{\underline{r}', \underline{\Omega}'} G(\underline{r}', \underline{\Omega}' \to \underline{r}) \left[S(\underline{r}', \underline{\Omega}') - S^D(\underline{r}', \underline{\Omega}') \right] d\underline{r}' d\underline{\Omega}'$$

Assume the source in the detector $S^D(\underline{r}, \underline{\Omega})$ due to the slowing down of neutrons is zero and the source due to slowing down of neutrons outside the detector.

$$S(\underline{r}, \underline{\Omega}) = \frac{\Sigma_a}{4\pi} \int_{\underline{\Omega}} \Phi(\underline{r}, \underline{\Omega})\, d\underline{\Omega} \quad .$$

Putting the spherical harmonic expansion for $\Phi(\underline{r}, \underline{\Omega})$ and $G(\underline{r}', \underline{\Omega}' \to \underline{r})$ into Equation (26) and integrating over all $\underline{\Omega}'$ gives:

$$\int_{\Omega} \Psi_1(\underline{r}, \underline{\Omega}) \, d\underline{\Omega} = (\Sigma_t^D - \Sigma_t) \sum_{a=o}^{l} \int_{\underline{r}} \Phi_a^b(\underline{r}') Y_a^b(\underline{r} - \underline{r}') \bar{G}_a(|\underline{r} - \underline{r}'|) \, d\underline{r}'$$

$$+ \frac{\Sigma_a - \Sigma_a^D}{4\pi} \int_{\underline{r}'} \psi(\underline{r}') \, \bar{G}_o(|\underline{r} - \underline{r}'|) \, d\underline{r}' \qquad (27)$$

$$+ \frac{\Sigma_s - \Sigma_s^D}{4\pi} \int_{\underline{r}'} \bar{G}_o(|\underline{r} - \underline{r}'|) \sqrt{4\pi} \, \Phi_o^o(\underline{r}') \, d\underline{r}'$$

$$+ \frac{\Sigma_a}{4\pi} \int_{\underline{r}'} \bar{G}_o(|\underline{r} - \underline{r}'|) \sqrt{4\pi} \, \Phi_o^o(\underline{r}') \, d\underline{r}'$$

In the case of a uniform isotropic initial flux, as noted earlier $\psi(\underline{r})$ and $\int_{\Omega} \Psi_1(\underline{r}, \underline{\Omega}) \, d\underline{\Omega}$ are identical. So the $\psi(\underline{r})$ for the isotropic initial flux case can be compared to the function $\int_{\underline{r}} \Psi_1(\underline{r}, \underline{\Omega}) \, d\underline{\Omega}$ for the non-isotropic initial flux case in order to evaluate the effect of a non-uniform non-isotropic flux upon the difference flux and upon the average flux within the detector.

It should be noted that in the case of an initially non-uniform non-isotropic flux only one iteration of Equation (6) can be carried out due to the fact that the general Green's function $G(\underline{r}', \underline{\Omega}' \rightarrow \underline{r}, \underline{\Omega})$ is not available, but this should not present a serious handicap for $\Psi_i(\underline{r}, \underline{\Omega})$ will be very close to $\Psi(\underline{r}, \underline{\Omega})$ for a large range of small detectors.

CHAPTER IV

RESULTS OF THE CALCULATION OF $\overline{G}_a(R)$

Rather than presenting the function $\overline{G}_a(R)$ which has a $1/R^2$ dependence for small R the graphs and tables all present $R^2 \times \overline{G}_a(R)$.

The upper limit for error specified in the calculation of $\overline{G}_a(R)$ is 1.0 per cent, but an examination of the convergence of the numerical calculations of $\overline{G}_a(R)$ shows that in all cases the actual error in $\overline{G}_a(R)$ is much less than 1.0 per cent. A more realistic error estimate is about 0.1 per cent or 0.2 per cent.

The value of $\overline{G}_a(R)$ was calculated at points $R = n/6$ cm. where n runs from 0 to 60. The function $R^2 \times \overline{G}_a(R)$ is then stored in tabular form for later use. The spacing of 1/6 cm. between points is used so that a linear interpolation scheme can be used in the table lookup process while restricting the interpolation error to 0.1 per cent. The results of the calculations show that the functions $R^2 \times \overline{G}_a(R)$ for water and graphite are smooth enough so that a larger spacing can be used and still maintain the interpolation error limit at about 0.1 per cent.

It is of interest to note that for R greater than several mean free paths the function $\overline{G}_o(R)$ agrees very well with the conventional diffusion approximation

$$\overline{G}_o(R) \approx \frac{e^{-R/L}}{DR}$$

The term L is the usual diffusion length and D is the diffusion coefficient.

The usual factor of 4π is missing from the denominator due to the fact that the $\bar{G}_o$ (R) has a source of 4π neutrons per second.

It is also observed that the $\bar{G}_a$ (R) curves fall off more rapidly for increasing "a." The terms in the spherical harmonic expansion of $G(\underline{r}', \underline{\Omega}' \rightarrow \underline{r})$ for "a" greater than zero correspond to higher order anisotropy in the source. This more rapid fall off corresponds to the physically observed phenomenon that the non-isotropic components of a point source are less important at a given observation point than the isotropic component.

Two sets of calculations are presented for $R^2 \times \bar{G}_o$ (R) for water. The only difference between the two calculations is the Σ_a used. In one case $\Sigma_a = 0.0196$ cm^{-1} and in the other $\Sigma_a = 0.0184$ cm^{-1}, As expected, increasing the absorption cross-section causes the neutron density to decrease at any given observation point.

Another set of calculations are presented for $R^2 \times \bar{G}_\phi$ (R) for water. In one calculation $\bar{\mu}$ is 0.3, in the other one $\bar{\mu}$ is 0.0. In this case the neutron density near the source is reduced for $\bar{\mu} = 0.3$. This is due to the fact that for $\bar{\mu} = 0.3$ scattered neutrons tend to be scattered forward rather than isotropically, which is the case when $\bar{\mu} = 0$. This preferential scattering allows the neutrons to penetrate greater distances into the medium. Since the source strength is unchanged the number of neutrons absorbed is unchanged:

$$\Sigma_a \int_{\underline{r}} \bar{G}_o \left(|\underline{r} - \underline{r}'|\right)_{\bar{\mu} = 0} d\underline{r} = \Sigma_a \int_{\underline{r}} \bar{G}_o \left(|\underline{r} - \underline{r}'|\right)_{\mu = .3} d\underline{r}$$

Although the $\bar{G}_o\,(R)_{\bar{\mu}=0} > \bar{G}_o\,(R)_{\bar{\mu}=.3}$ for small R the inequality must eventually reverse for some larger R.

The change of the shape of the $R^2 \times \bar{G}_o\,(R)$ curve with change in the value of $\bar{\mu}$ suggests a method for measuring $\bar{\mu}$ directly. Assume that several curves of $R^2\,\bar{G}_o\,(R)$ are available for several values of $\bar{\mu}$. The maximum for each curve will occur at a different point R depending upon the value of $\bar{\mu}$ used.

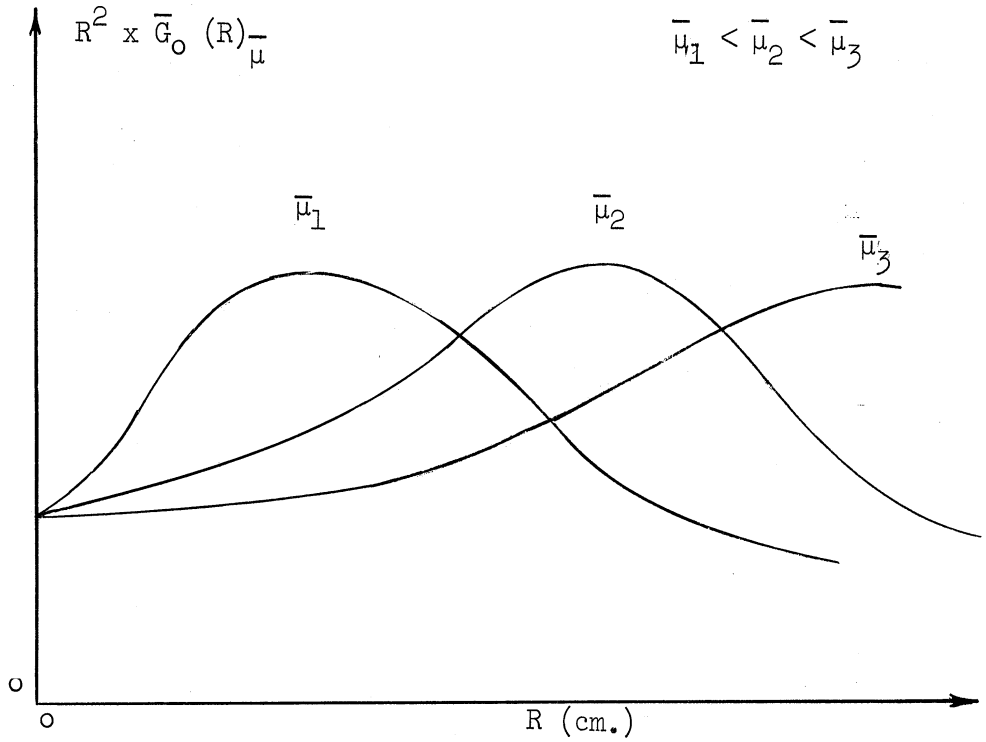

Figure 1. The Function $R^2\,\bar{G}_o\,(R)_{\bar{\mu}}$ for Several Values of $\bar{\mu}$.

Since $\overline{G}_o(R)$ is merely the neutron speed v times the neutron density at a distance R centimeters from an isotropic thermal neutron source emitting 4π neutrons per second, $\overline{G}_o(R)$ can be measured using activation techniques. From this type of measurement a plot of $R^2 G_o(R)$ can be obtained and the position of the maximum determined. The position of the maximum should then determine the proper value of $\overline{\mu}$.

It should be recalled that for the calculations carried out here $G_o(R)_{\overline{\mu}}$ was evaluated assuming that terms in $\overline{\mu}^2$ can be neglected compared to terms in $\overline{\mu}$. For the type of analysis outlined in the previous paragraph the terms in $\overline{\mu}^2$ can not be neglected, and a more careful calculation taking into account higher order terms in $\overline{\mu}$ should be made.

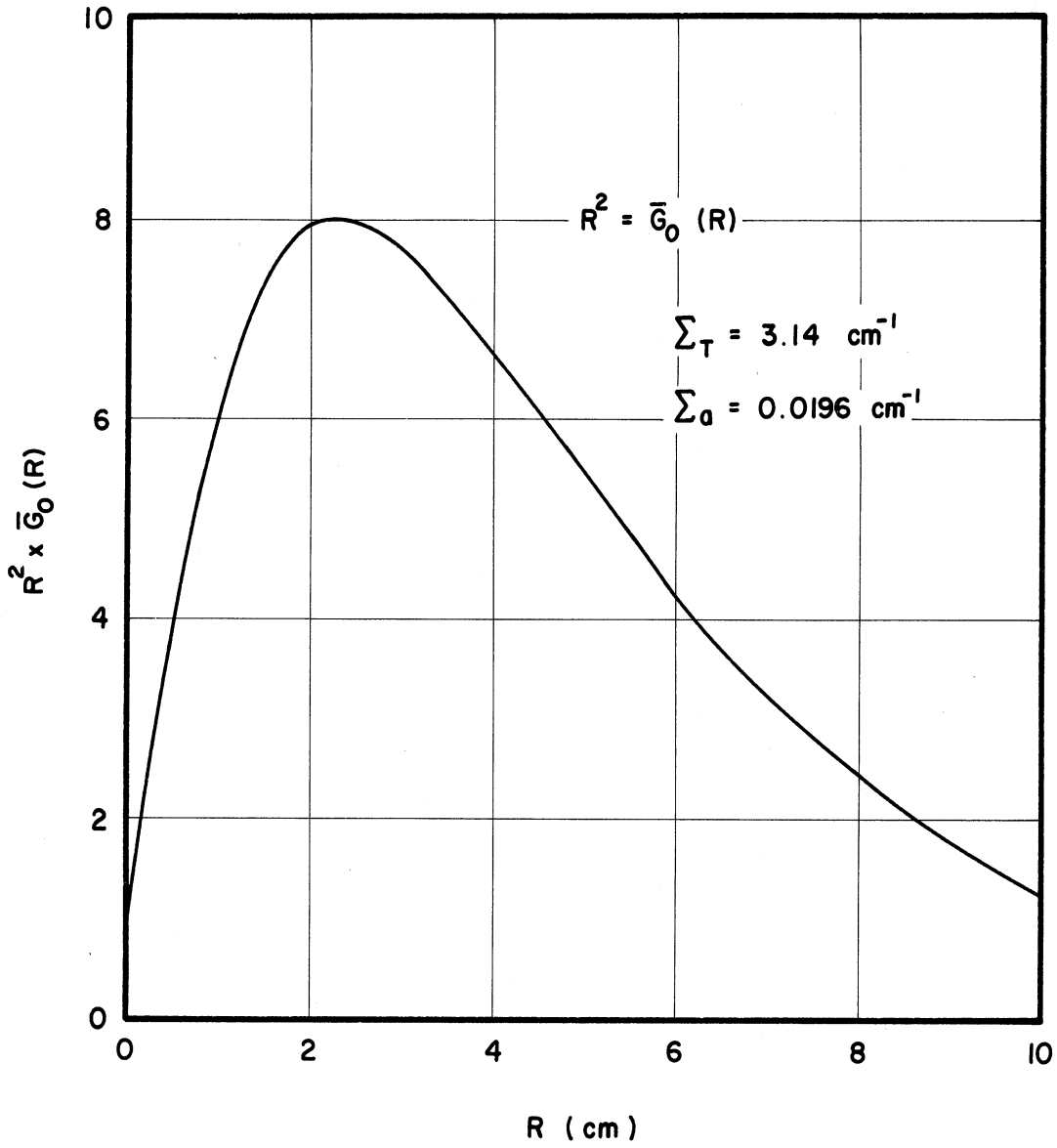

Figure 2. Zeroth Green's Function Coefficient for Water.

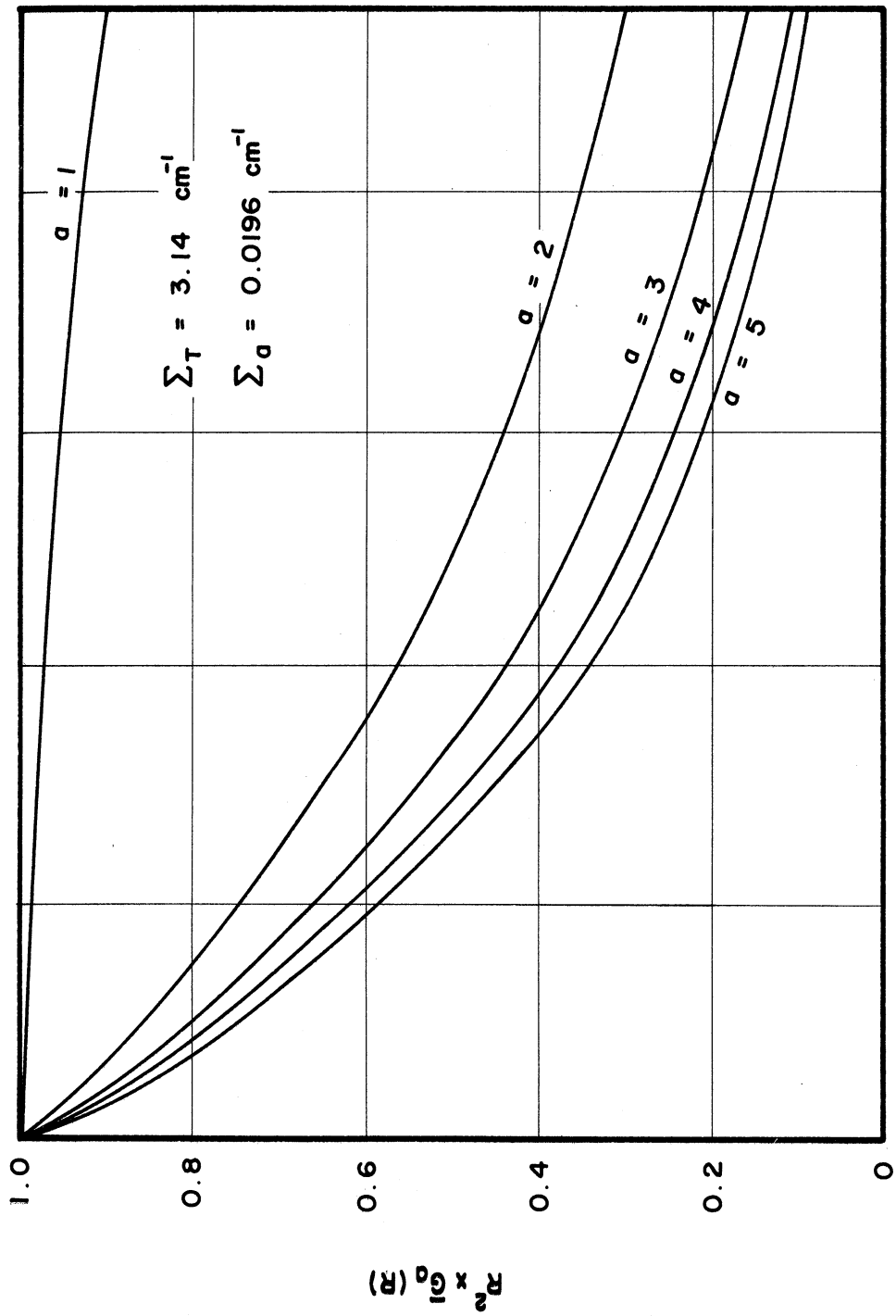

Figure 3. Higher Order Green's Function Coefficients for Water.

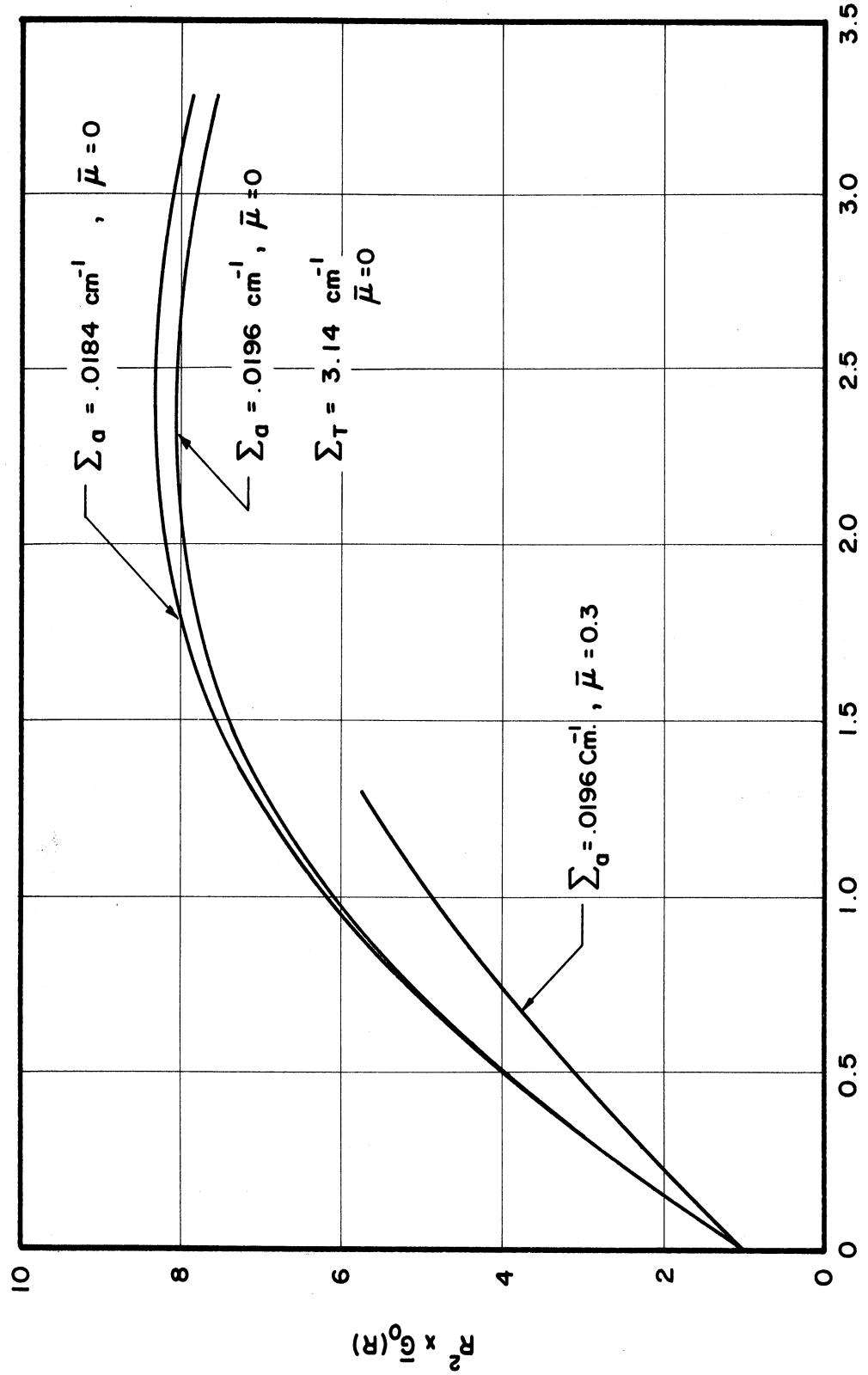

Figure 4. Zeroth Green's Function Coefficient for Water for Two Absorption Cross-Sections.

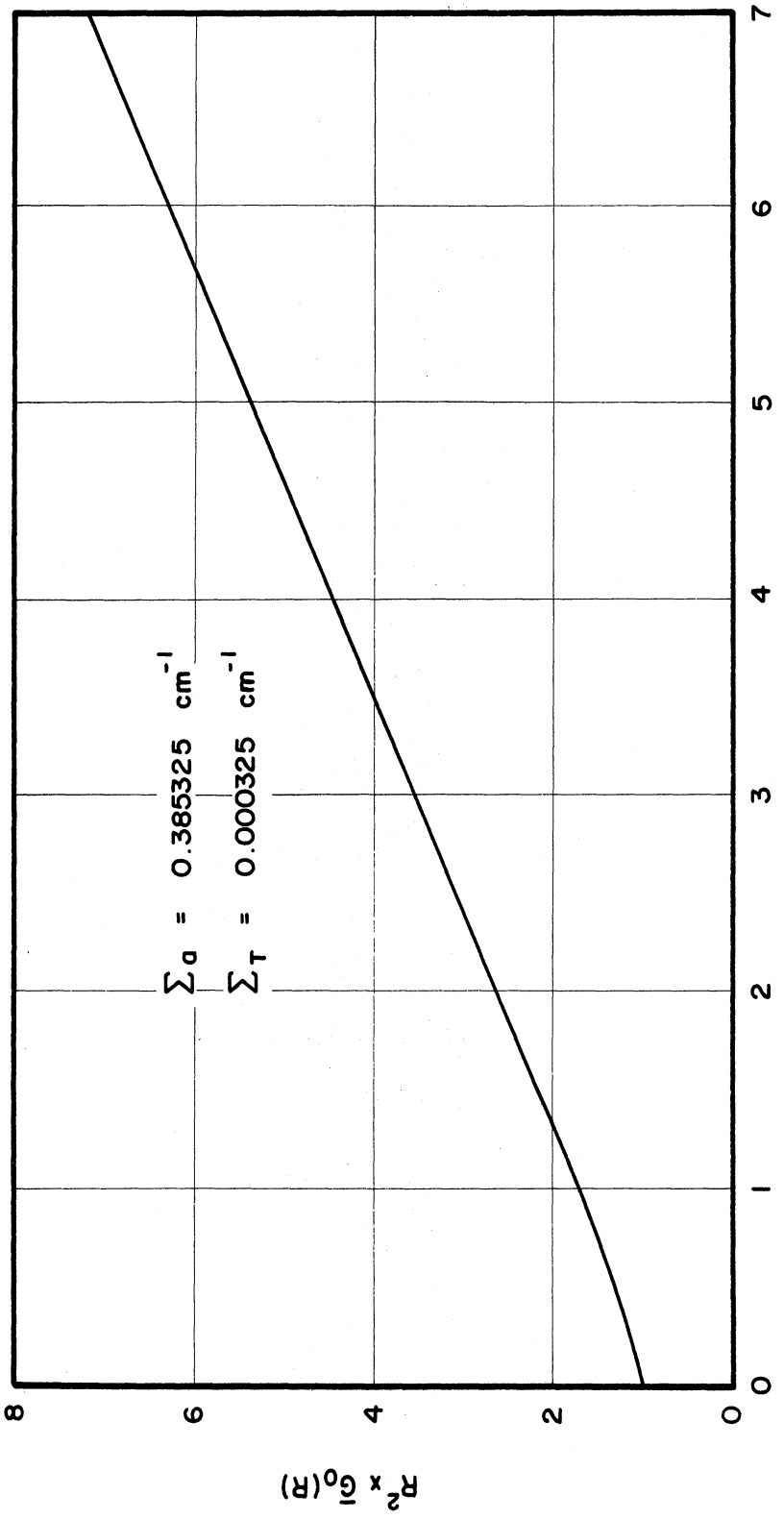

Figure 5. Zeroth Green's Function Coefficient for Graphite.

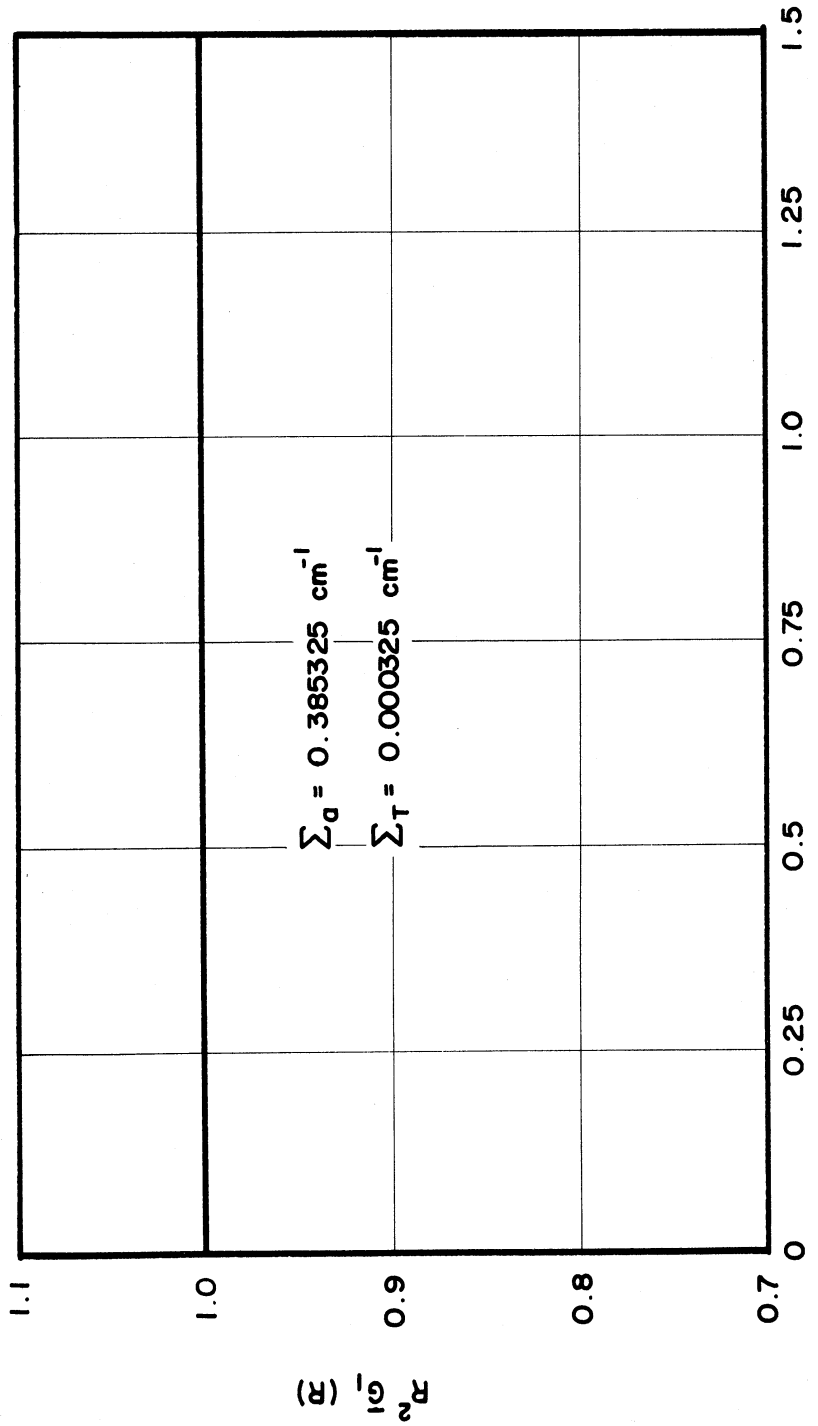

Figure 6. First Order Green's Function Coefficient for Graphite.

CHAPTER V

FLUX CALCULATIONS

In the calculation of the neutron population after the detector is put in place there are several assumptions made which are open to question. First it is assumed that the energy spectrum of the neutron population is independent of position before and after the detector is put in place and that it is the same before and after the detector is put in place. The validity of this assumption has not been investigated in this paper. Second it is assumed that the detector is placed in an infinite homogeneous medium. Third it is assumed that scatter is isotropic in the external medium. Fourth it is assumed that the integrals in Equations (6) and (15) can be replaced with the summations over a finite set of points as given in Appendix V. Fifth it is assumed that two iterations of the integral equation, Equation (6), will be suffcicient for reasonable accuracy. Sixth it is assumed in setting up the computer calculations that the source of thermal neutrons due to slowing-down of neutrons from higher energies within the detector is zero. Finally it is assumed that the source of thermal neutrons outside the detector is isotropic in angular distribution and equal to the capture rate before the detector is in place.

The assumption of an infinite homogeneous medium has the effect of limiting the application of this type of a calculation to detectors placed at least several mean free paths from any boundaries in the system.

Since the moderating material with the largest $\bar{\mu}$ is water it is used as the test case for the assumption of isotropic scattering. The zeroth

coefficient for the Green's function is calculated for $\bar{\mu} = 0$ and for $\bar{\mu} = 0.3$. Both of these Green's functions are then used to calculate the flux within a detector. For the case of a gold foil of 0.5 cm. radius and 0.0127 cm. (5 mil.) thickness the ratio of average flux in the detector to the flux before the detector is in place is 0.813 for $\bar{\mu} = 0$ and 0.840 for $\bar{\mu} = 0.3$. The effect is essentially the same for indium in water. Thus it is seen that the effect of non-isotropic scattering in the moderating material will effect the flux within the detector by 3 per cent in the case considered here.

The next assumption considered is the one that the integrals may be replaced by a summation over a finite set of points. One test of the validity of such an assumption is to repeat the summation, each time including a larger number of points. A given detector was calculated three different times. The only difference between calculations was that the axies were divided into four, five and six subdivisions. The greatest difference between the calculations was the order of 0.1 per cent. This indicates that the summations are essentially independent of subdivision size and that the summations are good approximations to the integrals when there are about five subdivisions along each axis.

It is not necessary to assume that a certain number of iterations of Equation (6) will be necessary for a given accuracy. For the quantities $\int_{\underline{r},\,\underline{\Omega}} \Psi_1(\underline{r},\,\underline{\Omega})\, d\underline{r}d\underline{\Omega}$ and $\int_{\underline{r},\,\underline{\Omega}} \Psi_2(\underline{r},\,\underline{\Omega})\, d\underline{r}d\underline{\Omega}$ are both available as the result of the numerical calculations. An estimate of the quantity K,

which is the maximum difference between $\Psi_{n+1}(\underline{r}, \underline{\Omega})$ and $\Psi_n(\underline{r}, \underline{\Omega})$ relative to the maximum difference for the previous iteration, is also available. From these quantities it will be possible to recognize that range of small detector dimensions, thickness for coins and radius for wires, where $\psi(\underline{r}, \underline{\Omega})$ will be sufficiently accurate. It will also be possible to recognize that range of larger dimensions where the second iteration will be sufficiently accurate.

In the case of the 0.5 cm. radius gold coin in water it is seen that the difference between $\int_{\underline{r}, \underline{\Omega}} \Psi_1(\underline{r}, \underline{\Omega})\, d\underline{r}d\underline{\Omega}$ and $\int_{\underline{r}, \underline{\Omega}} \Psi_2(\underline{r}, \underline{\Omega})\, d\underline{r}d\underline{\Omega}$ is 1.5 per cent for a 5 mil thickness and 10 per cent for a 10 mil thickness. It is further seen that the third iteration would differ from the second iteration by about 0.15 per cent and 0.2 per cent for the 5 mil and the 10 mil thick coins respectively. In the case of the 0.5 cm. radius gold coin in graphite it is seen that the second iteration differs from the first by 1 per cent and 12 per cent for the 7 mil and the 15 mil thickness respectively and that the third iteration would differ from the second by 0.1 per cent and 1.2 per cent for the 7 mil and 15 mil thickness respectively.

Inspection of Equation (13) shows that $\psi(\underline{r})$ is independent of the scattering cross section of the detector, but $\Psi_2(\underline{r}, \underline{\Omega})$ is dependent on it. Results of the calculation $\int_{\underline{r}, \underline{\Omega}} \Psi_2(\underline{r}, \underline{\Omega})\, d\underline{r}d\underline{\Omega}$ shows that for 0.5 cm. radius and 5 mil thick gold coin variation of the scattering cross-section from zero to 0.549 cm^{-1} changes the value of the flux in the detector by less than 0.1 per cent for both water and graphite.

TABLE I

THE EFFECT OF HIGHER ORDER CORRECTIONS ON THE AVERAGE SCALAR FLUX WITHIN THE DETECTOR

		Change Due To		
	$\frac{\varphi - \overline{\psi(\underline{r})}}{\varphi}$	$\bar{\mu} = 0.3$	Ψ_2	Ψ_3
Gold Coin in Water t = 5 mils, R = 0.5 cm.	.813	+.027	-.013	$\pm$.001
t = 10 mils, R = 0.5 cm.	.707		-.026	$\pm$.003
Gold Coin in Graphite t = 7 mils, R = 0.5 cm.	.827	*	-.024	$\pm$.002
t = 15 mils, R = 0.5 cm.	.730	*	-.118	$\pm$.011

L = 1.27 cm.
R = 20 mils

* The quantity π is assumed to be effectively zero for graphite.

As discussed in Chapter III the case of a non-uniform non-isotropic initial flux can be calculated. But due to the assumption of axial symmetry and symmetry across the midplane which were necessary only due to the computer time and space limitations the gradient problem was not carried to a numerical calculation.

The assumption of a zero source due to slowing-down of neutrons within the detector is not necessary due to the theory, merely convenient. It has the effect of limiting the application of the calculations to detectors which have high enough atomic weight so that the detector thermalizes very few neutrons. As the numerical problem now stands one could not calculate a detector made up of a solution of gold salt in plastic for example. But there is no reason in principle why the calculation could not be modified to take a non-zero source within the detector into account.

The assumption of a source of neutrons in the external medium which is isotropic and equal to the capture rate before the detector is introduced is again not necessary. The theory will permit the use of a completely arbitrary source. For the cases considered here, where the initial flux has a constant gradient in space, there is no net flow into any unit volume in the space. Thus the supply must equal the rate of loss, i.e. the absorption rate. In the absence of any reliable information about the anisotropy of neutrons as they slow down, the source in the external medium due to the slowing-down of neutrons is assumed isotropic.

CHAPTER VI

COMPARISON WITH OTHER THEORIES

It seems generally agreed that for finite foil detectors Skyrme's method [11] is the most adequate method available for calculating the average flux in the detector. It is of interest to see how the results of the integral technique developed in Chapter I compare with the results of Skyrme's method.

Let the quantity $\int_{\underline{\Omega}} \Phi' (\underline{r}, \underline{\Omega})\, d\underline{\Omega}$ be called the scalar flux.

A comparison of final results shows that for gold and indium in water the integral method consistantly gives average scalar fluxes in the detector which are higher than those calculated by Skyrme's method. The comparison of the integral method with Skyrme's method is presented graphically for gold in water only, the comparison for indium in water shows the same trends. For the case of gold and indium foil detectors in graphite the integral method is seen to agree within 1 per cent with Skyrme's method.

It would be desirable to show how the integral method reduces to the method used by Skyrme. But Skyrme superimposes two independent calculations, one for "self-shielding" within the detector and the other for "flux-depression" in the surrounding medium. This approach of separating the problem is basically inconsistant with the unified approach of the integral method. Skyrme also makes several other approximations which could not be included in the integral method.

An attempt was made to estimate the effect of these approximations upon the calculations, but no method of accounting for Skyrme's approximations

was found which could consistantly account for the differences between the integral method and Skyrme's method.

There is one other method of calculating foils with which comparison might be made. The method is the P_L Legendre polynomial method for infinite slab geometries. This method is discussed at some length by Bengston[1] and numerical solutions were carried out by him and are quoted in the report.

There is a basic difficulty with using the integral method discussed here to calculate infinite foils or foils with very large radii. The radius must be divided into a finite number of intervals. As larger and larger radii are considered the number of radial divisions must be increased to maintain accuracy. But the time required to carry out the computation on the computer goes as the third power of the number of radial divisions. Due to the limited amount of computer time available it does not seen desirable to push the calculations along this line.

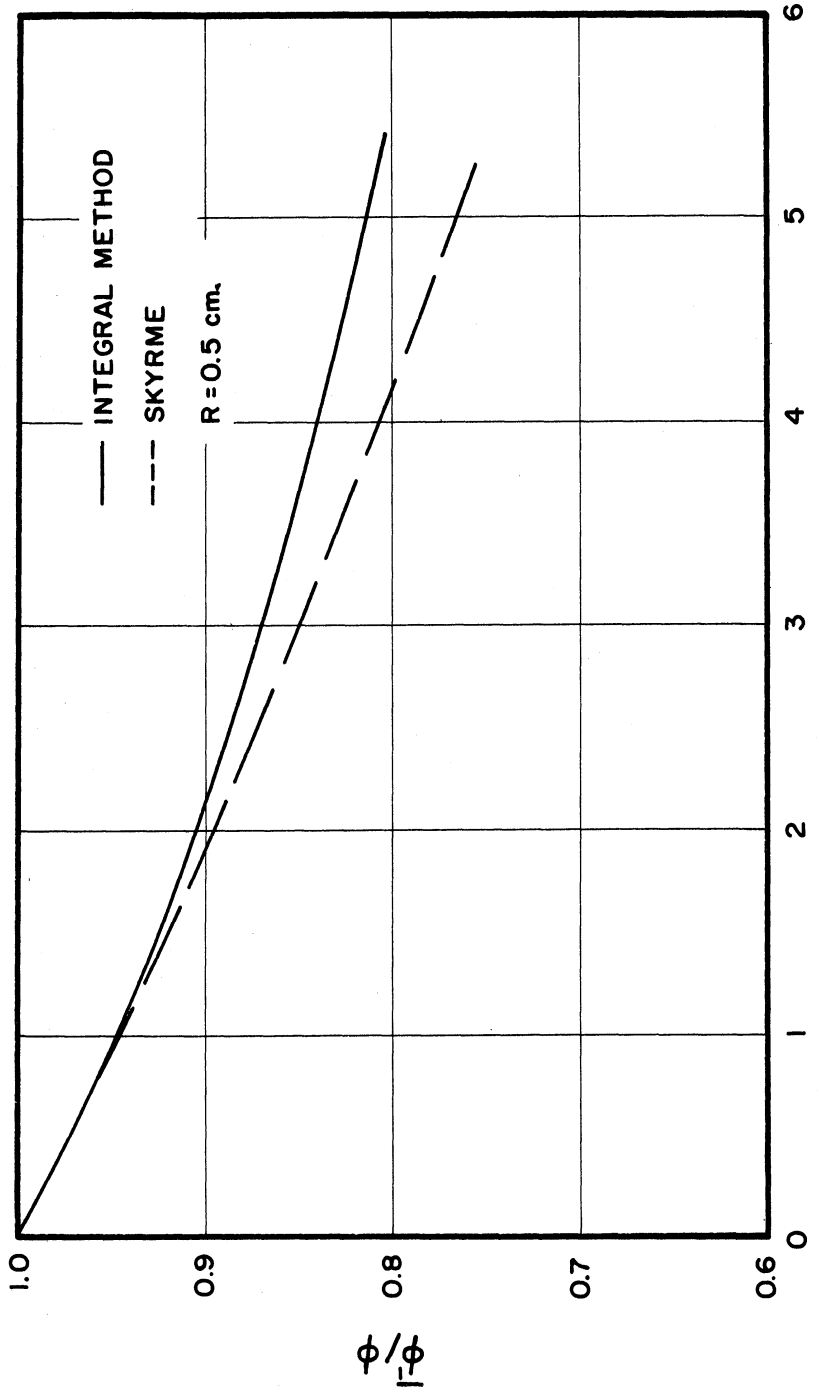

Figure 7. A Comparison of The Average Normalized Scalar Flux In A Coin Shaped Gold Detector of 0.5 cm. Radius In Water As Calculated By The Integral Method and Skyrme's.

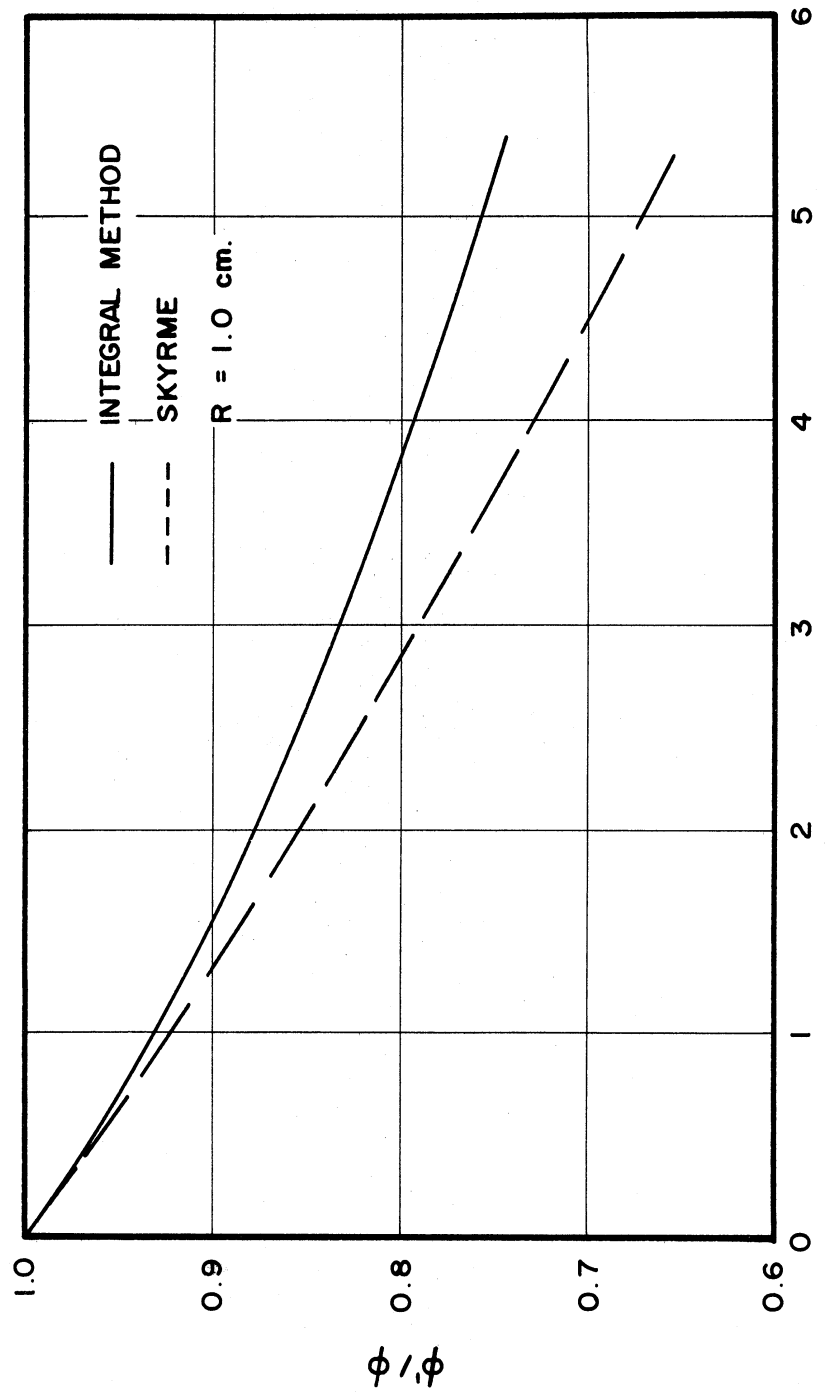

Figure 8. A Comparison of The Average Normalized Scalar Flux In A Coin Shaped Gold Detector of 1.0 cm. Radius In Water As Calculated By The Integral Method and Skyrme's Method.

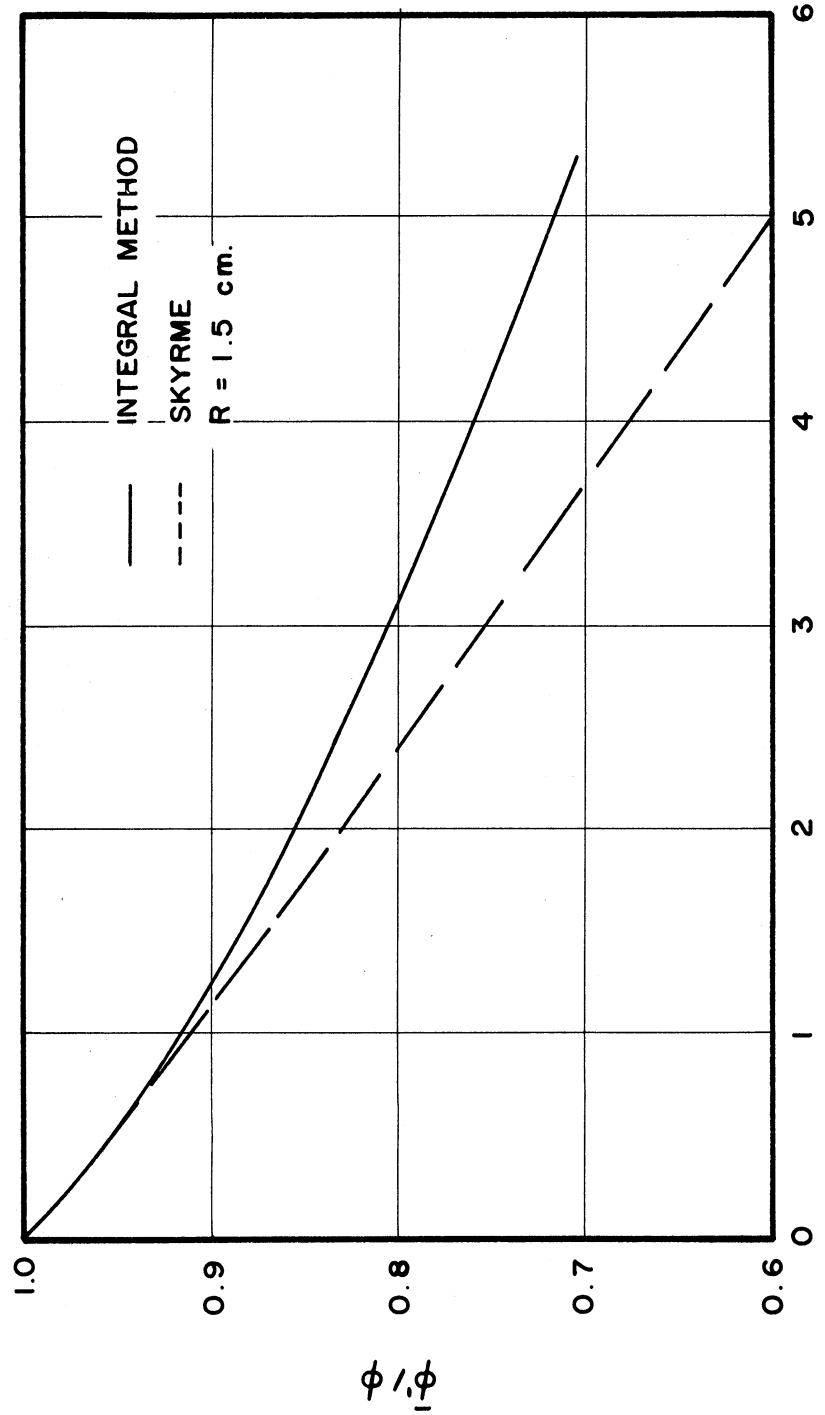

Figure 9. A Comparison of The Average Normalized Scalar Flux In A Coin Shaped Gold Detector of 1.5 cm. Radius In Water As Calculated By The Integral Method and Skyrme's Method.

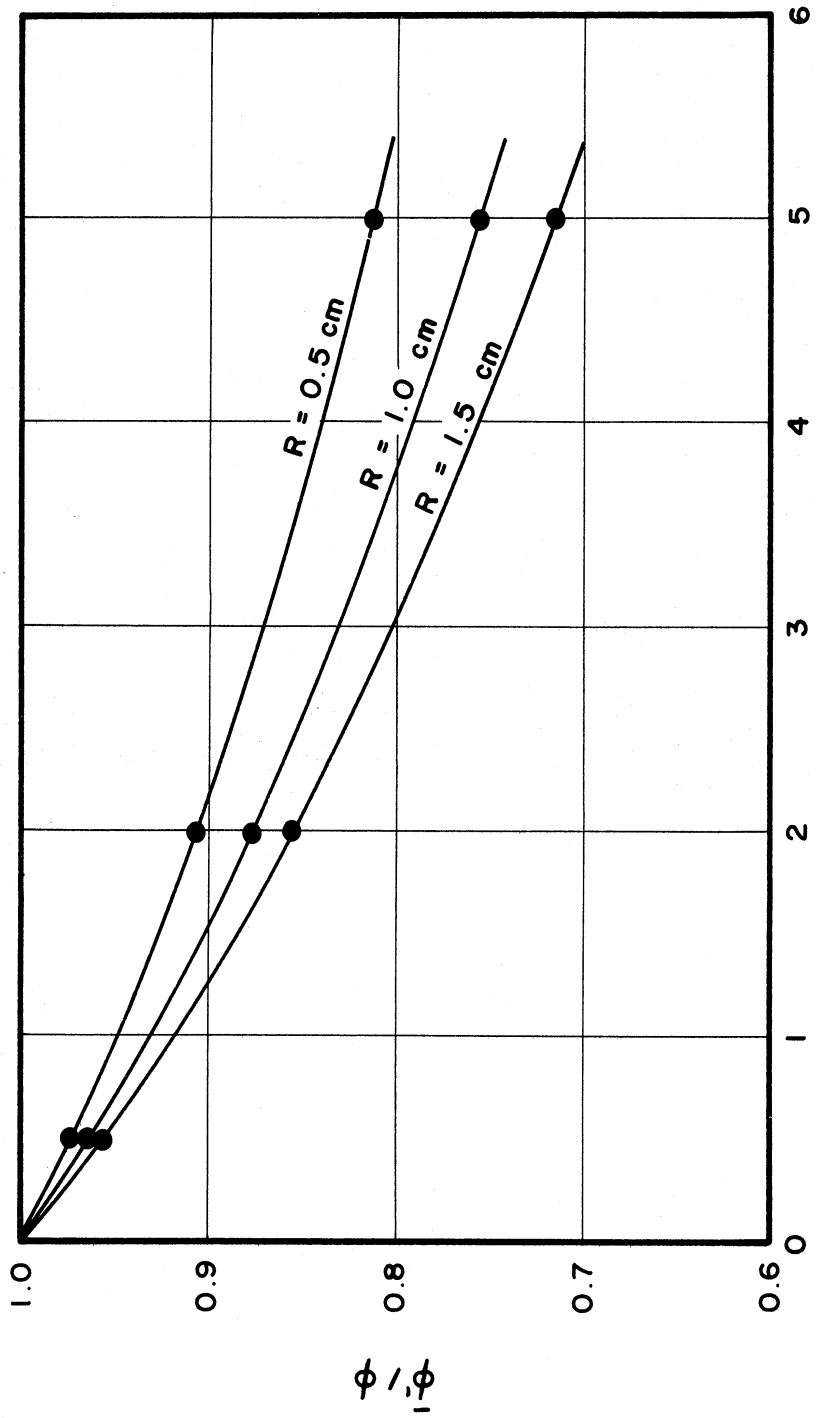

Figure 10. The Average Normalized Scalar Flux In A Coin Shaped Gold Detector In Water As Calculated By The Integral Method.

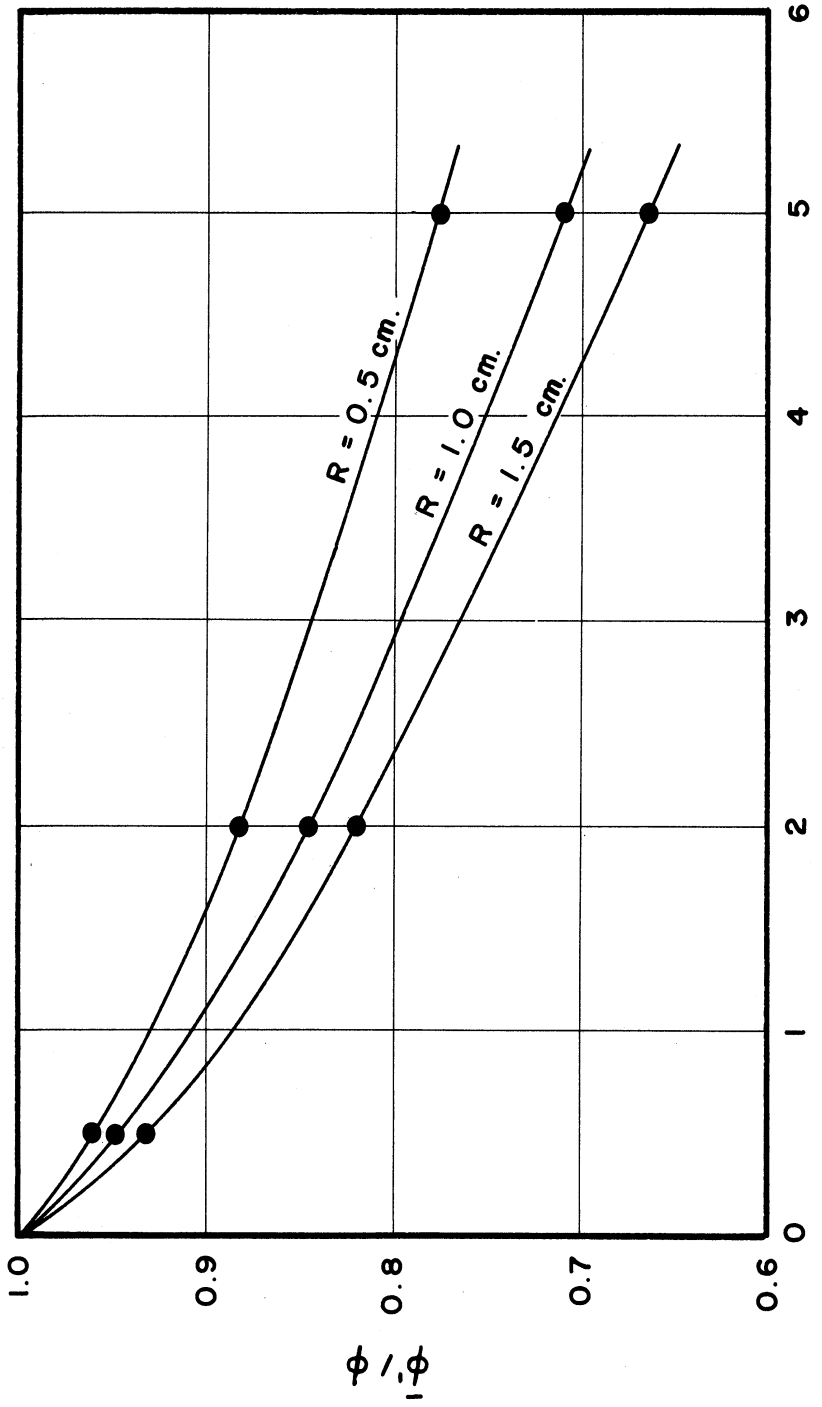

Figure 11. The Average Normalized Scalar Flux In A Coin Shaped Indium Detector In Water As Calculated By The Integral Method.

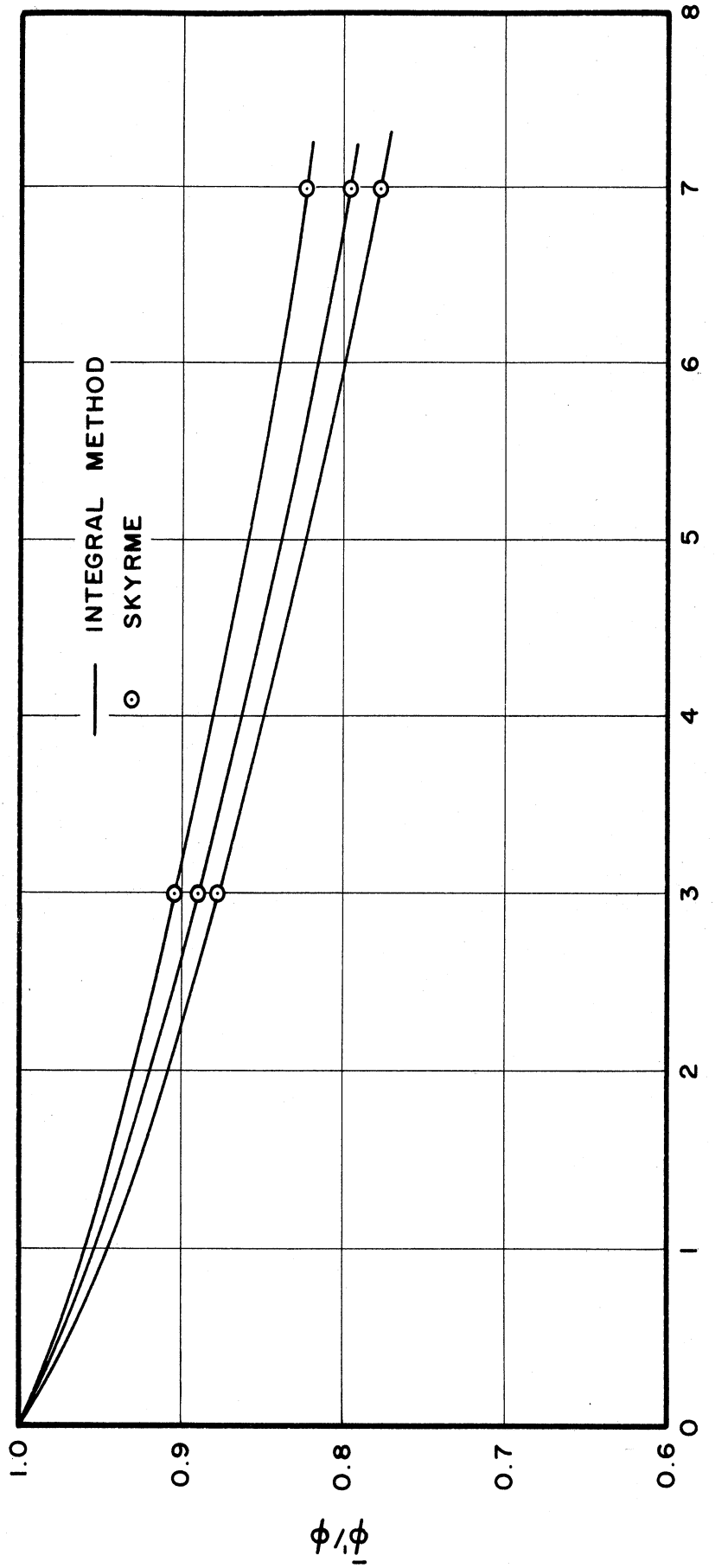

Figure 12. A Comparison of The Average Normalized Scalar Flux In A Coin Shaped Gold Detector In Graphite As Calculated By the Integral Method and By Skyrme's Method.

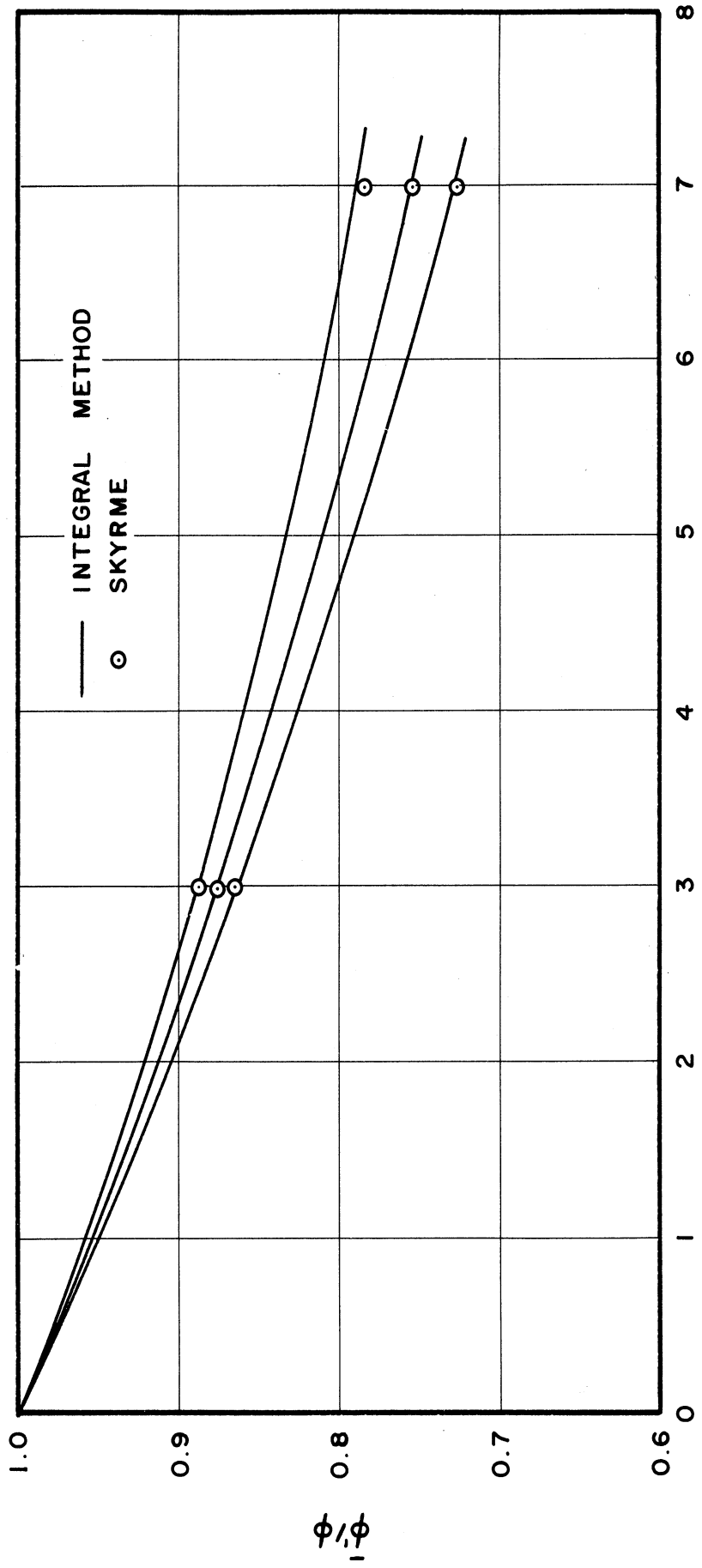

Figure 13. A Comparison of The Average Normalized Scalar Flux In a Coin Shaped Indium Detector In Graphite As Calculated By the Integral Method and By Skyrme's Method.

CHAPTER VII

COMPARISON WITH EXPERIMENTS

In Figures 14 through 21 a comparison of the results of the calculations using the integral method with various experiments is presented. It should be noted that the error bounds indicated on the experimental points vary considerably in meaning from one set of results to another. At one extreme Zobel [13] attempts to estimate the total uncertainty from all causes in his measurements and he quotes a very large range of uncertainty. At the other extreme is the work of Fitch and Drummond [4] where no indication is given of the possible errors. In between the two extremes is the work of Klema and Ritchie [8] who specifically state that their error estimates reflect only the uncertainty of the counting process and nothing else.

An examination of the comparison for indium and gold detectors in graphite shows that most of the experimental results fall slightly above the theoretical curve. But the most complete and well documented work, that of Thompson,[12] consistantly falls below the theoretical curve. Even with the somewhat uncertain error bounds available a minor renormalization of the experimental results within these bounds produces in almost every case an excellent fit with the theoretical curves.

For the case of gold and indium in water the meager amount of experimental data shows a qualitative agreement with the theoretical calculations. The largeness, or complete lack, of error estimates will not permit any qualitative comments about the agreement with the theory.

Similarly for the case of indium wires in water the lack of error

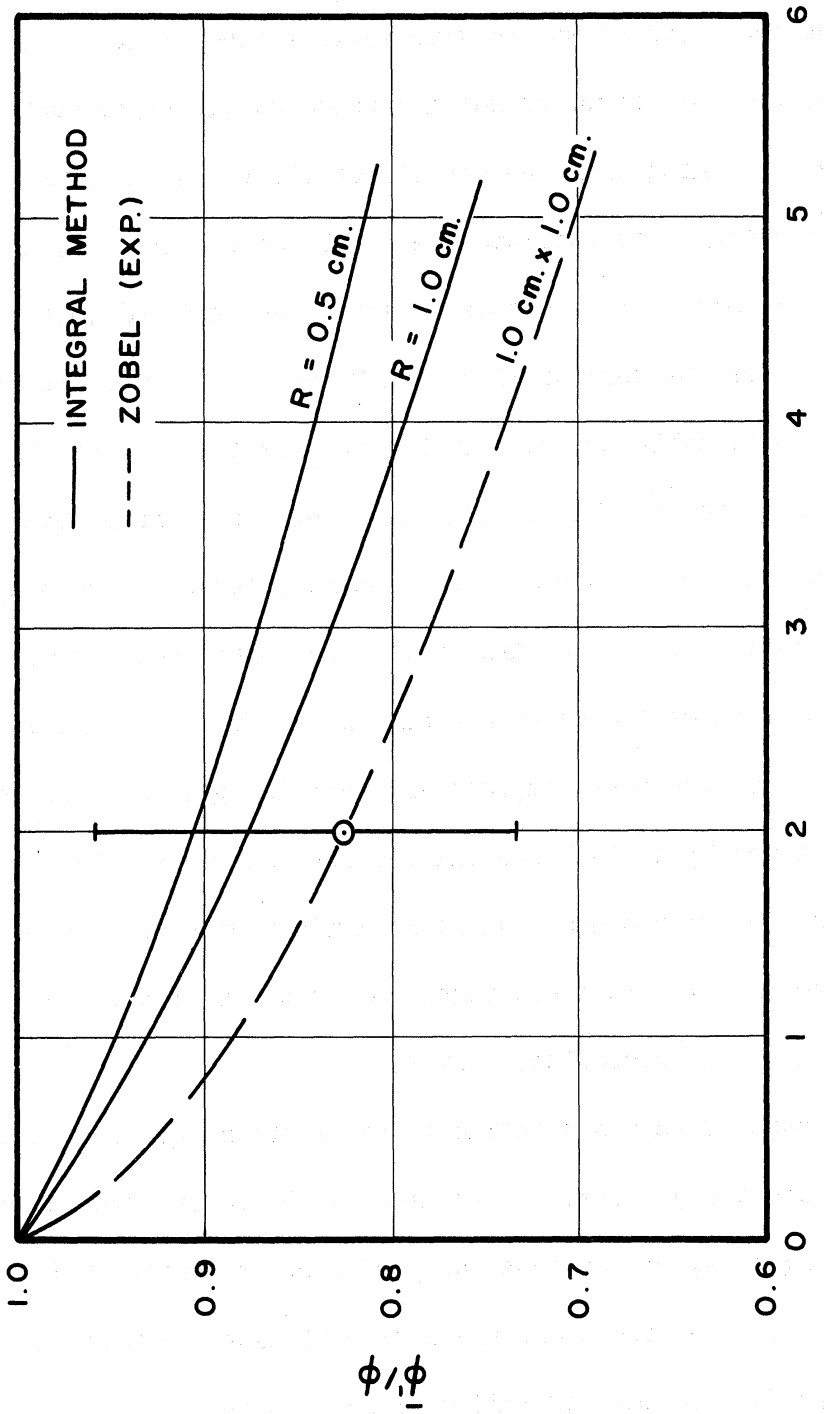

Figure 14. A Comparison of The Average Normalized Scalar Flux In A Coin Shaped Gold Detector In Water As Calculated By the Integral Method and As Measured By Zobel.

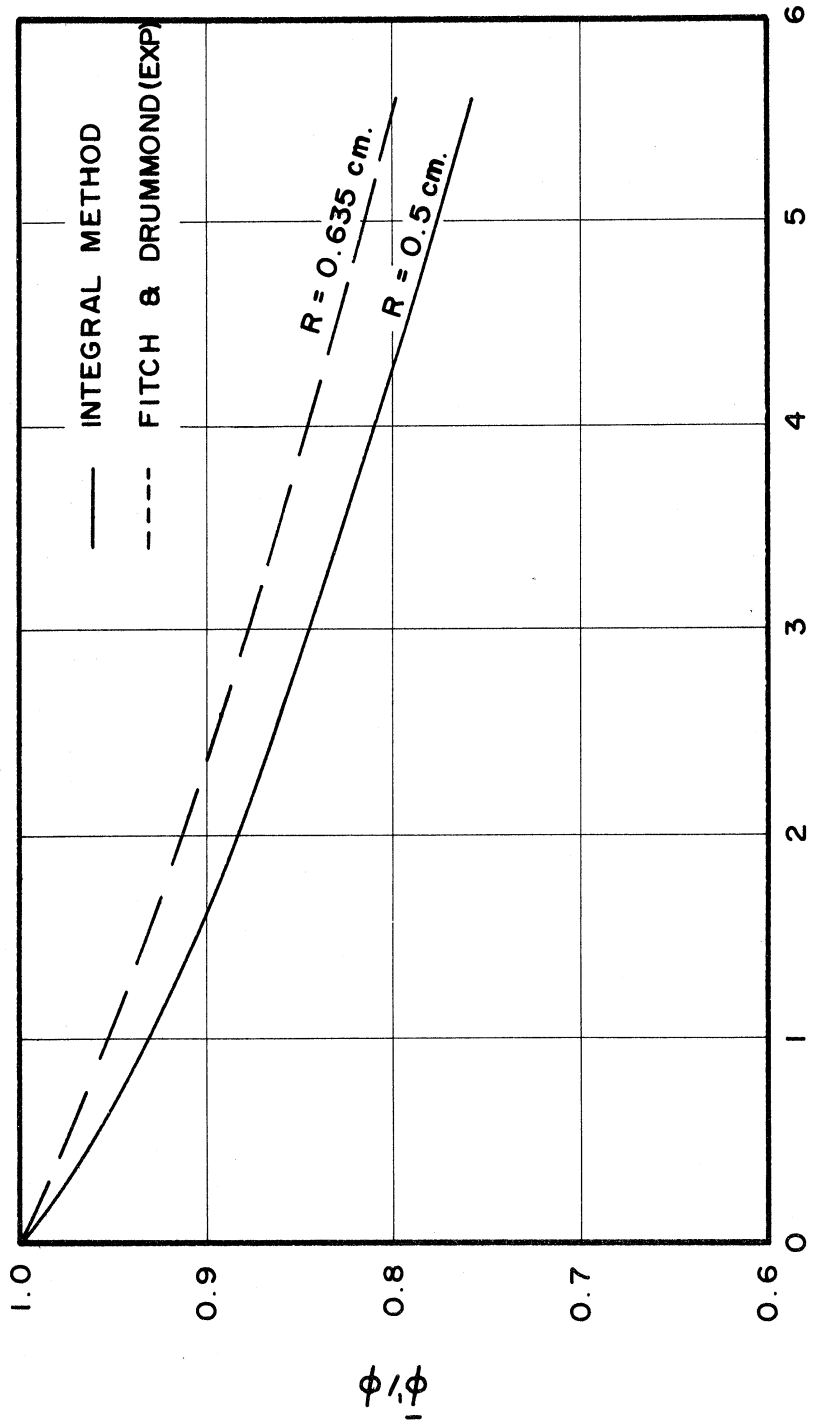

Figure 15. A Comparison of The Average Normalized Scalar Flux In A Coin Shaped Indium Detector In Water As Calculated By the Integral Method and As Measured By Fitch and Drummond.

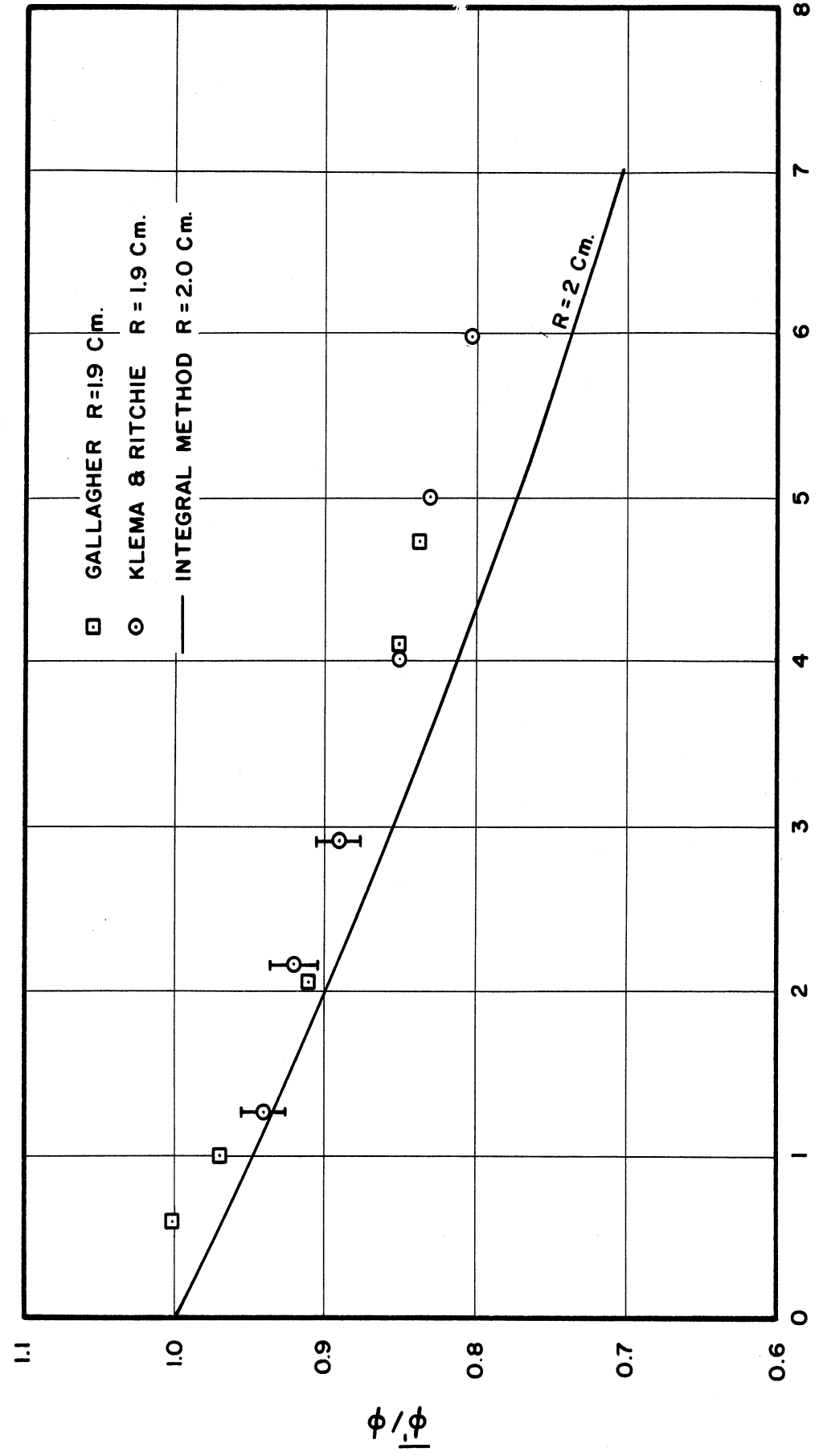

Figure 16. A Comparison of The Average Normalized Scalar Flux In A Coin Shaped Indium Detector In Graphite As Calculated By the Integral Method and As Measured By Ritchie and Klema and By Gallagher.

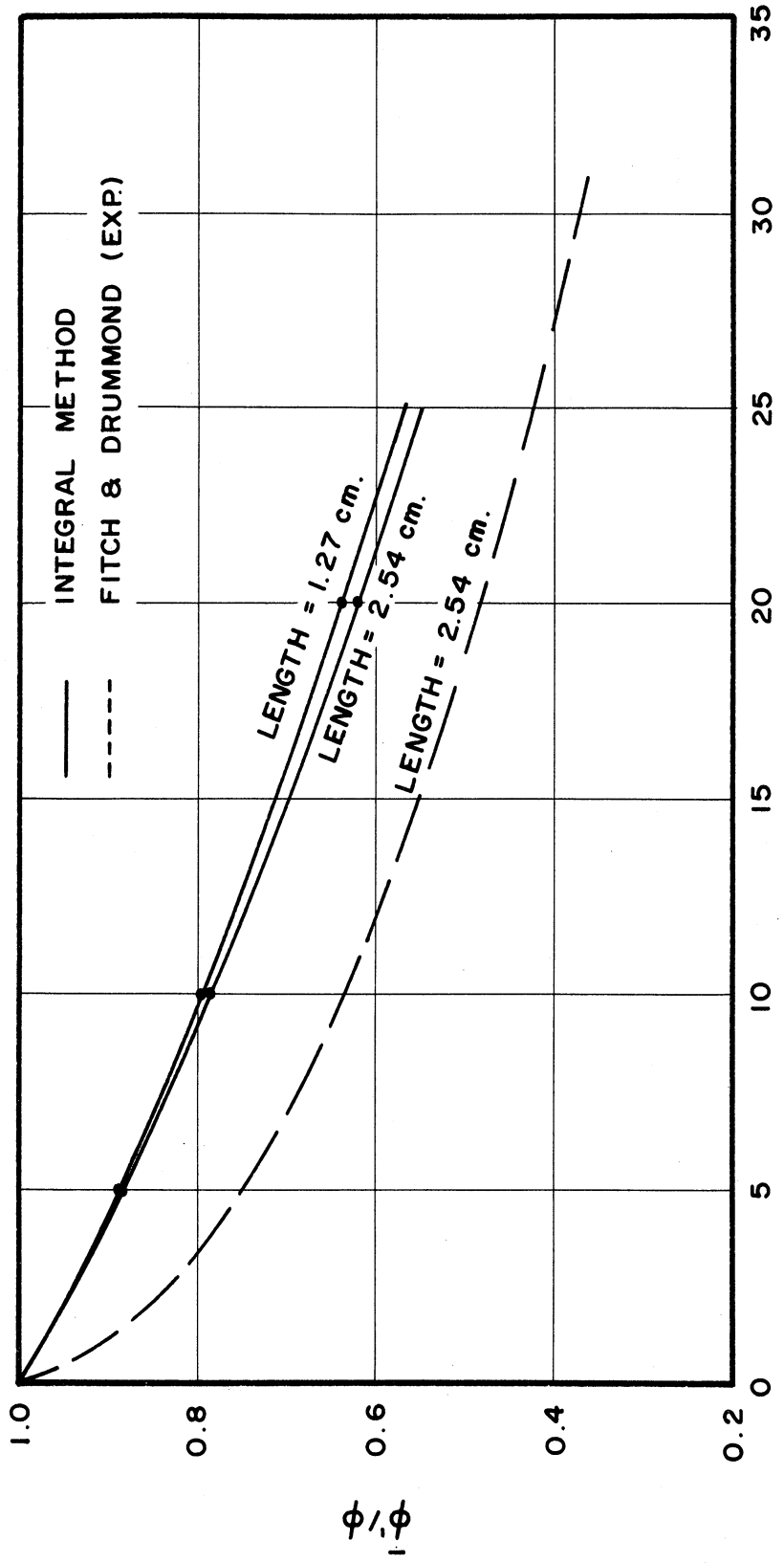

Figure 17. A Comparison of The Average Normalized Scalar Flux In A Wire Shaped Indium Detector In Water As Calculated By The Integral Method And As Measured By Fitch and Drumm

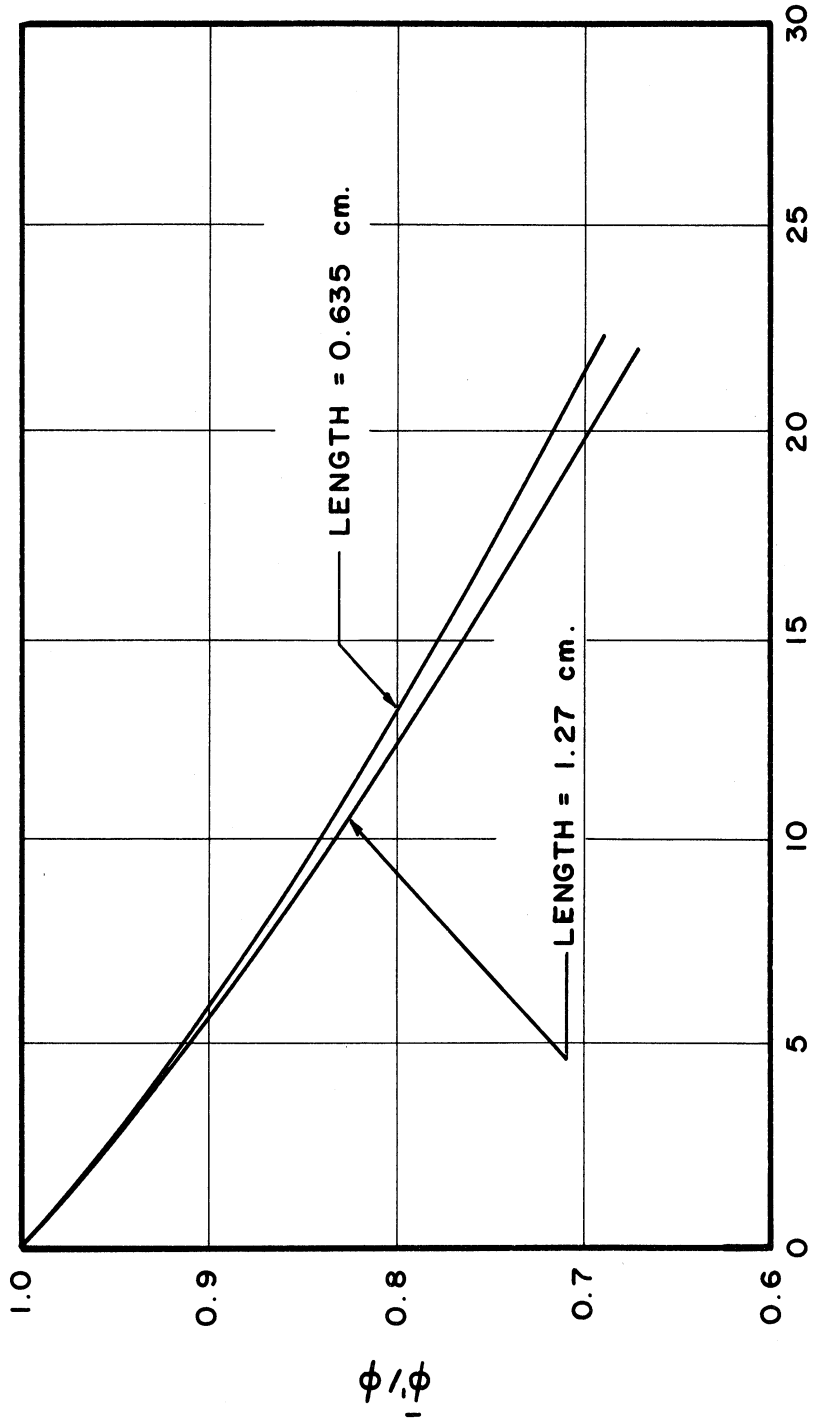

Figure 18. A Comparison of The Average Normalized Scalar Flux In A Wire Shaped Gold Detector In Water As Calculated By the Integral Method and As Measured By Fitch and Drummond.

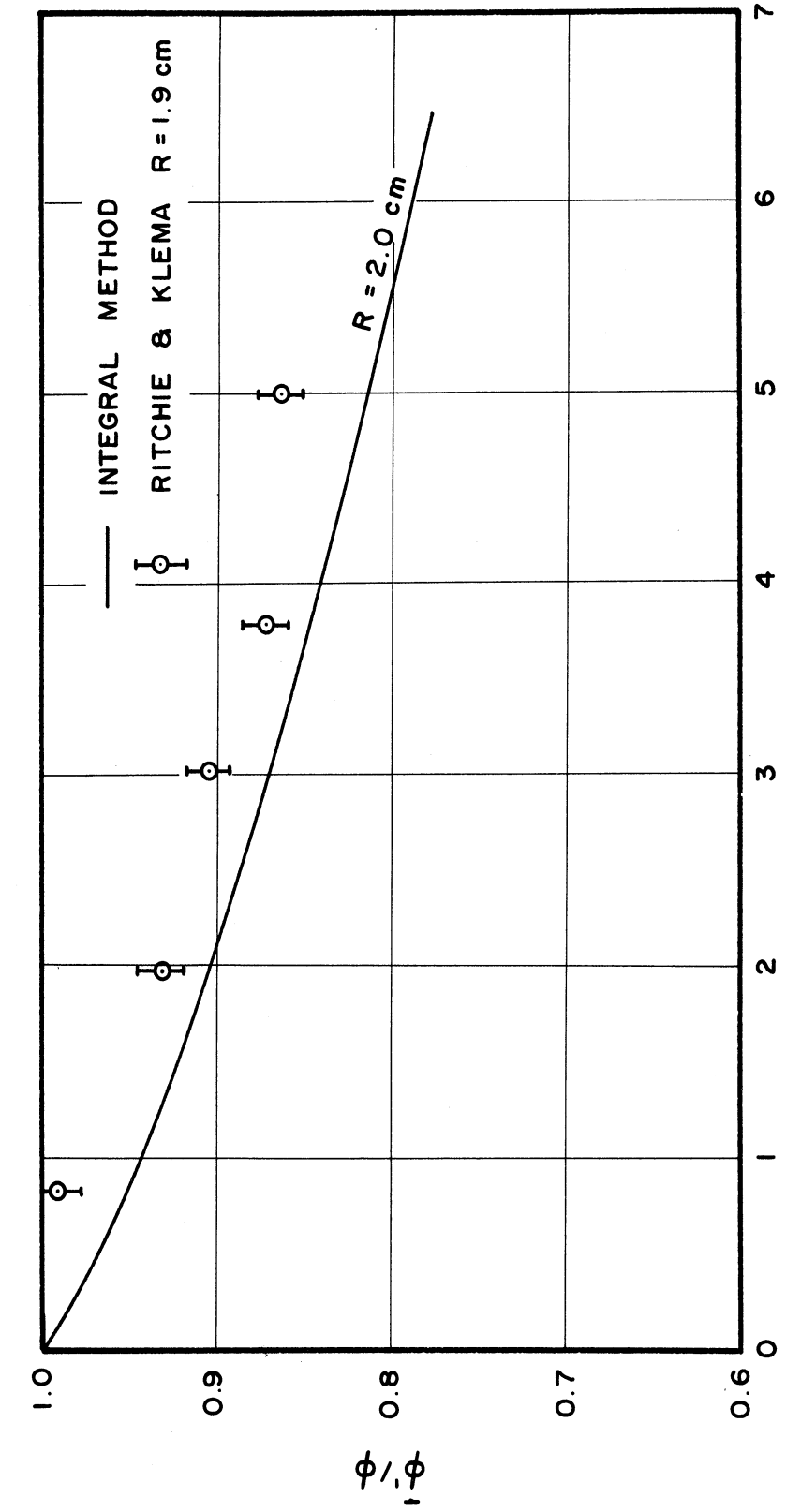

Figure 19. A Comparison of The Average Normalized Scalar Flux In A Coin Shaped Gold Detector In Graphite As Calculated By the Integral Method and As Measured By Ritchie and Klema.

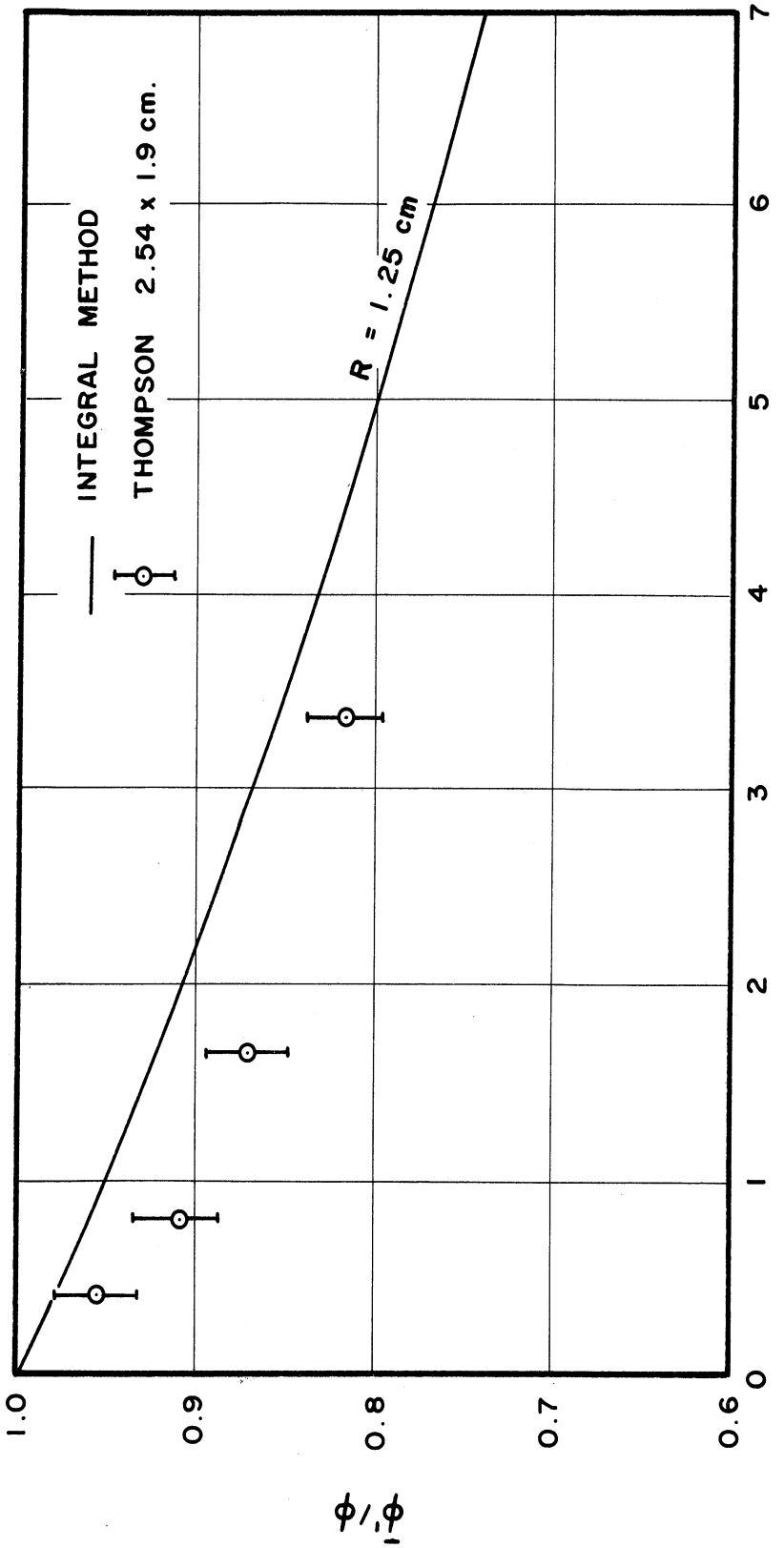

Figure 20. A Comparison of The Average Normalized Scalar Flux In A Coin Shaped Indium Detector In Graphite As Calculated By the Integral Method and As Measured By Thompson.

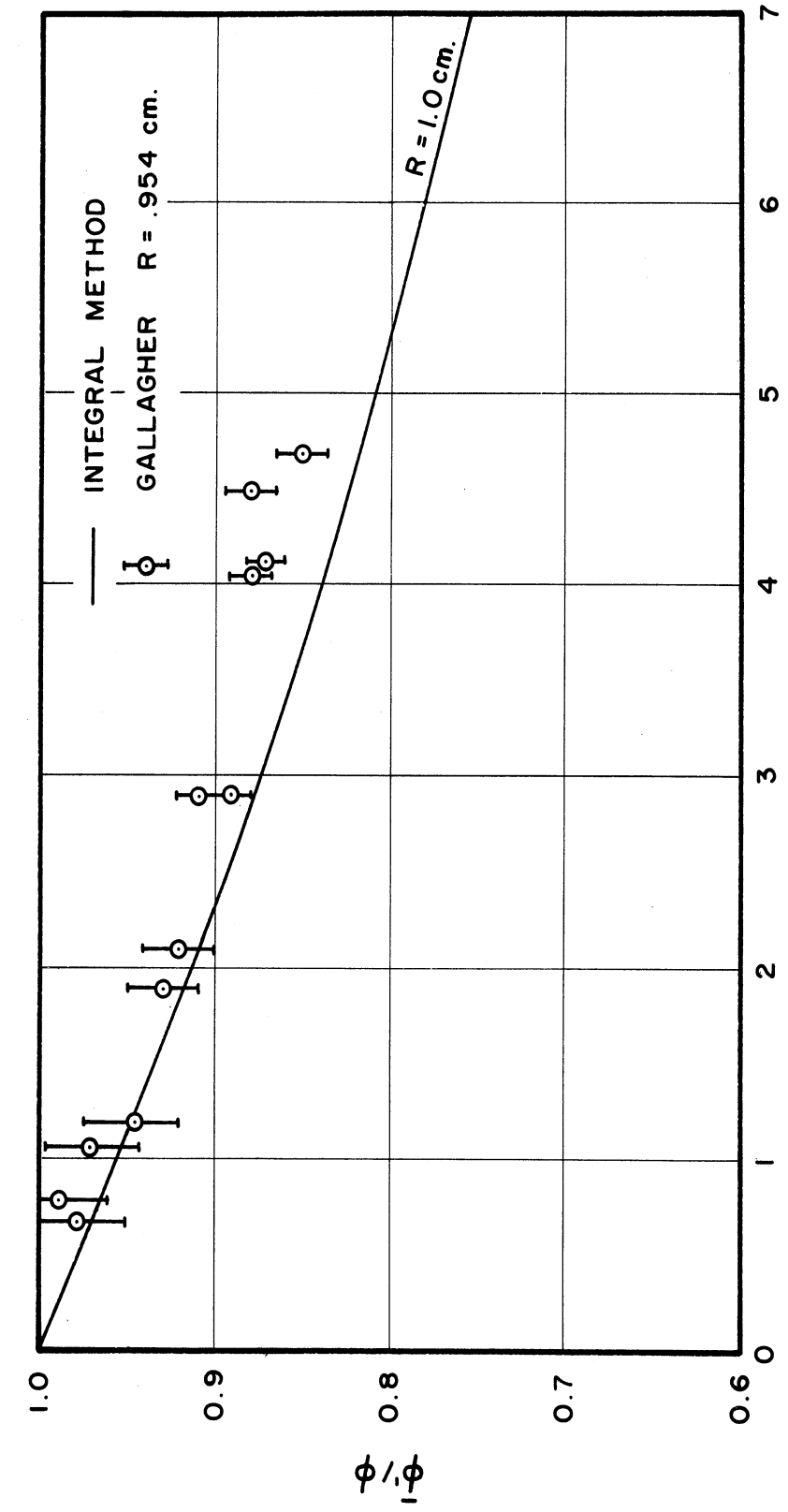

Figure 21. A Comparison of The Average Normalized Scalar Flux In A Coin Shaped Indium Detector In Graphite As Calculated By the Integral Method and As Measured By Gallagher.

estimates will allow no more than the comment that the qualitative agreement is good.

Maps of the scalar flux are presented for the 5 mil thick gold coin shaped detectors in water and in graphite. The maps for the coins of 0.5 and 2.0 mil thickness are not presented due to their great similarity to the plots for the 5 mil coins. The only essential difference between the 5 mil coins and the thinner ones is in the average value of the scalar flux within the coins and in the quantity the average scalar flux less the minimum scalar flux. Both of these quantities are presented for all coins. Similarly the maps of the indium coins are not presented due to their great similarity to the maps for the gold coins.

Graphs of the normalized scalar flux for points along the central Z axis outside the detector are presented for the 5 mil thick gold detectors in water and in graphite. Graphs of the normalized scalar flux for points along a radius in the mid-plane outside the detector are presented for the 0.5 inch long indium wire in water, and for the 0.5 inch long gold wire in water.

A question which is frequently discussed in the literature is the relation of the scalar flux at the surface of a detector to the average scalar flux in the detector. When examined in detail it is found that the scalar flux on the surface of the detector is not a single number but is a strong function of the position on the surface. In fact, the scalar flux on the surface varies from several per cent below the average scalar neutron flux to several per cent above. Since there is no obvious method for defining a "surface flux" no attempt is made to present the relation of surface to average scalar flux.

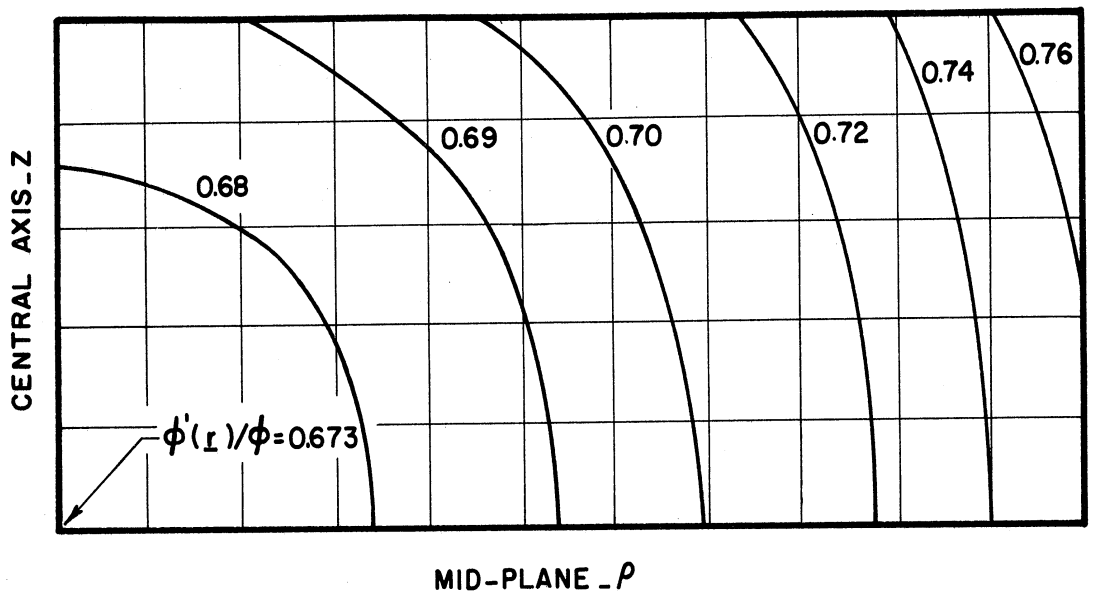

Figure 22. A Map of The Normalized Scalar Flux Within A Coin Shaped Gold Detector In Water, Radius of 1.5 cm. and Thickness of 5 mils.

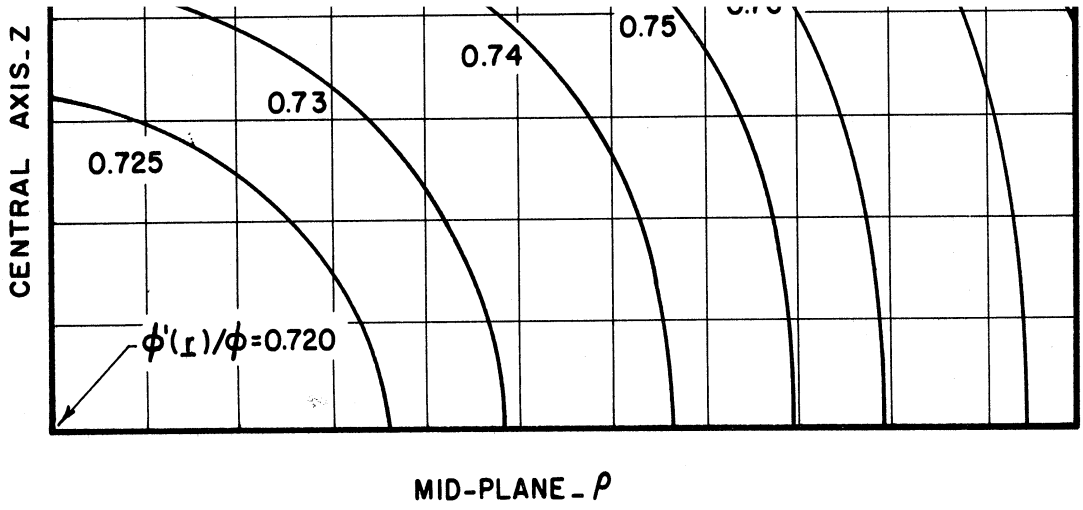

Figure 23. A Map of The Normalized Scalar Flux Within A Coin Shaped Gold Detector In Water, Radius of 1.0 cm. and Thickness of 5 mils.

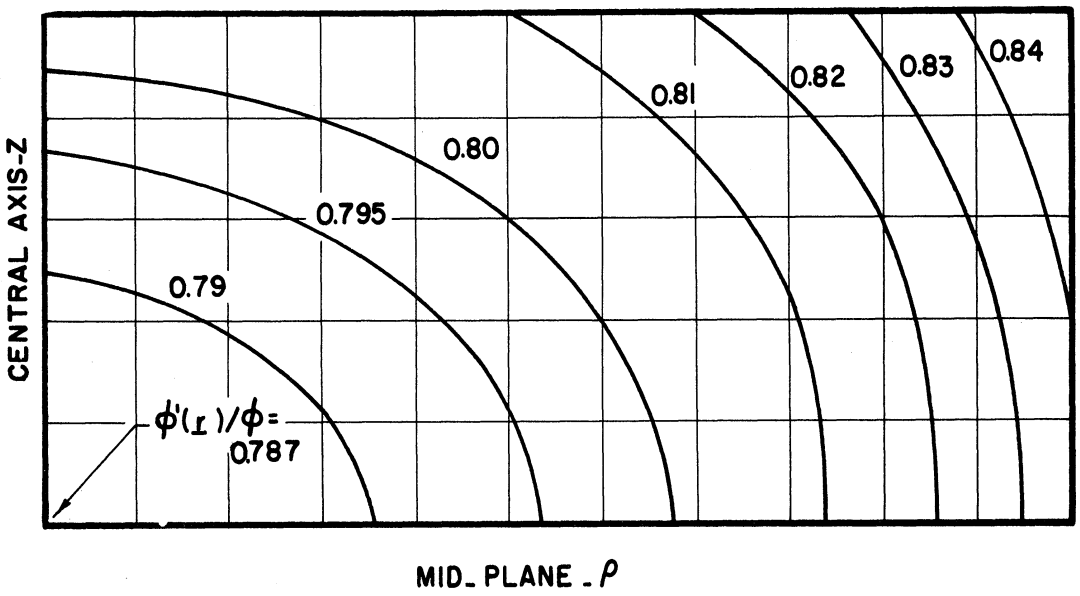

Figure 24. A Map of The Normalized Scalar Flux Within A Coin Shaped Gold Detector In Water, Radius 0.5 cm. and Thickness of 5 mils.

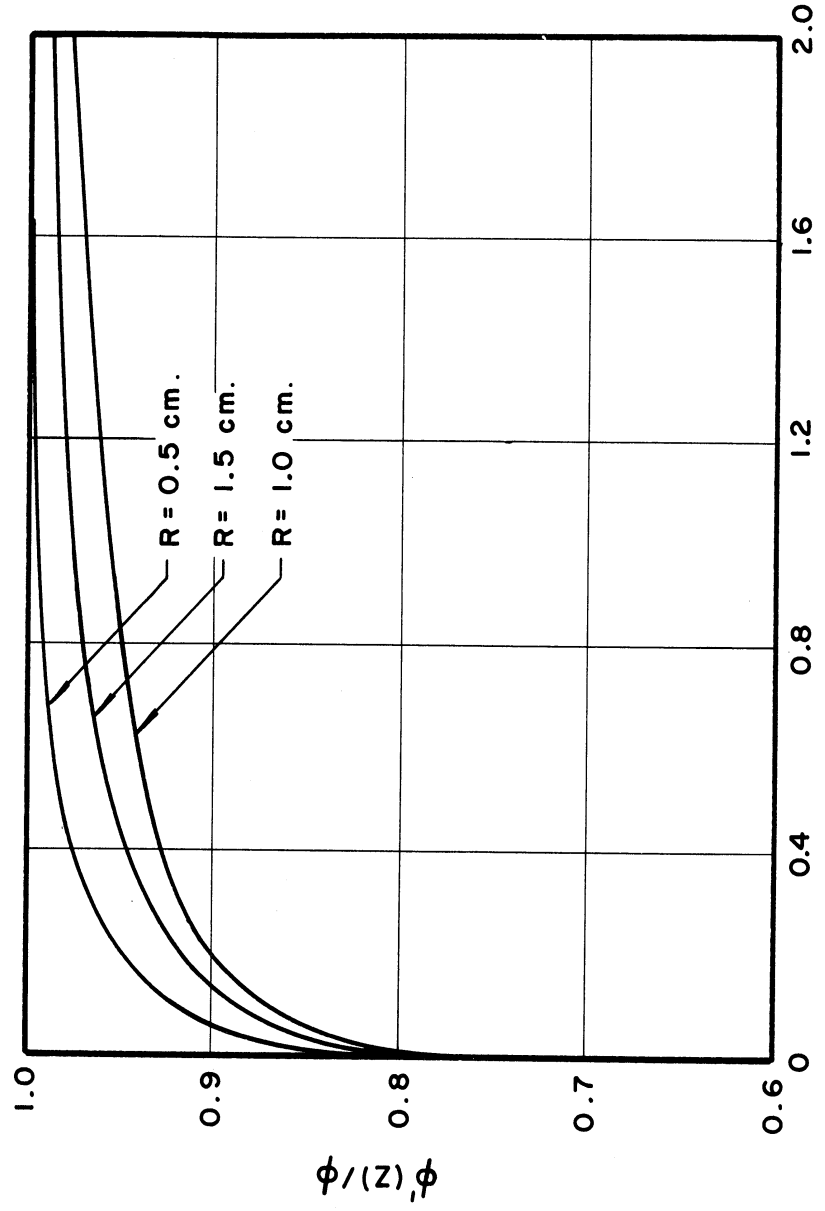

Figure 25. A Plot of The Normalized Scalar Fluxes Along the Central Axis Outside of A Set of Gold Coin Shaped Detectors In Graphite, Thickness of 5 mils.

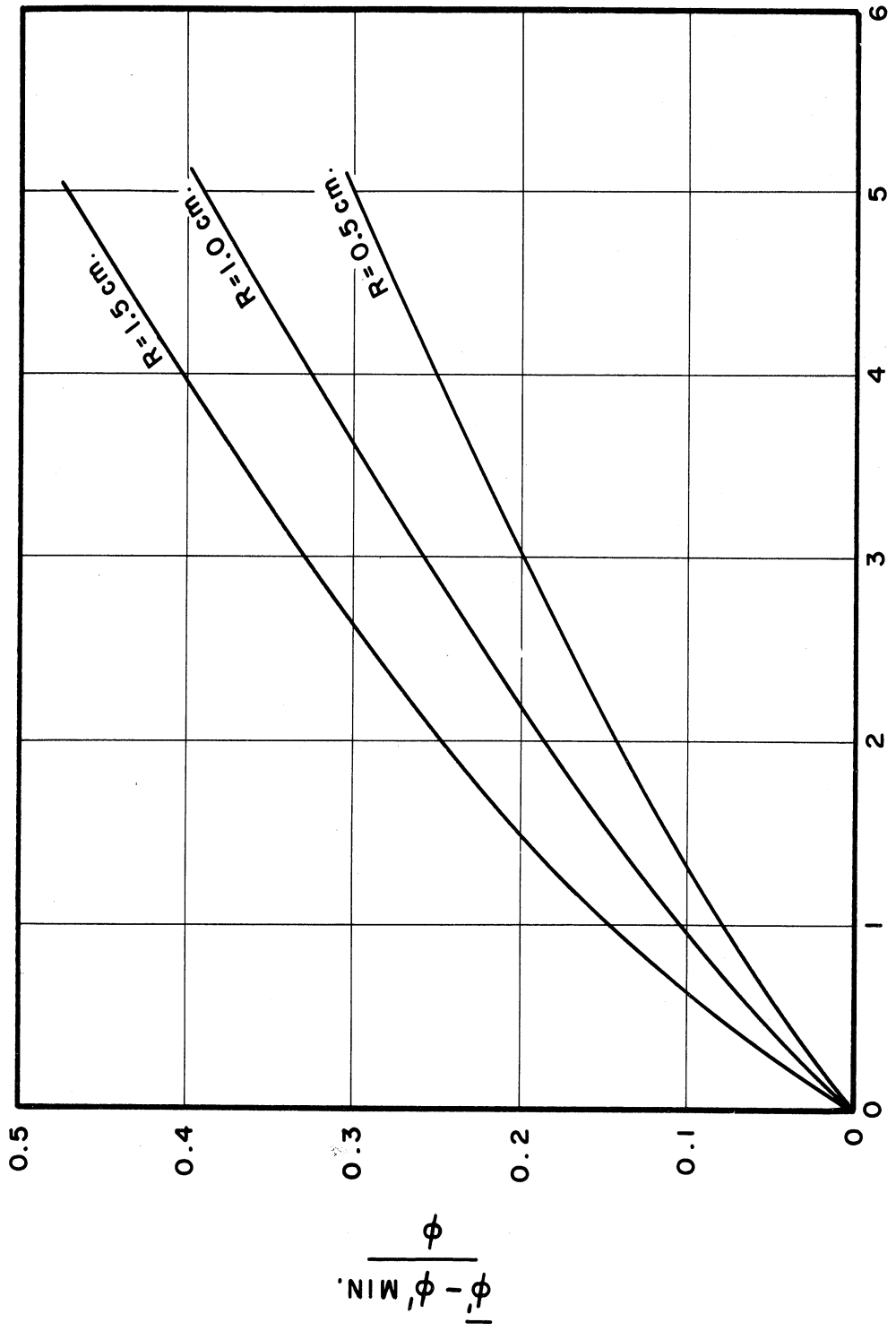

Figure 26. A Plot of the Average Normalized Scalar Flux Minus the Minimum Normalized Scalar Flux In A Coin Shaped Indium Detector In Water.

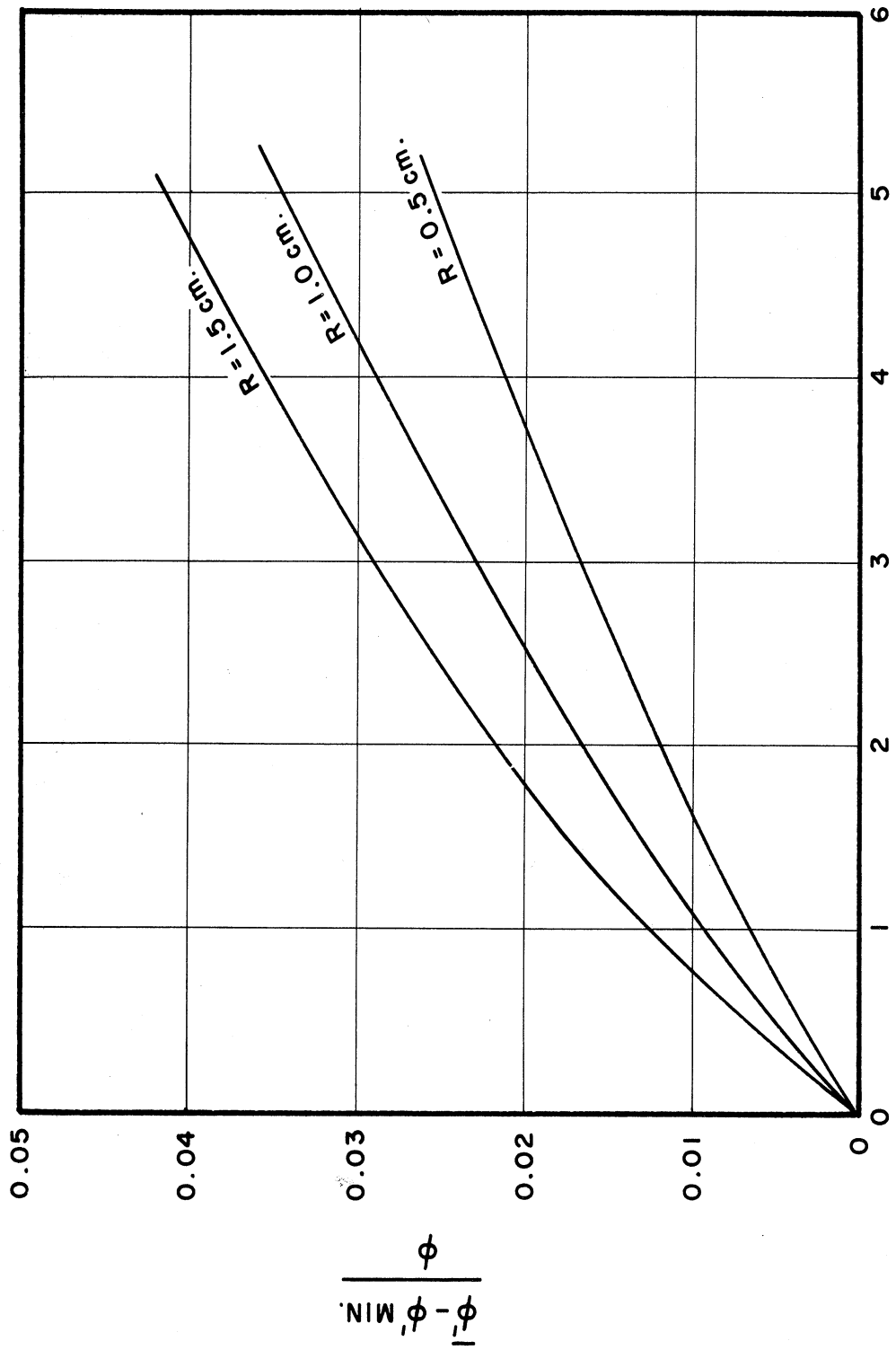

Figure 27. A Plot of the Average Normalized Scalar Flux Minus the Minimum Normalized Scalar Flux In A Coin Shaped Gold Detector In Water.

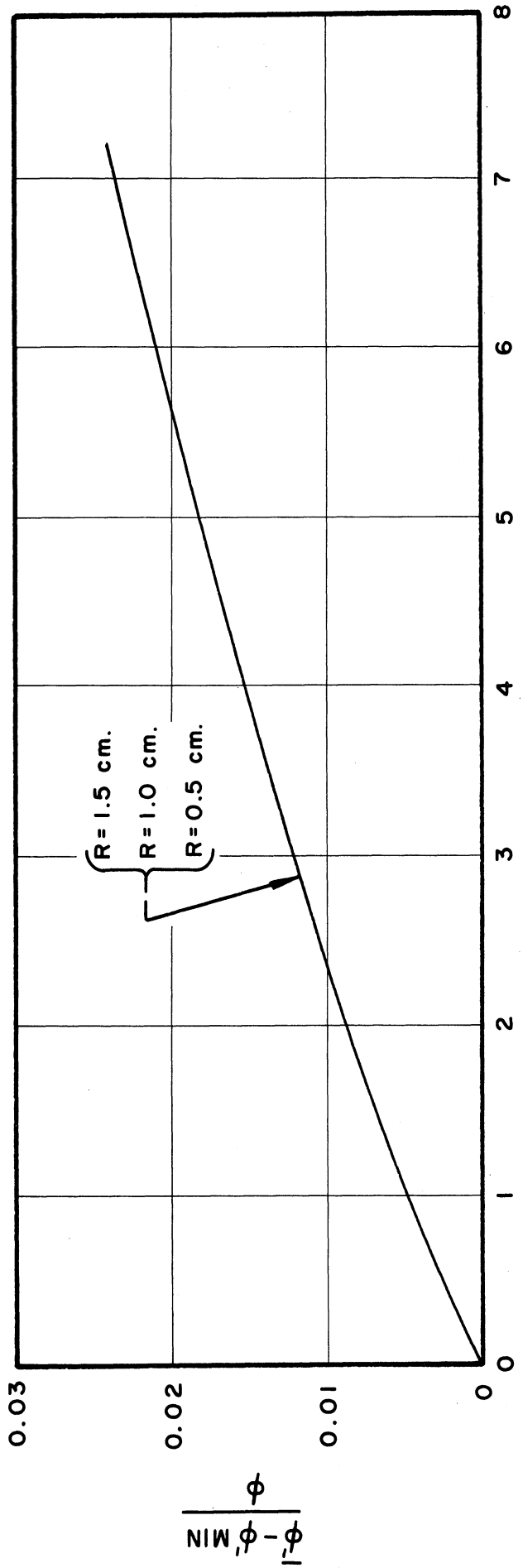

Figure 28. A Plot of the Average Normalized Scalar Flux Minus the Minimum Normalized Scalar Flux In A Coin Shaped Gold Detector In Graphite.

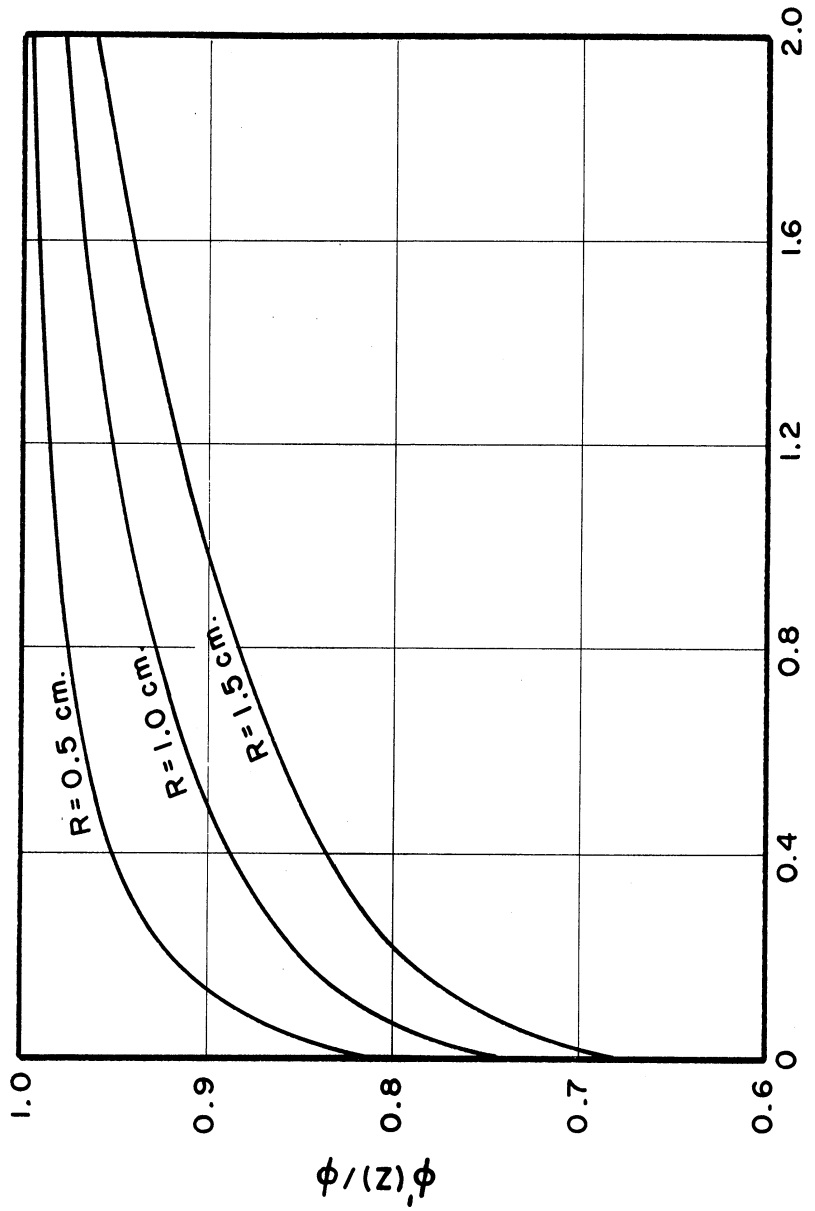

Figure 29. A Plot of The Normalized Scalar Fluxes Along the Central Axis Outside of A Set of Gold Coin Shaped Detectors In Water, Thickness of 5 mils.

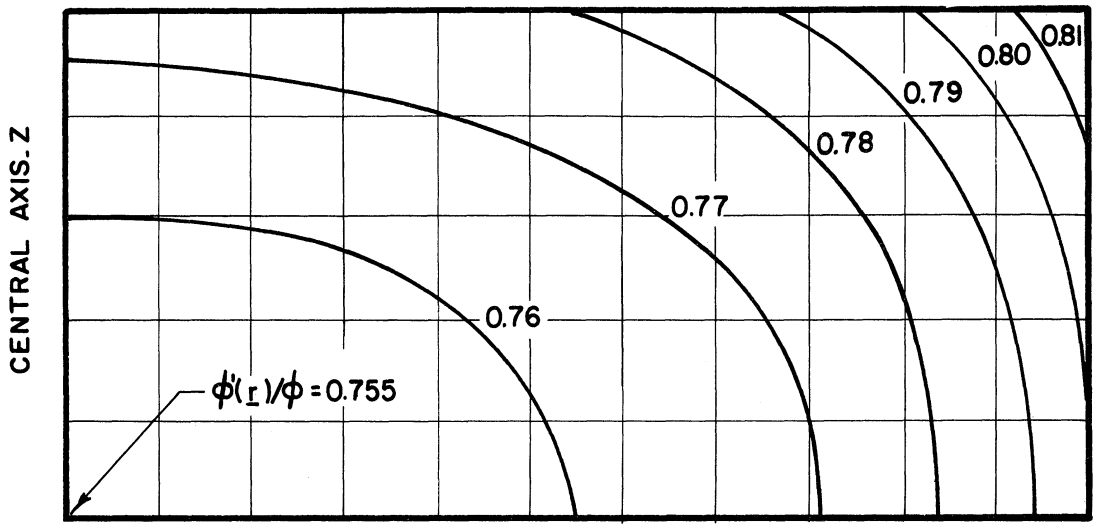

Figure 30. A Map of The Normalized Scalar Flux Within A Coin Shaped Gold Detector In Graphite, Radius of 1.5 cm. and Thickness of 7 mils.

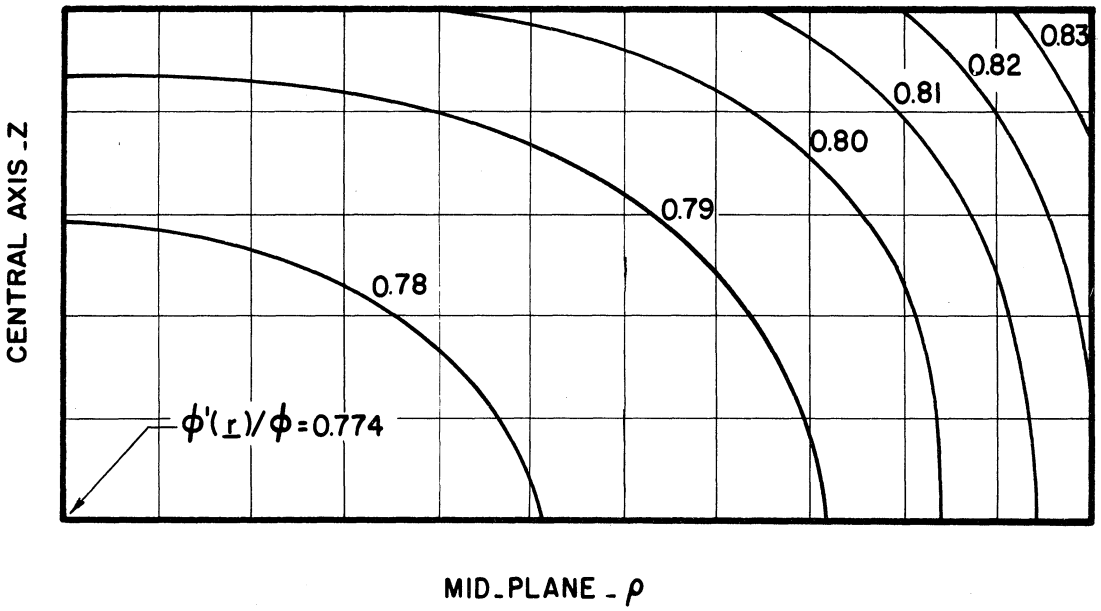

Figure 31. A Map of The Normalized Scalar Flux Within A Coin Shaped Gold Detector In Graphite, Radius of 1.0 cm. and Thickness of 7 mils.

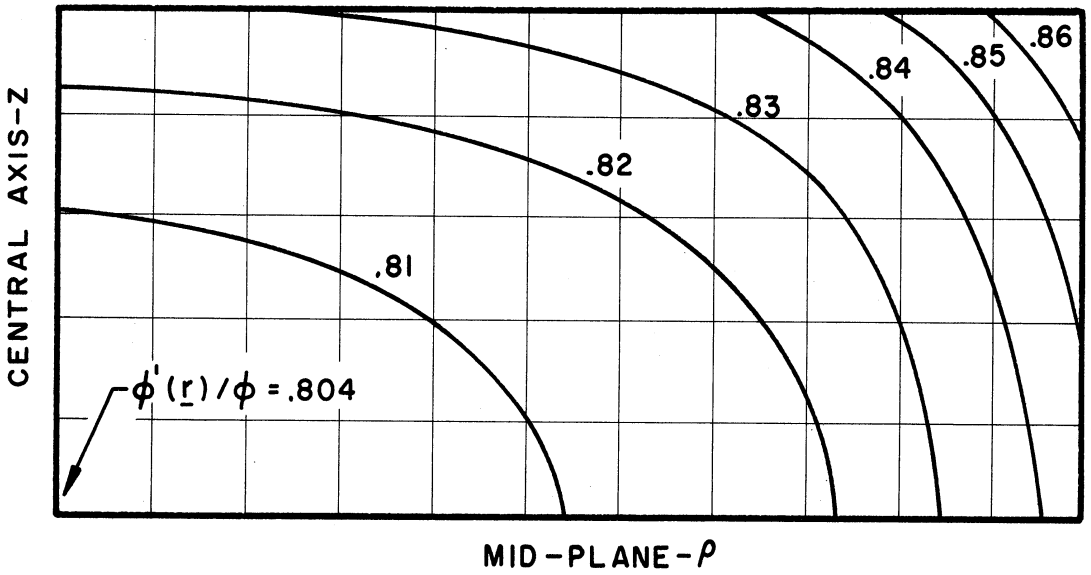

Figure 32. A Map of The Normalized Scalar Flux Within A Coin Shaped Gold Detector In Graphite, Radius of 0.5 cm. and Thickness of 7 mils.

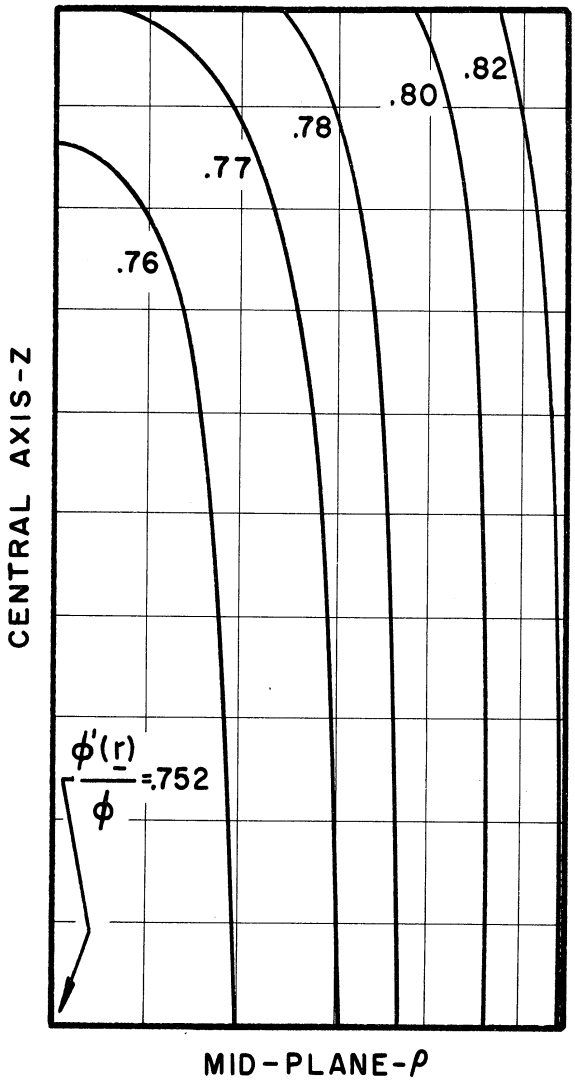

Figure 33. A Map of The Normalized Scalar Flux Within A Wire Shaped Indium Detector In Water, Radius of 10 mils and Length of 2.54 cm.

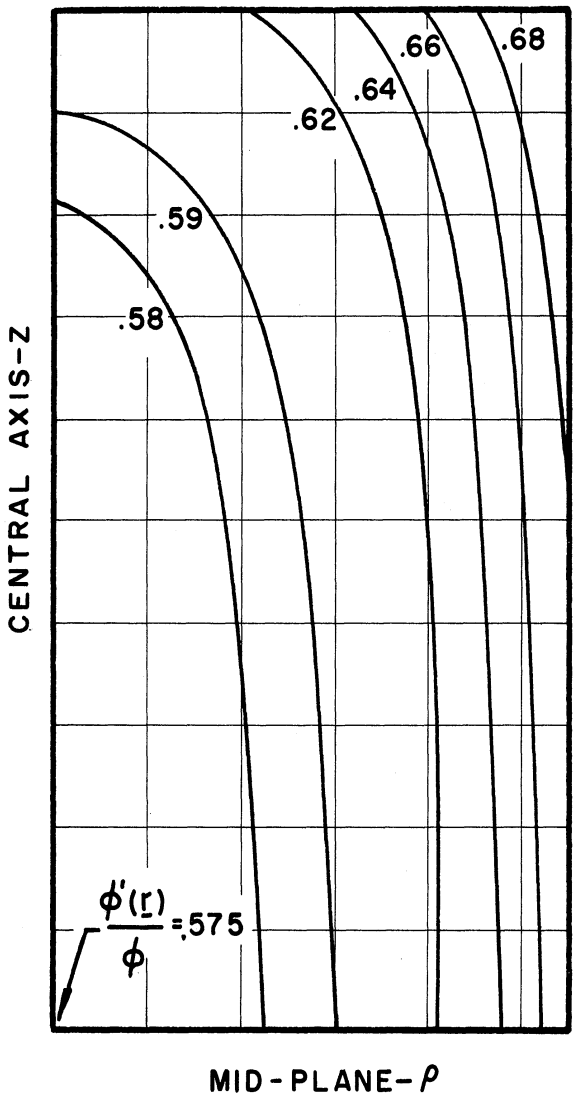

Figure 34. A Map of The Normalized Scalar Flux Within A Wire Shaped Indium Detector In Water, Radius of 20 mils and Length of 2.54 cm.

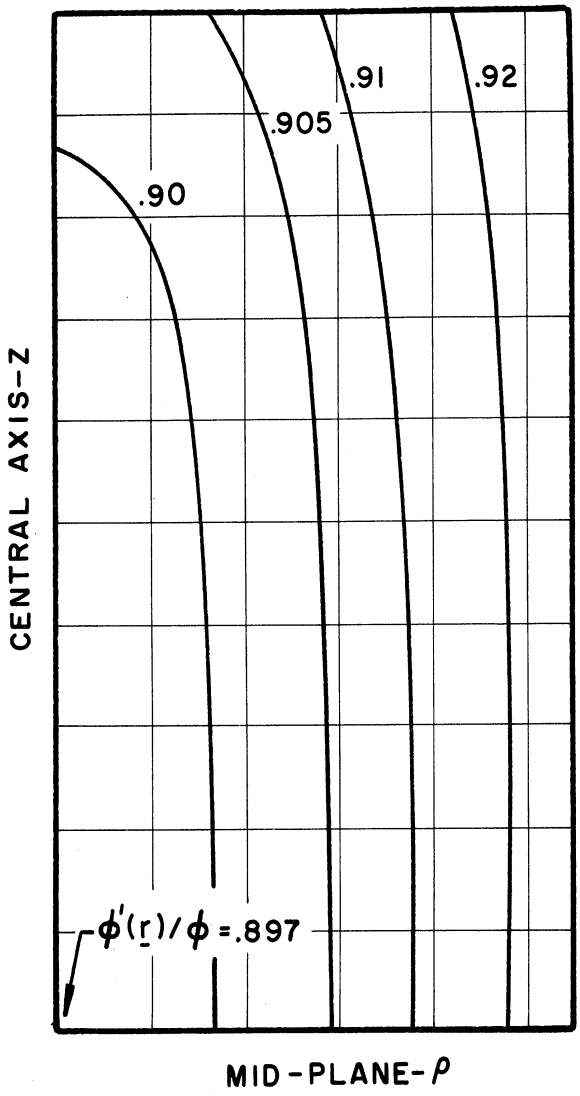

Figure 35. A Map of The Normalized Scalar Flux Within A Wire Shaped Gold Detector In Water, Radius of 5 mils and Length of 1.27 cm.

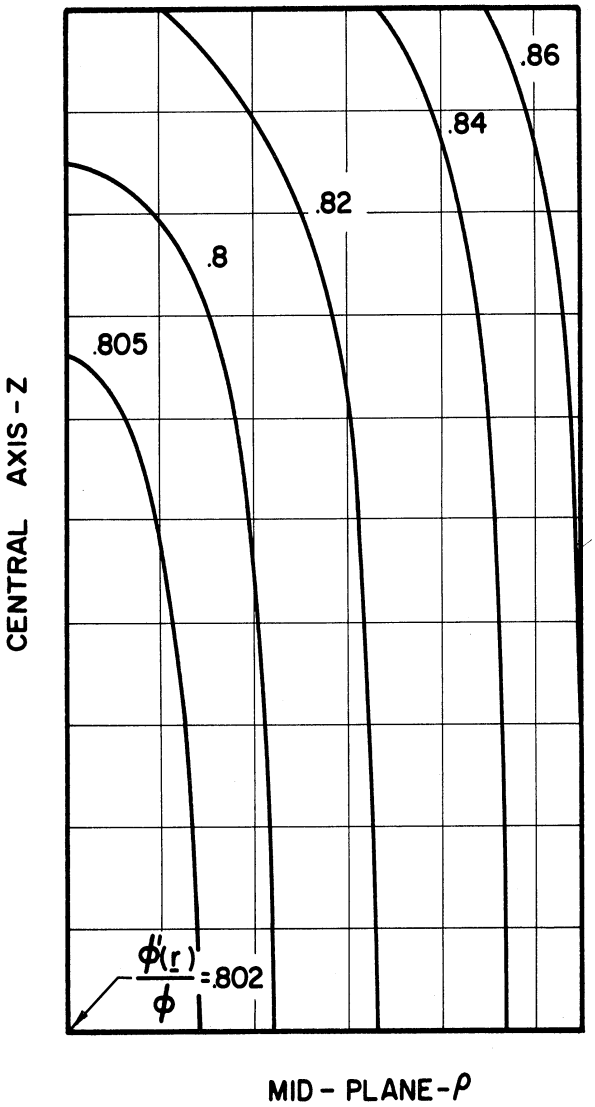

Figure 36. A Map of The Normalized Scalar Flux Within A Wire Shaped Gold Detector In Water, Radius of 10 mils and Length of 1.27 cm.

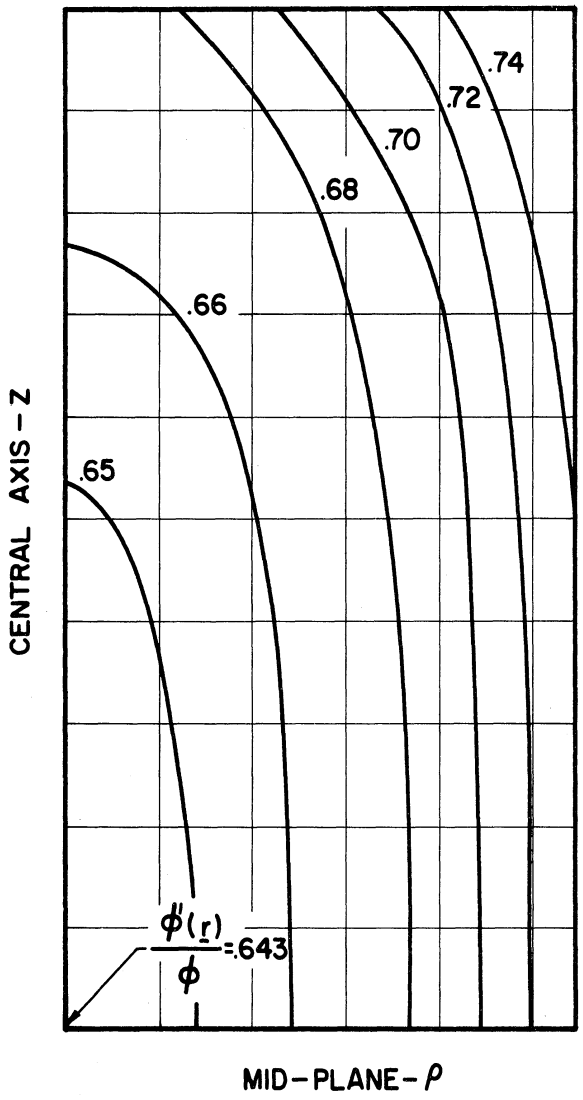

Figure 37. A Map of The Normalized Scalar Flux Within A Wire Shaped Gold Detector In Water, Radius of 20 mils and Length of 1.27 cm.

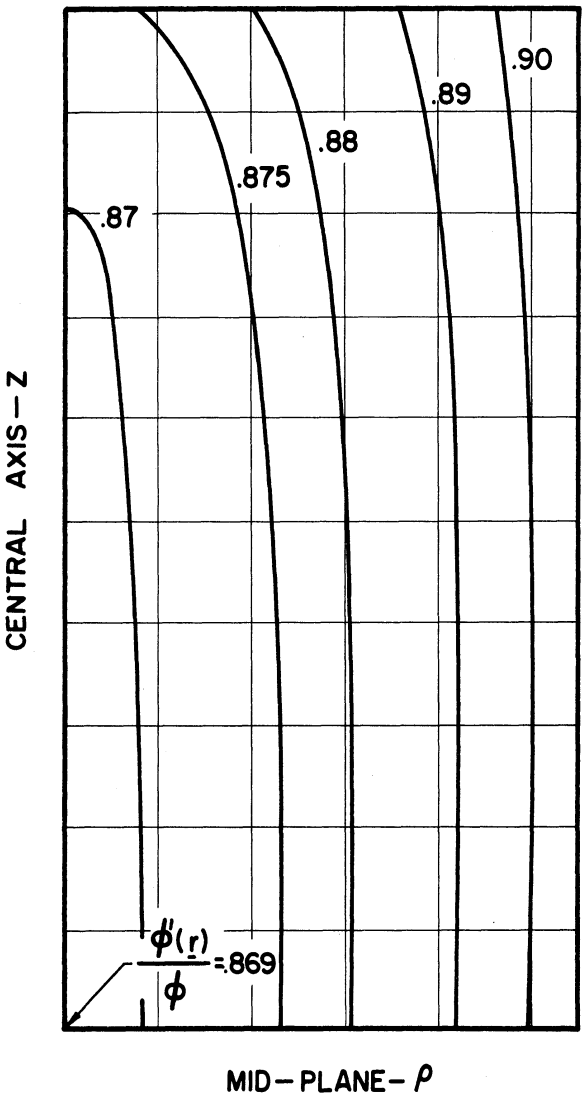

Figure 38. A Map of The Normalized Scalar Flux Within A Wire Shaped Indium Detector In Water, Radius of 5 mils and Length of 2.54 cm.

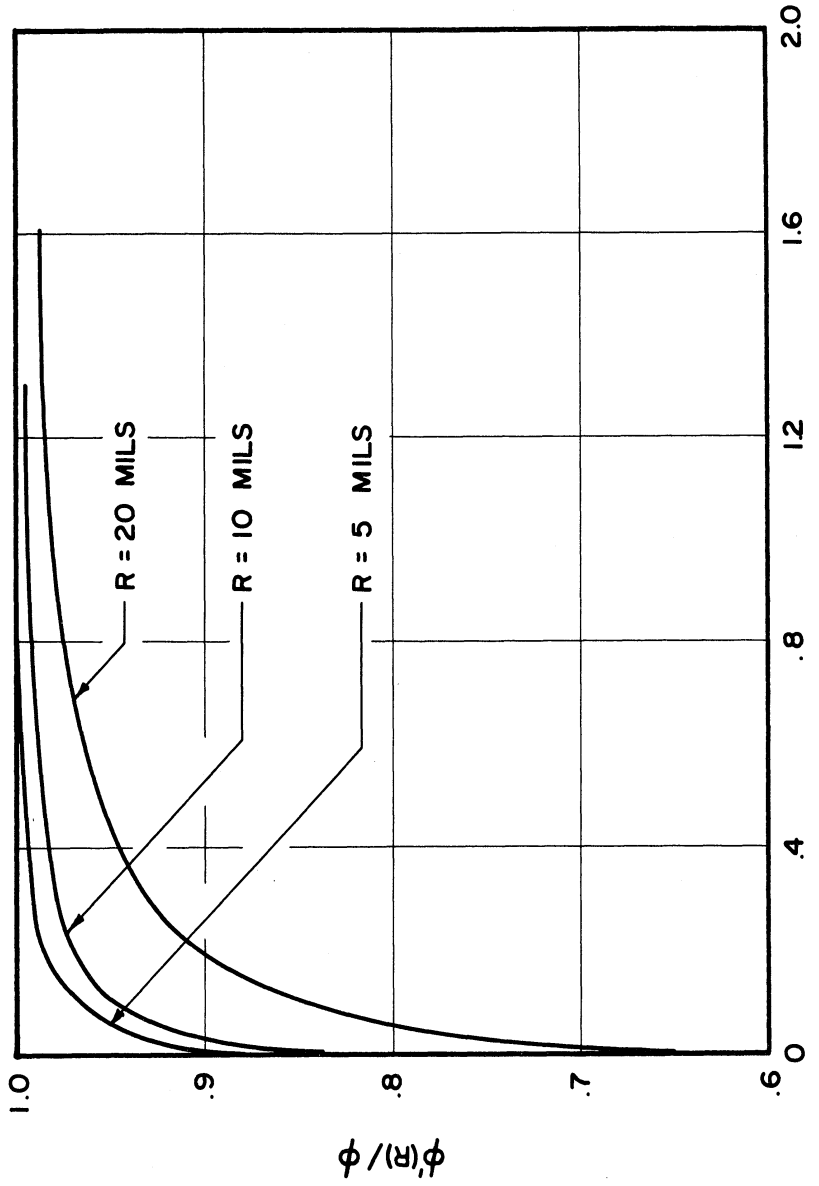

Figure 39. A Plot of The Normalized Scalar Fluxes Along A Radius In The Mid-Plane of A Set of Indium Wire Shaped Detectors In Water, Length of 0.5 Inches.

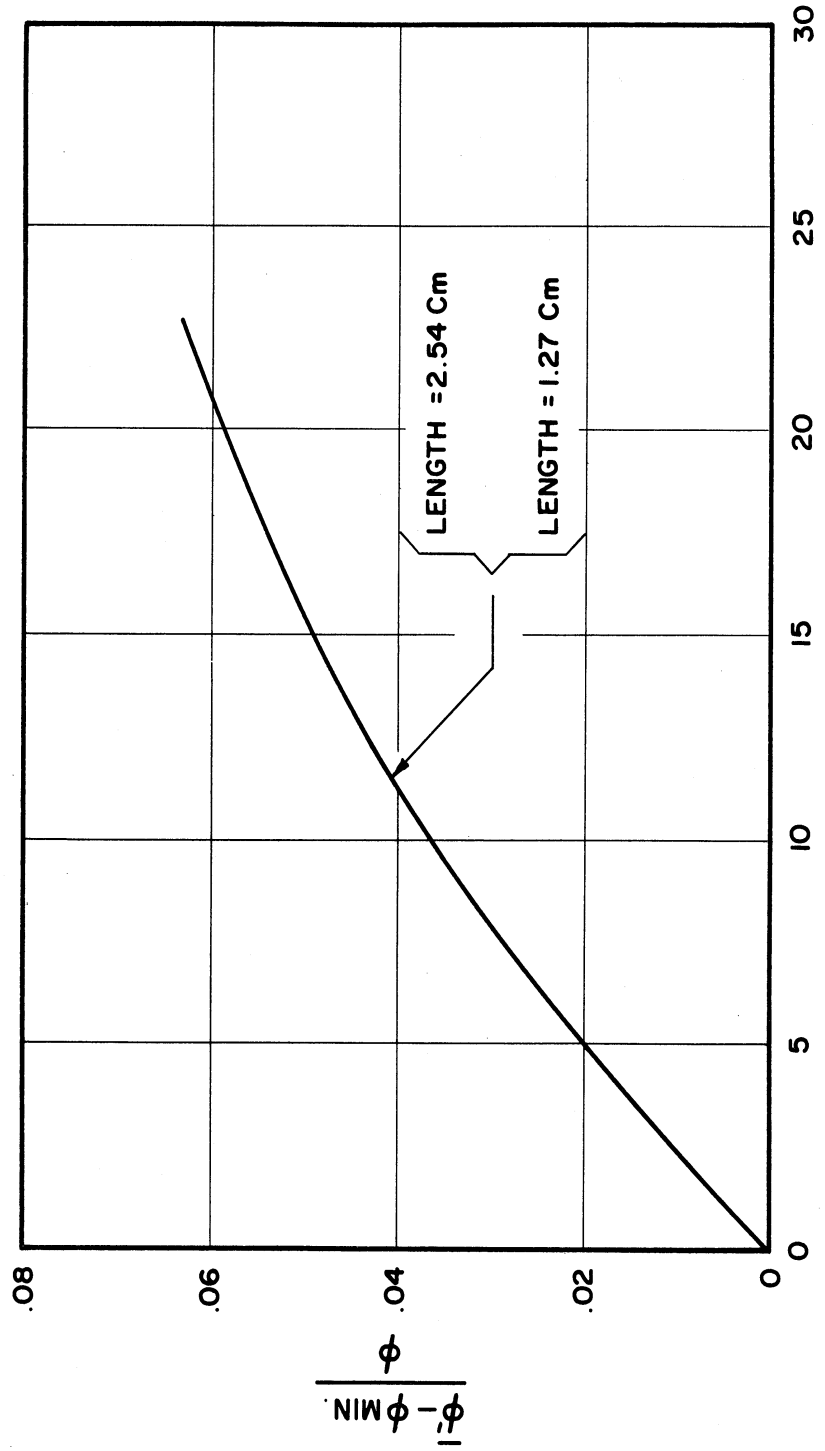

Figure 40. A Plot of the Average Normalized Scalar Flux Minus the Minimum Normalized Scalar Flux In A Wire Shaped Indium Detector In Water.

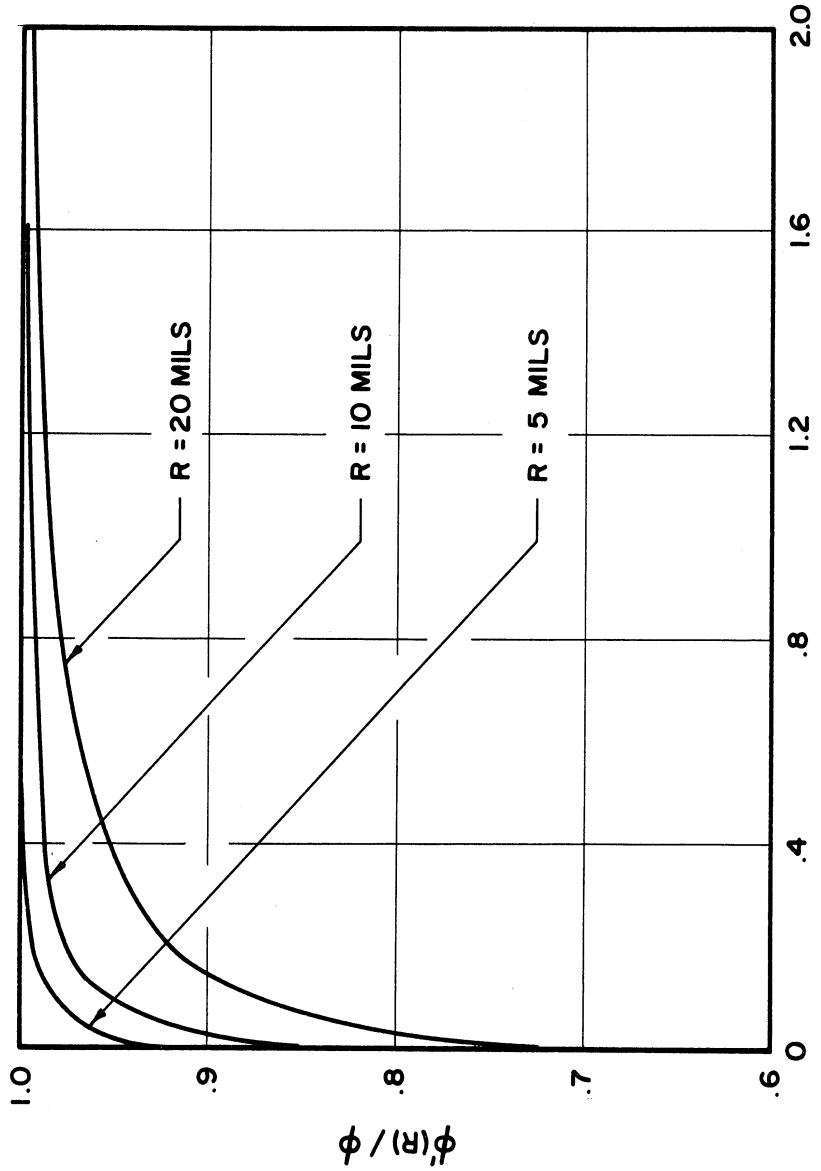

Figure 41. A Plot of the Normalized Scalar Fluxes Along a Radius In the Mid-Plane of A Set of Gold Wire Shaped Detectors in Water, Length of 0.5 Inches.

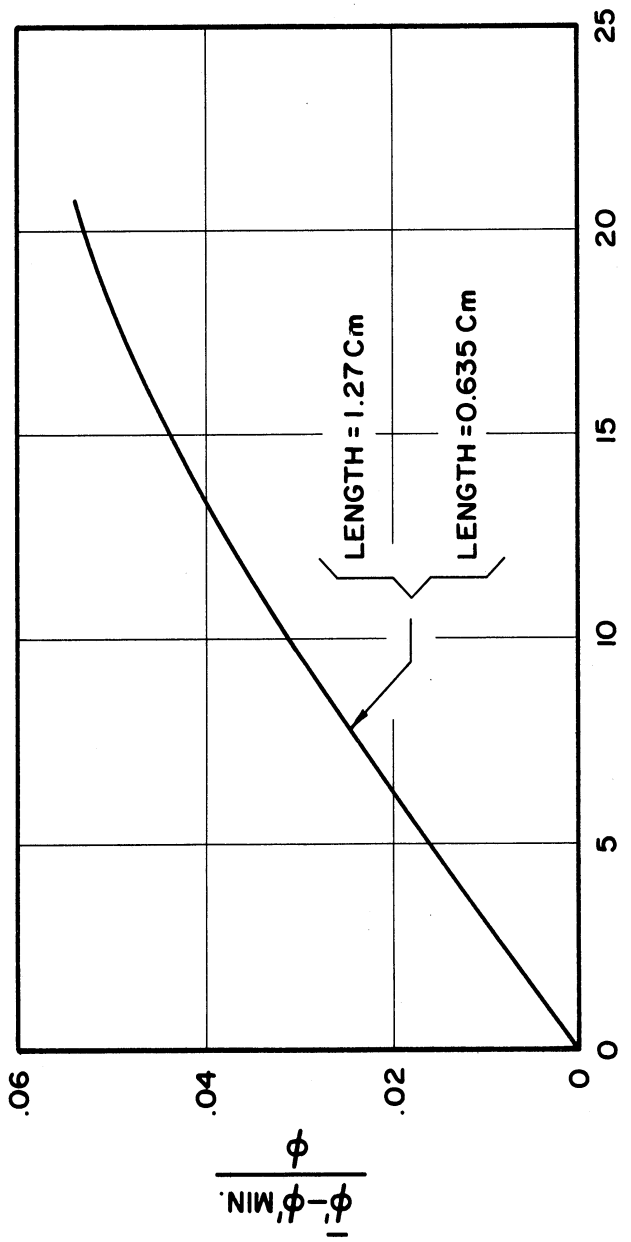

Figure 42. A Plot of the Average Normalized Scalar Flux Minus the Mimimum Normalized Scalar Flux in A Wire Shaped Gold Detector In Water.

CHAPTER VIII

CONCLUSIONS

In conclusion it can be observed that for neutron absorbers commonly used in neutron population measurements the conversion of the transport equation, Equation (2), to an integral equation, Equation (5), is a very practical method of treating the thermal neutron population and around a neutron detector. For a large range of detector sizes it is, in fact, necessary to consider only the zeroth spherical harmonic of the neutron population, Equation (13). For these cases such problems as:

1. Initially anisotropic neutron population.
2. Non-isotropic scattering by the surrounding material.
3. Detailed spatial dependence of the neutron population.
4. Arbitrary three dimensional detector geometry.

can be calculated with an accuracy of 1 per cent using only the zeroth spherical harmonic of the neutron population.

For the larger detector sizes the calculation of two iterations of Equation (6) must be carried out, where the higher spherical harmonics are included, in order to achieve an accuracy of 1 per cent. For very large absorbers, e.g. reactor control rods, the iterations of Equation (6) should be continuted beyond the second iteration, but as noted earlier this is not possible due to the limited amount of information available about the Green's function $G(\underline{r}', \underline{\Omega}' \rightarrow \underline{r}, \underline{\Omega})$.

In the case of water there is still another limiting factor. Even for the small detectors where the higher spherical harmonics need not be

considered the variation of $\bar{\mu}$ from zero to 0.3 causes the average scalar flux in the thickest detectors to increase by as much as 3 per cent. Thus, the limiting factor for the calculations presented here for the case of water is the value of $\bar{\mu}$ used. The value of $\bar{\mu}$ was taken as zero for all of the calculations except the one case of $\bar{\mu}$ of 0.3 . So, the average scalar flux in water may be low by as much as 3 per cent in the case of thick coins in water.

Aside from the uncertainty caused by the two factors mentioned above there are no other known sources of error which could contribute a correction of more than about 0.1 per cent.

APPENDIX I

Part 1

EVALUATION OF $G(\underline{r}', \underline{\Omega}' \rightarrow \underline{r})$

By definition $G(\underline{r}', \underline{\Omega}' \rightarrow \underline{r}, \underline{\Omega})$ satisfies the equation (1)

$$\underline{\Omega} \cdot \nabla G(\underline{r}', \underline{\Omega}' \rightarrow \underline{r}, \underline{\Omega}) + \Sigma_t G(\underline{r}', \underline{\Omega}' \rightarrow \underline{r}, \underline{\Omega}) -$$

$$\int_{\underline{\omega}} \Sigma_s (\underline{\omega} \rightarrow \underline{\Omega}) G(\underline{r}', \underline{\Omega}' \rightarrow \underline{r}, \underline{\omega}) \, d\underline{\omega} = \delta(\underline{r}'-\underline{r}) \, \delta(\underline{\Omega}'-\underline{\Omega})$$

Again by definition

$$G(\underline{r}', \underline{\Omega}' \rightarrow \underline{r}) \equiv \int_{\underline{\Omega}} G(\underline{r}', \underline{\Omega}' \rightarrow \underline{r}, \underline{\Omega}) \, d\underline{\Omega}$$

Assume isotropic scattering in the laboratory coordinate system. Then

$$\Sigma_s (\underline{\omega} \rightarrow \underline{\Omega}) = \frac{1}{4\pi} \Sigma_s \tag{2}$$

Next let $\mathcal{G}(\underline{r}'', \underline{\Omega}'' \rightarrow \underline{r}, \underline{\Omega})$ denote the solution to the following equation:

$$\underline{\Omega} \cdot \nabla \mathcal{G}(\underline{r}'', \underline{\Omega}'' \rightarrow \underline{r}, \underline{\Omega}) + \Sigma_t \mathcal{G}(\underline{r}'', \underline{\Omega}'' \rightarrow \underline{r}, \underline{\Omega}) \tag{3}$$

$$= \delta(\underline{r}''-\underline{r}) \, \delta(\underline{\Omega}''-\underline{\Omega})$$

It is well known that [2]

$$\mathcal{G}(\underline{r}'', \underline{\Omega}'' \rightarrow \underline{r}, \underline{\Omega}) = \frac{e^{-\Sigma_t |\underline{r}-\underline{r}''|}}{|\underline{r}-\underline{r}''|^2} \tag{4}$$

$$\delta(\underline{\Omega}''-\underline{\Omega}) \, \delta(\underline{\Omega} - [\underline{r}-\underline{r}'']^{\wedge})$$

The function $\mathcal{G}(\underline{r}'', \underline{\Omega}'' \rightarrow \underline{r}, \underline{\Omega})$ is a Green's function for Equation (1) thus

$$G(\underline{r}', \underline{\Omega}' \rightarrow \underline{r}, \underline{\Omega}) = \int_{\underline{r}'', \underline{\Omega}''} G(\underline{r}'', \underline{\Omega}'' \rightarrow \underline{r}, \underline{\Omega}) \left[\frac{\Sigma_s}{4\pi} \right. \tag{5}$$

$$\left. \int_{\underline{\omega}} G(\underline{r}', \underline{\Omega}' \rightarrow \underline{r}'', \underline{\omega})\, d\underline{\omega} + \delta(\underline{r}'-\underline{r}'')\, \delta(\underline{\Omega}'-\underline{\Omega}'') \right] d\underline{r}''d\underline{\Omega}''$$

Spatial integrations are over all $\underline{r}$ space. Making the indicated substitutions yields:

$$G(\underline{r}', \underline{\Omega}' \rightarrow \underline{r}, \underline{\Omega}) = \int_{\underline{r}''} \frac{e^{-\Sigma_t |\underline{r}-\underline{r}''|}}{|\underline{r}-\underline{r}''|^2} \frac{\Sigma_s}{4\pi} \tag{6}$$

$$\int_{\underline{\omega}} G(\underline{r}', \underline{\Omega}' \rightarrow \underline{r}'', \underline{\omega})\, d\underline{\omega}\ \delta(\underline{\Omega} - [\underline{r}-\underline{r}''])\, d\underline{r}'' +$$

$$+ \frac{e^{-\Sigma_t |\underline{r}'-\underline{r}|}}{|\underline{r}'-\underline{r}|^2}\ \delta(\underline{\Omega}'-\underline{\Omega})$$

Now integrating over all $\underline{\Omega}$ yields:

$$G(\underline{r}', \underline{\Omega}' \rightarrow \underline{r}) = \frac{\Sigma_s}{4\pi} \int_{\underline{r}''} \frac{e^{-\Sigma_t |\underline{r}-\underline{r}''|}}{|\underline{r}-\underline{r}''|^2} G(\underline{r}', \underline{\Omega}' \rightarrow \underline{r}'')\, d\underline{r}'' \tag{7}$$

$$+ \frac{e^{-\Sigma_t |\underline{r}-\underline{r}'|}}{|\underline{r}-\underline{r}'|^2}\ \delta(\underline{\Omega}'-[\underline{r}-\underline{r}'])$$

Expand $G(\underline{r}', \underline{\Omega}' \rightarrow \underline{r})$ as

$$G(\underline{r}', \underline{\Omega}' \rightarrow \underline{r}) = \sum_{a,b} G_a^b(\underline{r}', \underline{r})\, Y_a^b(\underline{\Omega}') \tag{8}$$

Thus

$$\sum_{a,b} G_a^b(\underline{r}', \underline{r})\ Y_a^b(\underline{\Omega}') = \frac{\Sigma_s}{4\pi} \sum_{a,b} Y_a^b(\underline{\Omega}')\ x \tag{9}$$

$$\int_{\underline{r}''} G_a^b(\underline{r}',\underline{r}'') \frac{e^{-\Sigma_t|\underline{r}-\underline{r}''|}}{|\underline{r}-\underline{r}''|^2} d\underline{r}'' +$$

$$\frac{e^{-\Sigma_t|\underline{r}-\underline{r}'|}}{|\underline{r}-\underline{r}'|^2} \delta(\underline{\Omega}'-[\underline{\hat{r}}-\underline{\hat{r}}'])$$

Now multiply by $Y_1^{*m}(\underline{\Omega}')$ and integrate over all $\underline{\Omega}'$.

$$G_1^m(\underline{r}', \underline{r}) \frac{\Sigma_s}{4\pi} \int_{\underline{r}''} G_1^m(\underline{r}', \underline{r}'') \frac{e^{-\Sigma_t|\underline{r}-\underline{r}''|}}{|\underline{r}-\underline{r}''|^2} d\underline{r}'' + \qquad (10)$$

$$Y_1^m(\underline{\hat{r}}-\underline{\hat{r}}') \frac{e^{-\Sigma_t|\underline{r}-\underline{r}'|}}{|\underline{r}-\underline{r}'|^2}$$

For the sake of convenience let $\underline{r}' = 0$. Now take the Fourier transform of Equation (10).

$$G_1^m(\underline{K}) = \frac{\Sigma_s}{4\pi} \int_{\underline{r}'', \underline{r}} G_1^m(\underline{r}'') \frac{e^{-\Sigma_t|\underline{r}-\underline{r}''|-i\underline{K}\cdot\underline{r}}}{|r-r''|^2 (2\pi)^{3/2}} d\underline{r}''d\underline{r} + \qquad (11)$$

$$+ \frac{1}{(2\pi)^{3/2}} \int_{\underline{r}} Y_1^{*m}(\underline{r}) \frac{e^{-\Sigma_t r-i\underline{K}\cdot\underline{r}}}{r^2} d\underline{r}$$

where

$$G_1^m(\underline{K}) \equiv \frac{1}{(2\pi)^{3/2}} \int_{\underline{r}} G_1^m(\underline{r}) e^{-i\underline{K}\cdot\underline{r}} d\underline{r} \qquad (12)$$

Using the expansion for $e^{\pm i\underline{K}\cdot\underline{r}}$ given in part 4 of this appendix:

$$\int_{\underline{r}} Y_1^{*m}(\underline{\hat{r}}) \frac{e^{-\Sigma_t r-i\underline{K}\cdot\underline{r}}}{r^2} d\underline{r} = \qquad (13)$$

$$= \int_{r=0}^{\infty} \frac{r^2 e^{-\Sigma_t r}}{r^2} \int_{\underline{\hat{r}}} e^{-i\underline{K}\cdot\underline{r}} \; Y_l^{m*}(\underline{\hat{r}}) \, d\underline{\hat{r}} dr =$$

$$= \int_{r=0}^{\infty} e^{-\Sigma_t r} \, 4\pi \sum_{a,b} (-i)^a j_a(Kr) \; Y_a^{b*}(\underline{\hat{K}}) \int_{\underline{\hat{r}}} Y_l^{m*}(\underline{\hat{r}}) \; Y_a^b(\underline{\hat{r}}) \, d\underline{\hat{r}} dr$$

$$= \int_{r=0}^{\infty} 4\pi \, (-i)^l \, j_l(Kr) \, dr \; Y_l^m(\underline{\hat{K}})$$

Define $F_l(K, \Sigma_t) \equiv 4\pi \, (-i)^l \int_{r=0}^{\infty} j_l(Kr) \, e^{-\Sigma_t r} \, dr; \; l = 0, 1, 2 \ldots$ (14)

Thus

$$\int Y_l^{m*}(\underline{\hat{r}}) \frac{e^{-\Sigma_t r - i\underline{K}\cdot\underline{r}}}{r^2} \, d\underline{r} = Y_l^{m*}(\underline{\hat{K}}) \, F_l(K, \Sigma_t) \qquad (15)$$

Note that in the special case of $l = m = 0$ the integral in Equation (14) can be done directly yielding

$$F_o(K, \Sigma_t) = \frac{4\pi}{K} \; \text{Arctangent}\left(\frac{K}{\Sigma_t}\right) \qquad (16)$$

Next examine the integral:

Let $\underline{x} = \underline{r}'' - \underline{r}$

$$\int_{\underline{r}} \frac{e^{-\Sigma_t |\underline{r}-\underline{r}''| \, i\underline{K}\cdot\underline{r}}}{|\underline{r}-\underline{r}''|^2} \, d\underline{r} = e^{-i\underline{K}\cdot\underline{r}''} \, x \qquad (17)$$

$$\int_{\underline{x}} \frac{e^{-\Sigma_t x - i\underline{K}\cdot\underline{x}}}{x^2} \, d\underline{x} =$$

$$e^{-i\underline{K}\cdot\underline{r}''} \; F_0 \; (K, \Sigma_t)$$

Combining Equations 11 and 15 gives:

$$G_1^m \; (\underline{K}) = \frac{1}{(2\pi)^{3/2}} \; \frac{\Sigma_s}{4\pi} \int_{\underline{r}''} G_1^m \; (\underline{r}'') \; e^{-i\underline{K}\cdot\underline{r}} \; F_0 \; (K, \Sigma_t) \; d\underline{r}''$$

$$+ \frac{1}{(2\pi)^{3/2}} \quad Y_1^{*m} \; (\underline{K}) \; F_1 \; (K, \Sigma_t) \tag{18}$$

Using the definition in Equation 12 and solving for $G_1^m \; (\underline{K})$

$$G_1^m \; (\underline{K}) = \frac{1}{(2\pi)^{3/2}} \quad \frac{Y_1^{*m} \; (\hat{\underline{K}}) \; F_1 \; (K, \Sigma_t)}{1 - \frac{\Sigma_s}{4\pi} \; F_0 \; (K, \Sigma_t)} \tag{19}$$

Now take the inverse Fourier transform:

$$G_1^m \; (\underline{r}) = \frac{1}{(2\pi)^3} \int_{\underline{K}} \frac{e^{-i\underline{K}\cdot\underline{r}} \; Y_1^{*m} \; (\hat{\underline{K}}) \; F_1 \; (K, \Sigma_t)}{1 - \frac{\Sigma_s}{4\pi} \; F_0 \; (K, \Sigma_t)} \, d\underline{K} \tag{20}$$

Again using the expansion for $e^{\pm i\underline{K}\cdot\underline{r}}$ it is easily shown that

$$\int_{\hat{\underline{K}}} e^{i\underline{K}\cdot\underline{r}} \; Y_1^{*m} \; (\hat{\underline{K}}) \; d\hat{\underline{K}} = 4\pi \; (i)^l \; j_1 \; (Kr) \; Y_1^{*m} \; (\hat{\underline{r}}) \tag{21}$$

Thus

$$G_l^m(\underline{r}) = \frac{2(i)^l}{(2\pi)^3} Y_l^{*m}(\hat{\underline{r}}) \int_{K=0}^{\infty} \frac{j_l(Kr)\, F_l(K, \Sigma_t)\, K^2}{1 - \frac{\Sigma_s}{4\pi} F_0(K, \Sigma_t)}\, dK$$

In order to regain the dependance on $\underline{r}'$ replace $\underline{r}$ with $\underline{r}-\underline{r}'$.

$$G_l^m(\underline{r}-\underline{r}') = \frac{2i^l}{(2\pi)^3} Y_l^{*m}(\hat{\underline{r}-\underline{r}'})\, x \tag{22}$$

$$\int^{\infty} \frac{j_l(K|\underline{r}-\underline{r}'|)\, F_l(K, \Sigma_t)}{1 - \frac{\Sigma_s}{4\pi} F_0(K, \Sigma_t)}\, K^2 dK$$

Define

$$\bar{G}_a(|\underline{r}-\underline{r}'|) = \frac{2i^l}{(2\pi)^3} \int_{K=0}^{\infty} \frac{j_a(K|\underline{r}-\underline{r}'|)\, F_a(K, \Sigma_t)\, K^2}{1 - \frac{\Sigma_s}{4\pi} F_0(K, \Sigma_t)}\, dK \tag{23}$$

Thus

$$G(\underline{r}', \Omega' \rightarrow \underline{r}) = \sum_{a}^{l} \sum^{b} Y_a^b(\Omega')\, Y_a^{*b}(\hat{\underline{r}-\underline{r}'})\, \bar{G}_a(|\underline{r}-\underline{r}'|) \tag{24}$$

APPENDIX I

Part 2

THE FUNCTION $F_a(K, \Sigma_t)$

In Equation (14) of Part 1 of this Appendix $F_a(K, \Sigma_t)$ was defined as

$$F_a(K, \Sigma_t) = 4\pi\ (-i)^a \int_{x=0}^{\infty} j_a\ (Kx)\ e^{-\Sigma_t x}\ dx \qquad (25)$$

$$= 4\pi\ (-i)^a\ \frac{\Gamma(\frac{1}{2})\Gamma(a+1)}{2^{a+1}\Gamma(a + 3/2)}\ x\ \frac{K^a}{(K^2+\Sigma_t^2)^{\frac{1}{2}(a + 1)}}\ x$$

$$x\ F\left(\frac{a + 1}{2};\ \frac{a + 1}{2}\ |\ \frac{2a + 3}{2}\ |\ \frac{K^2}{K^2 + \Sigma_t^2}\right)^{(9)}$$

The function $F(A;\ B|C|Z)$ is the hypergeometric function.[9]

$$F(A;B|C|Z) = 1 + \frac{AB}{C}\ Z + \frac{A(A+1)B(B+1)}{C(C+1)\ x\ 2!}\ Z^2 + \ldots\ . \qquad (26)$$

For Z near 1 it is useful to note

$$F(A;B|C|Z) = \frac{\Gamma(C)\Gamma(C-A-B)}{\Gamma(C-A)\Gamma(C-B)}\ F(A;B|A+B-C+1|1-Z) + \qquad (27)$$

$$\frac{\Gamma(C)\Gamma(A+B-C)}{\Gamma(A)\Gamma(B)}\ (1-Z)^{C-A-B}\ F(C-A;\ C-B|C-A-B+1|1-Z)$$

---

* Note that Equation (25) should contain the term

$$\frac{\Gamma(\frac{1}{2})\Gamma(A+1)}{2^{a+1}\Gamma(a+3/2)}\ \text{NOT}\ \frac{\Gamma(\frac{1}{2})\Gamma(a+1)}{2^{a+1}\Gamma(a+\frac{1}{2})}\ \text{as given in Reference (9).}$$

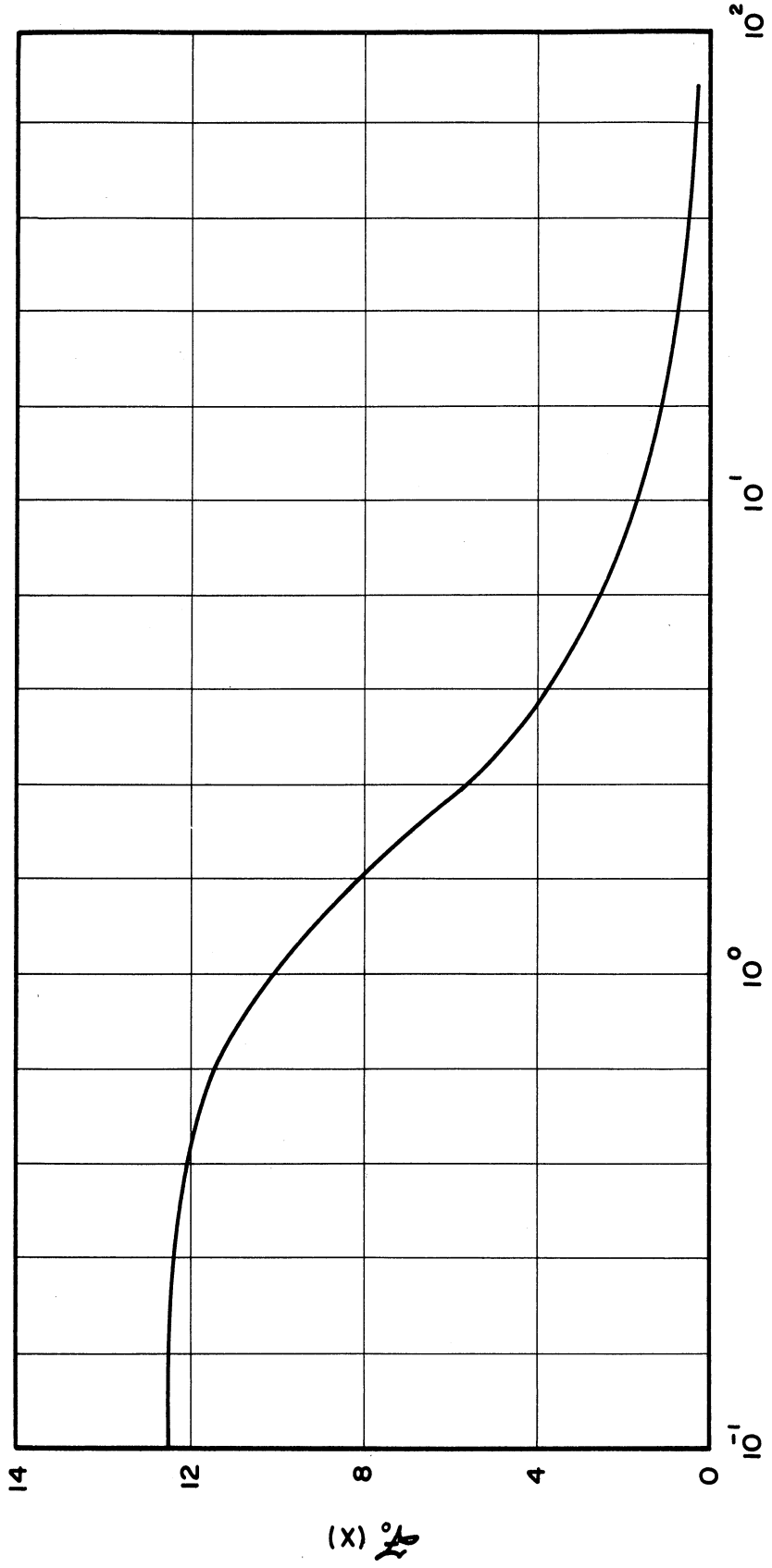

Figure 43. A Graph of The Function $\mathcal{Z}_0(x)$.

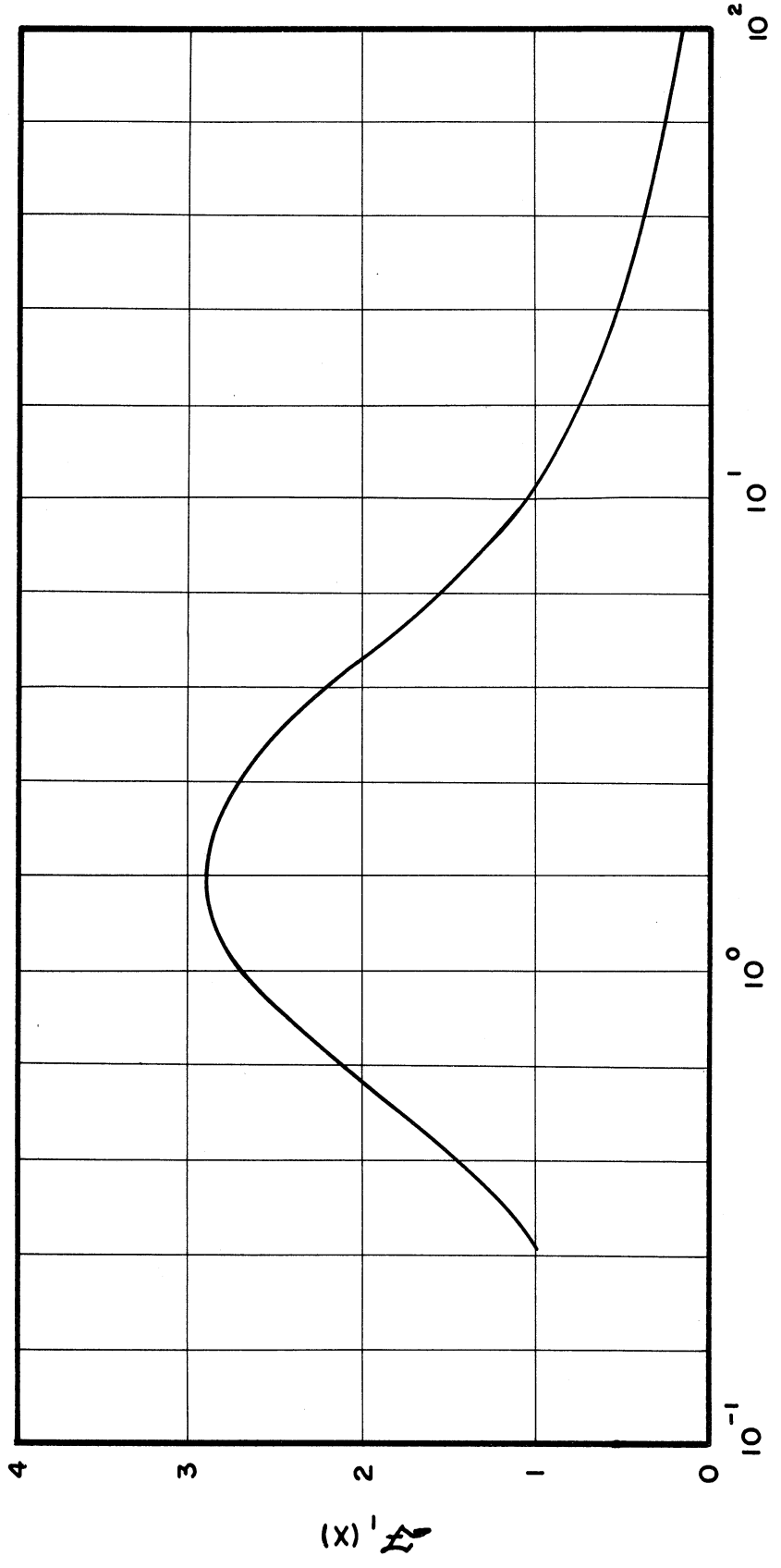

Figure 44. A Graph of The Function $\mathcal{J}_1(x)$.

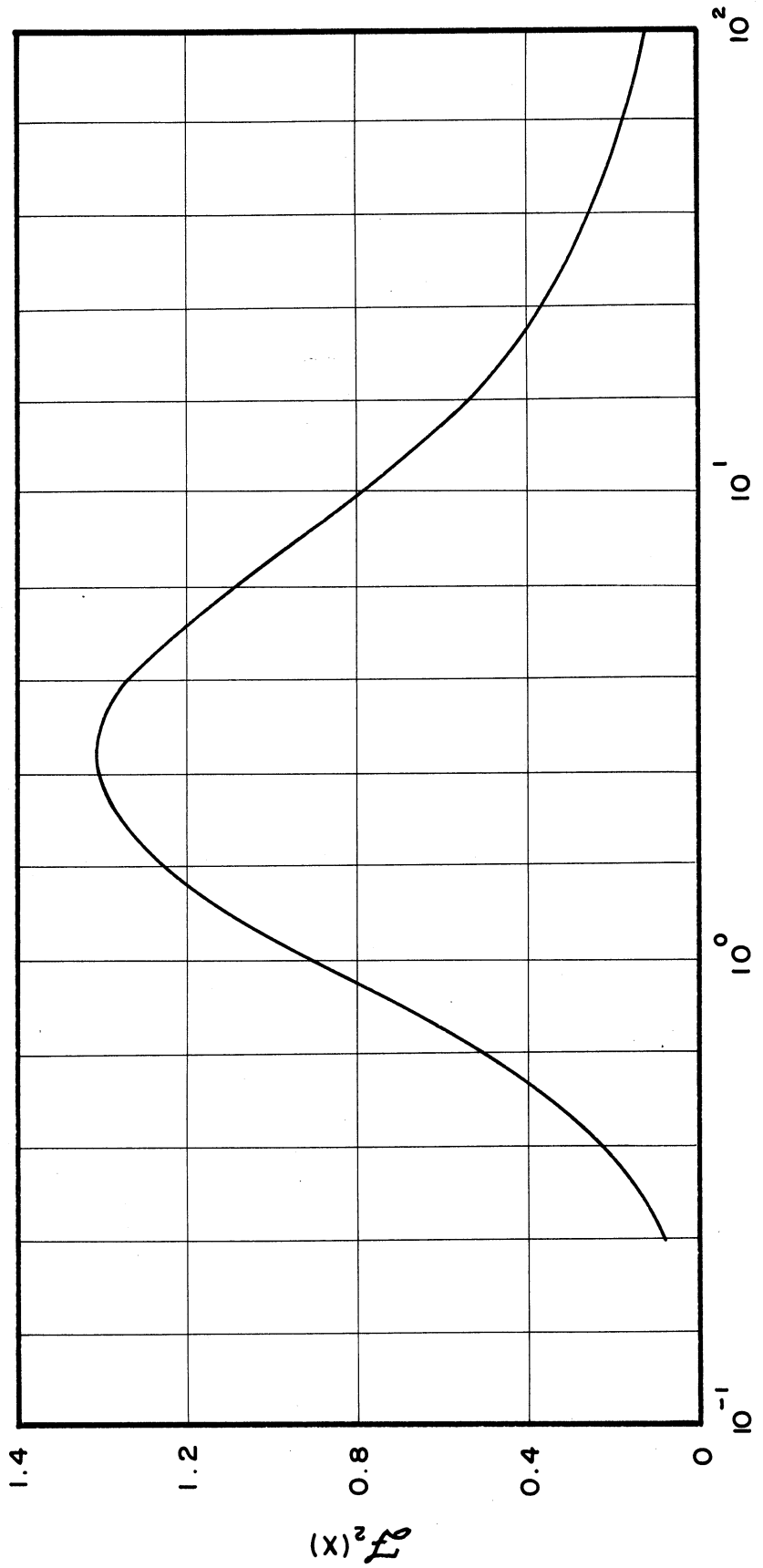

Figure 45. A Graph of the Function $\mathcal{J}_2(x)$.

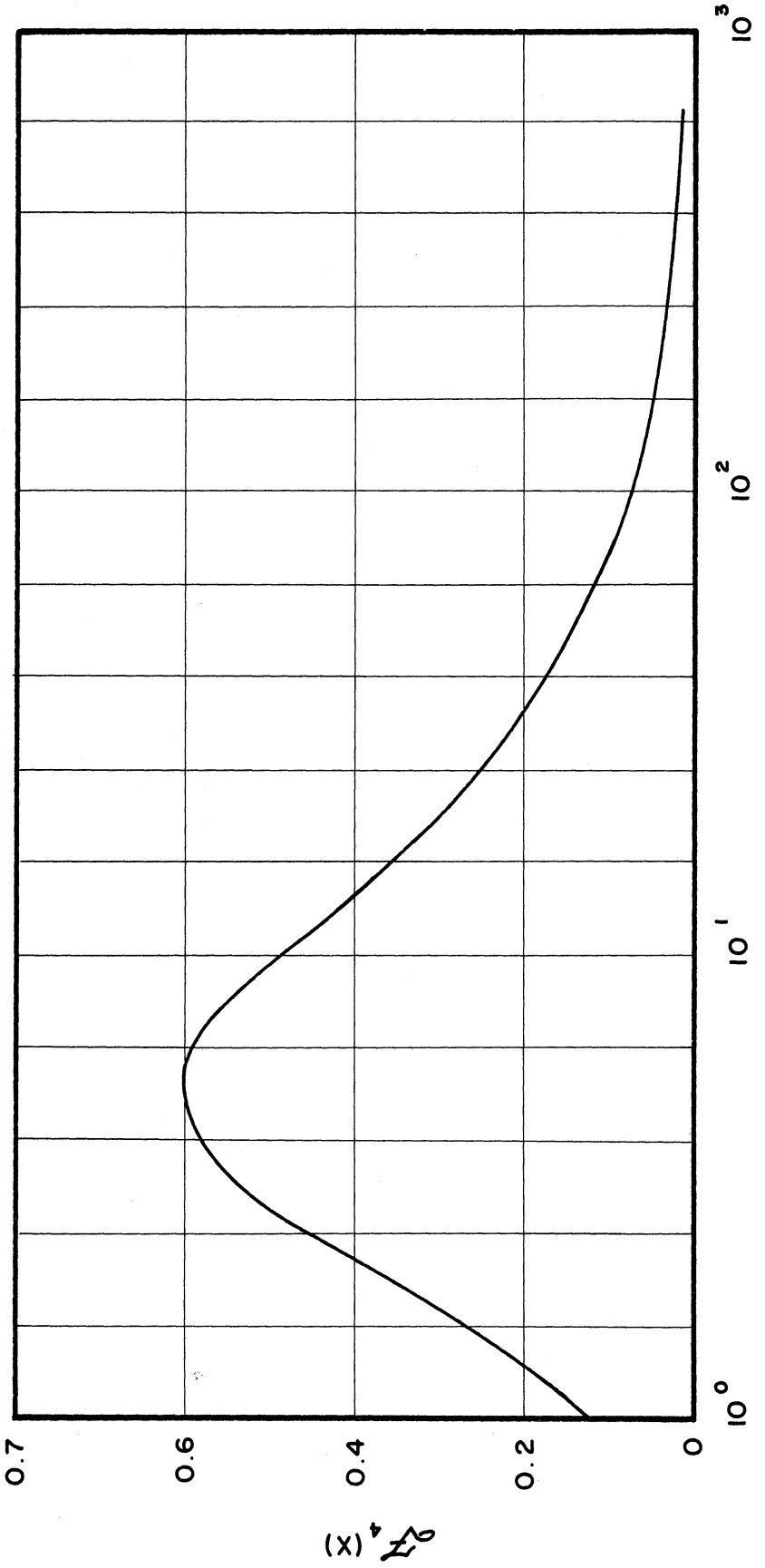

Figure 46. A Graph of the Function $\mathcal{F}_4(x)$.

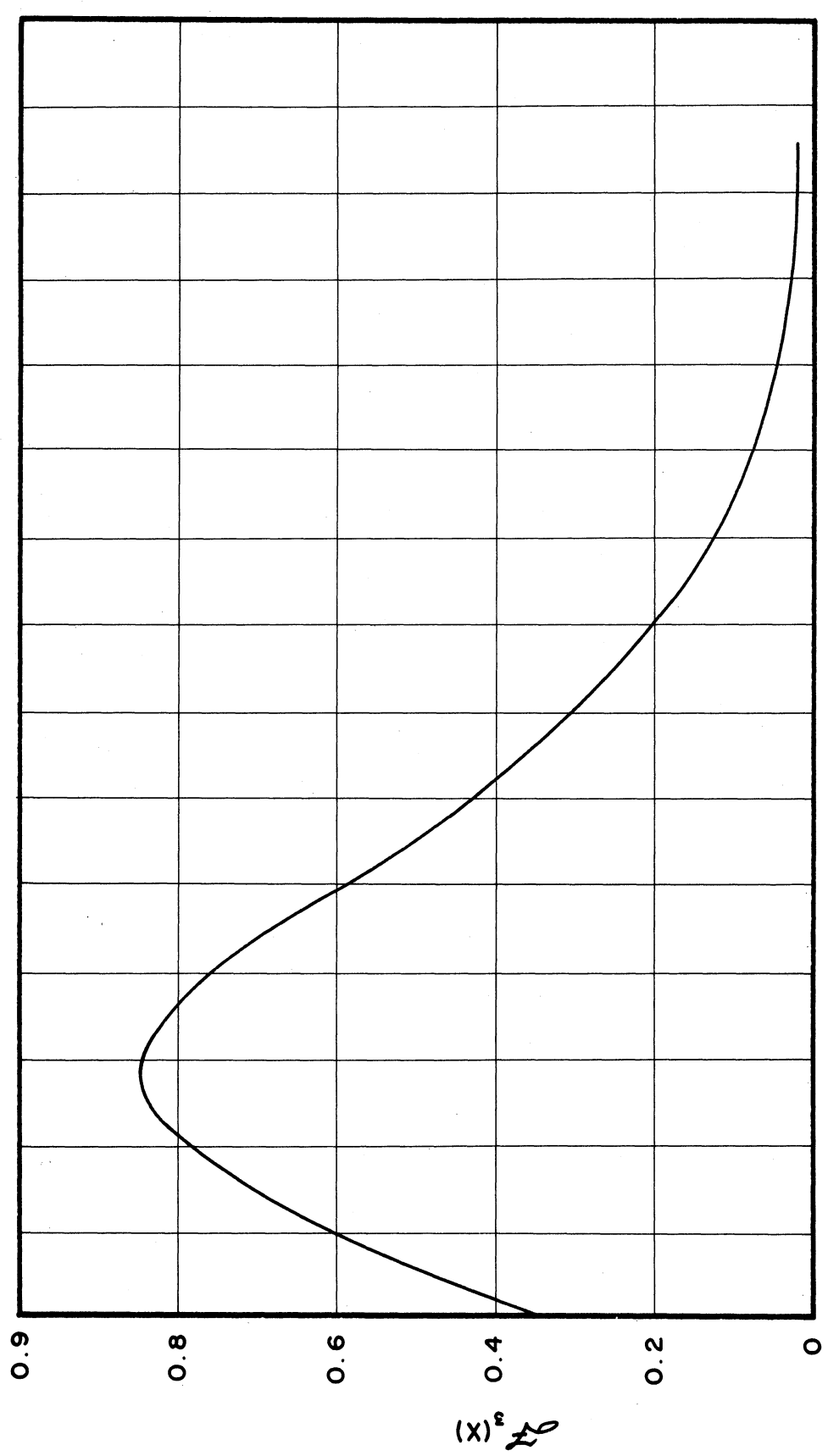

Figure 47. A Graph of The Function $\mathcal{J}_3(x)$.

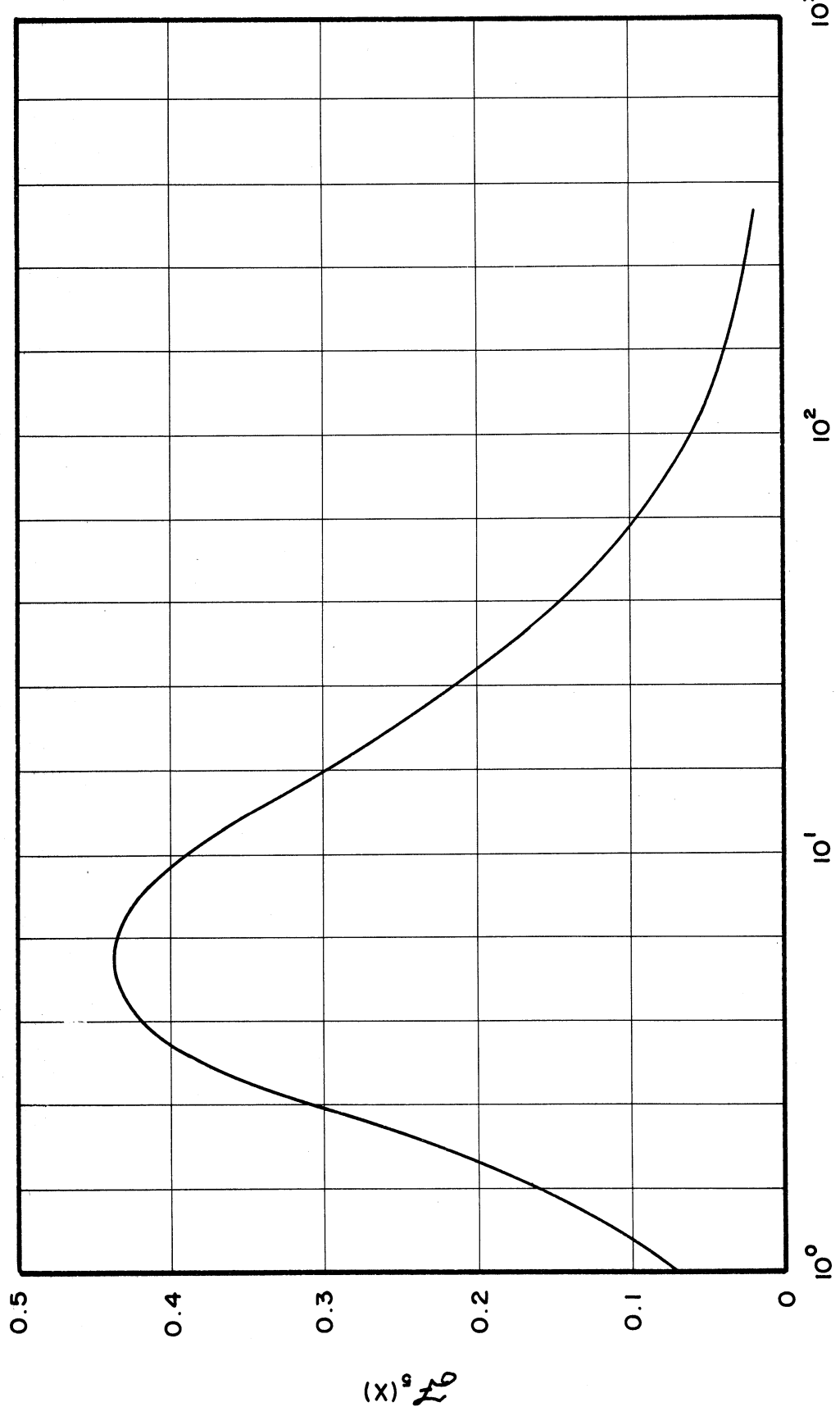

Figure 48. A Graph of The Function $\mathcal{Z}_5(x)$.

For the large K, i.e. Z near 1, it will be more convenient to use Equation (3) with its power series expansions in (1-Z) rather than the slowly converging power series in Z given by Equation (2). From the power series expansion it is obvious that

$$F(A;B|C|Z) \underset{Z \to \infty}{\to} 1$$

Thus for large K

$$F_a(K, \Sigma_t) \underset{K \to \infty}{\to} \frac{4\pi(-i)^a \Gamma^2(\frac{1}{2})\Gamma(a+1)}{2^{a+1}\Gamma^2(\frac{a}{2}+1)} \times \frac{1}{K} \tag{28}$$

Define

$$\mathcal{F}_a(K/\Sigma_t) = \Sigma_t \times F_a(K, \Sigma_t) \tag{29}$$

The function $\mathcal{F}_a(K/\Sigma_t)$ is dimensionless and depends only upon a and K/Σ_t. The functions $\mathcal{F}_a(K/\Sigma_t)$ are displayed graphically in Figures 43 through 48.

APPENDIX I

Part 3

SPHERICAL BESSEL FUNCTIONS

$$j_n(Z) = (-1)^n Z^n \left(\frac{d}{Z dZ}\right)^n \left(\frac{\text{Sin } Z}{Z}\right) \quad (9) \qquad (30)$$

$$j_0(Z) = \frac{\text{Sin } Z}{Z} \qquad (31)$$

$$j_1(Z) = -\frac{\text{Cos } Z}{Z} + \frac{\text{Sin } Z}{Z^2} \qquad (32)$$

$$j_2(Z) = -\frac{\text{Sin } Z}{Z} - 3\frac{\text{Cos } Z}{Z^2} + 3\frac{\text{Sin } Z}{Z^3} \qquad (33)$$

$$j_3(Z) = \frac{\text{Cos } Z}{Z} - 6\frac{\text{Sin } Z}{Z^2} - 15\frac{\text{Cos } Z}{Z^3} + 15\frac{\text{Sin } Z}{Z^4} \qquad (34)$$

$$j_4(Z) = \frac{\text{Sin } Z}{Z} + 10\frac{\text{Cos } Z}{Z^2} - 45\frac{\text{Sin } Z}{Z^3} \qquad (35)$$

$$-105\frac{\text{Cos } Z}{Z^4} + 105\frac{\text{Sin } Z}{Z^5}$$

$$j_5(Z) = -\frac{\text{Cos } Z}{Z} + 15\frac{\text{Sin } Z}{Z^2} + 105\frac{\text{Cos } Z}{Z^3} \qquad (36)$$

$$-420\frac{\text{Sin } Z}{Z^4} - 945\frac{\text{Cos } Z}{Z^5} + 945\frac{\text{Sin } Z}{Z^6}$$

$$j_n(Z) \rightarrow \frac{Z^n}{1.3..(2n+1)} \quad \text{as} \quad Z \rightarrow 0 \tag{37}$$

$$j_n(Z) \rightarrow \frac{\text{Cos}[Z - \frac{\pi}{2}(n+1)]}{Z} \quad \text{as} \quad Z \rightarrow \infty \tag{38}$$

APPENDIX I

Part 4

SPHERICAL HARMONICS

$$Y_l^m(\underline{\Omega}) = \frac{2l+1}{4\pi} \frac{(l-m)!}{(l+m)!} e^{im\theta} P_l^m(\mu) \tag{39}$$

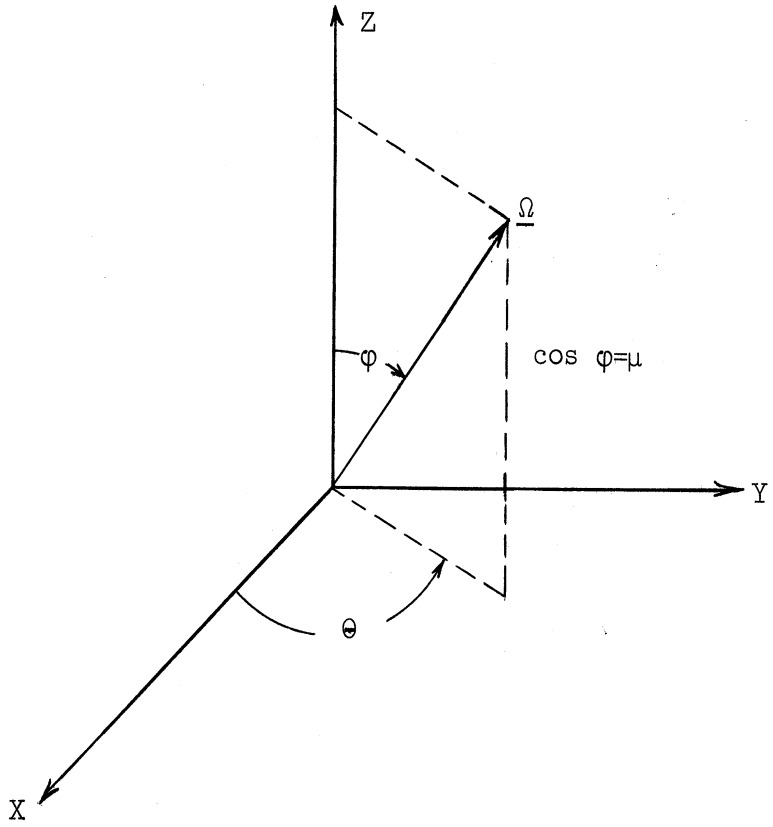

$P_l^m(\mu)$ = Legendre's associated function of the first kind,[7]

$$\int_{\underline{\Omega}} Y_l^m(\underline{\Omega}) \, Y_a^{b*}(\underline{\Omega}) \, d\underline{\Omega} = \delta(a-l)\,\delta(b-m) \tag{40}$$

$$Y_l^{m*}(\underline{\Omega}) = \frac{2l+1}{4\pi} \frac{(l-m)!}{(l+m)!} e^{-im\theta} P_l^m(\mu) \tag{41}$$

Note that $P_l^{-m}(\mu) = \frac{(l-m)!}{(l+m)!} P_l^m(\mu)$ (42)

$$Y_l^{-m}(\underline{\Omega}) = \frac{2l+1}{4\pi} \frac{(l+m)!}{(l-m)!} e^{-im\theta} P_l^{-m}(\mu) \quad (43)$$

$$= \frac{2l+1}{4\pi} \frac{(l-m)!}{(l+m)!} e^{-im\theta} P_l^{|m|}(\mu)$$

Thus

$$Y_l^m(\mu) = \frac{2l+1}{4\pi} \frac{(l-|m|)!}{(l+|m|)!} e^{im\theta} P_l^{|m|}(\mu) \quad (44)$$

Another useful formula is:

$$e^{i\underline{k}\cdot\underline{r}} = \sum_{n=0}^{\infty} (2n+1)\, i^n P_n(\hat{\underline{k}} \cdot \hat{\underline{r}})\, j_n(kr) \quad (9) \quad (45)$$

$$P_n(\hat{\underline{k}} \cdot \hat{\underline{r}}) = \frac{2}{2n+1} \sum_{n=0}^{n} \frac{2n+1}{2} \frac{(n-m)!}{(n+m)!} P_n^m(\cos\varphi_k) \times \quad (46)$$

$$\frac{2n+1}{2} \frac{(n-m)!}{(n+m)!} P_n^m(\cos\varphi_r)\, e^{im(\theta_k - \theta_r)}$$

Thus

$$P_n(\hat{\underline{k}} \cdot \hat{\underline{r}}) = \frac{4\pi}{2n+1} \sum_{m=-n}^{n} Y_n^m(\hat{\underline{k}})\, Y_n^{*m}(\hat{\underline{r}}) \quad (47)$$

Thus Equation (7) becomes:

$$e^{\pm i\underline{k}\cdot\underline{r}} = \sum_{n,m} 4\pi(\pm i)^n\, Y_n^m(\hat{\underline{k}})\, Y_n^{*m}(\hat{\underline{r}})\, j_n(kr) \quad (48)$$

Using the definitions and results of the above work it is easily shown that:

$$Y_a^b(-\underline{\Omega}) = (-1)^a Y_a^b(\underline{\Omega}) \tag{49}$$

$$\sum_{b=-a}^{a} f(b, \ldots\ldots) Y_a^b(\underline{\Omega}) \overset{*}{Y}{}_a^b(\underline{\Omega}') = \tag{50}$$

$$\sum_{b=-a}^{a} f(b, \ldots\ldots) \overset{*}{Y}{}_a^b(\underline{\Omega}) Y_a^b(\underline{\Omega}')$$

if $f(b, \ldots\ldots) = f(-b, \ldots\ldots)$

APPENDIX I

Part 5

NUMERICAL INTEGRATION

Consider the integral of Equation (23) of Appendix I, Part 1.

$$\bar{G}_a(R) = \frac{2}{(2\pi)^2} \int_{K=0}^{\infty} \frac{i^a j_a(KR)\, F_a(K, \Sigma_t)\, K^2}{1 - \frac{\Sigma_s}{4\pi} F_o(K, \Sigma_t)} \tag{51}$$

Examination of the integrand in Equation (51) will show that for large K it becomes

$$\frac{i^a\, j_a(KR)\, F_a(K, \Sigma_t)\, K^2}{1 - \frac{\Sigma_s}{4\pi} F_o(K, \Sigma_t)} \quad \underset{K \to \infty}{\to} \tag{52}$$

$$\frac{\text{Cos}\left[KR - \frac{\pi}{2}(a+1)\right] 4\pi \Gamma^2\left(\frac{1}{2}\right)\Gamma(a+1)}{R \times 2^{a+1}\, \Gamma^2\left(\frac{a}{2}+1\right)}$$

The value of the integral will oscillate with constant amplitude about some mean value as K goes to infinity.

As Davison [3] notes when the Fourier transform integral oscillates, the mean value about which the oscillations take place is the appropriate value for the integral. The upper limit for the integral (51) will then be changed from infinity to some number T. The number T must be large enough so that all of the terms in the integrand of Equation (51) are near to

their assymptotic form. Further T must be selected so that the mean value requirement can be satisfied.

For small K

$$1 - \frac{\Sigma_s}{4\pi} F_o(K, \Sigma_t) \underset{K \to 0}{\to} \frac{\Sigma_a}{\Sigma_t} \tag{53}$$

Due to the denominator the integrand will be changing very rapidly near $K = 0$. On the other hand for large K the integrand becomes a cosine of period R . The integral is evaluated using Simpson's rule in four separate ranges of K . Region one is $0 < K < \Sigma_t$, region two is $\Sigma_t < K < 100\pi/4R$, region three is $100\pi/R4 < K < (602 + 2a)\pi/4R$, region four is $(602 + 2a)\pi/4R < K < (642 + 2a)\pi/4R$. In each of these regions the step size is subdivided until two successive values of the integral over the region are within epsilon of each other. The epsilon is specified as input data and is usually taken as 0.01 .

The end point $K = (642 + 2a)\pi/4R$ is chosen so that the mean value requirement will be satisfied. If the value of the integral over region four is greater than epsilon times the sum of all the other three integrals then a region five is added. Region five is the same length as region four. If the end point of region five is large enough so that all of the terms in the integrand have reached their assymptotic value then the integral over region five will be very small. Successive regions are integrated until the K is large enough so that the integral over the last region is very small.

Let us now examine the assymptotic form of $\bar{G}_a(|\underline{r} - \underline{r}'|)$ for $|\underline{r} - \underline{r}'|$ going to zero.

Rename $|\underline{r} - \underline{r}'| = R$

Rewriting Equation (51)

$$\bar{G}_a(R) = \frac{2i^a}{(2\pi)^2} \int_{K=0}^{\infty} \frac{j_a(KR)\, F_a(K, \Sigma_t)\, K^2}{1 - \frac{\Sigma_s}{4\pi} F_o(K, \Sigma_t)}\, dK \tag{54}$$

Define $Z = KR$; $dK = dZ/R$

$$\bar{G}_a(R) = \frac{2i^a}{(2\pi)^2} \int_{Z=0}^{\infty} \frac{j_a(Z)\, F_a(Z/R, \Sigma_t)\, \frac{Z^2}{R^3}}{1 - \frac{\Sigma_s}{4\pi} F_o(\frac{Z}{R}, \Sigma_t)}\, dZ \tag{55}$$

$\lim_{R \to 0} \bar{G}_a(R) =$

$$\frac{2i^a}{(2\pi)^2} \int_{Z=0}^{\infty} \lim_{R \to 0} \left[\frac{j_a(Z)\, F_a(\frac{Z}{R}, \Sigma_t)\, \frac{Z^2}{R^2}}{1 - \frac{\Sigma_s}{4\pi} F_o(\frac{Z}{R}, \Sigma_t)} \right] dZ \tag{56}$$

Recalling Equation (28)

$$\lim_{R \to 0} F_a(\frac{Z}{R}, \Sigma_t) = \frac{4\pi\, \Gamma^2(\frac{1}{2})\Gamma(a+1)(-i)^a R}{2^{a+1}\Gamma^2(\frac{a}{2}+1)\, Z} \tag{57}$$

Combining equations

$$\lim_{R \to 0} \bar{G}_a(R) = \frac{\Gamma^2(\frac{1}{2})\Gamma(a+1)}{2^{a+1}\, \Gamma^2(\frac{a}{2}+1) 2\pi R^2} \int_{Z=0}^{\infty} j_a(Z) Z dZ \tag{58}$$

$$\int_{Z=0}^{\infty} j_a(Z) Z dZ = \frac{\Gamma(\frac{1}{2})\Gamma(a+2)}{2^{a+1}\Gamma(a+3/2)}\, F(\frac{a+2}{2};\ \frac{a}{2} \middle| a+\frac{3}{2} \middle| 1) \quad (9) \tag{59}$$

Where F is the Hypergeometric Function and equal to

$$F\left(\frac{2+a}{2};\ \frac{a}{2}\middle|a+\frac{3}{2}\middle|1\right) = \frac{\Gamma(a+\frac{3}{2})\Gamma(\frac{1}{2})}{\Gamma(\frac{a+1}{2})\Gamma(\frac{a+3}{2})} \tag{60}$$

Thus

$$\lim_{R \to 0} \bar{G}_a(R) =$$

$$\frac{\Gamma^4(\frac{1}{2})\Gamma(a+1)\Gamma(a+2)}{2^{2a}2\pi\ \Gamma^2(\frac{a}{2}+1)\Gamma(\frac{a+1}{2})\Gamma(\frac{a+3}{2})} \times \frac{1}{R^2}$$

Evaluation of the term on the right of equation shows that

$$\lim_{R \to 0} \bar{G}_a(R) = \frac{1}{R^2} \tag{62}$$

APPENDIX II

NON-ISOTROPIC SCATTERING

Consider a point source of thermal neutrons located at point $\underline{r}'$ in an infinite homogeneous medium. This source is emitting 4π neutrons per second isotropically. Scattering of neutrons in the medium is allowed to be non-isotropic in the laboratory coordinate system.

Assume that the spherical harmonic expansion for $\Sigma_s(\underline{\omega} \to \underline{\Omega})$ is known.

$$\Sigma_s(\underline{\omega} \to \underline{\Omega}) = \sum_{a,\ b} \Sigma_{sa}^{b}\ Y_a^b\ (\underline{\omega})\ \overset{*b}{Y}_a\ (\underline{\Omega}) \tag{1}$$

The usual representation for $\Sigma_s\ (\underline{\omega} \to \underline{\Omega})$ is

$$\Sigma_s\ (\underline{\omega} \to \underline{\Omega}) = \sum_{l=0}^{l} \frac{2\,l+1}{4\pi}\ P_l\ (\underline{\omega} \cdot \underline{\Omega})\ \Sigma_{sl} \tag{2}$$

Where the $P_l\ (\underline{\omega} \cdot \underline{\Omega})$ are the Legendre polynomials. In this case

$$\Sigma_{so} = \int_{\underline{\Omega}} \Sigma_s\ (\underline{\omega} \to \underline{\Omega})\ d\underline{\Omega} \tag{3}$$

The average of the cosine of the scattering angle $\overline{\mu}$ is defined

$$\overline{\mu} = \frac{\int_{\underline{\Omega}} \Sigma_s(\underline{\omega} \to \underline{\Omega})\ \underline{\omega} \cdot \underline{\Omega} d\underline{\Omega}}{\int_{\underline{\Omega}} \Sigma_s(\underline{\omega} \to \underline{\Omega})\ d\underline{\Omega}} = \frac{\Sigma_{sl}}{\Sigma_{so}} \tag{4}$$

Using the results of Appendix I, Part 4, Equation (2) becomes:

$$\Sigma_s(\underline{\omega} \to \underline{\Omega}) = \sum_{a,b}^{l} \Sigma_{sa}\ Y_a^b\ (\underline{\omega})\ \overset{*}{Y}_a^b\ (\underline{\Omega}) \tag{5}$$

Where $\Sigma_{sl} = \Sigma_{so} \times \overline{\mu}$ and Σ_{so} is the atomic density times the isotropic

component of the scattering cross-section which is found tabulated in Nuclear Cross Sections.(6)

Note that all spatial integrations in this appendix extend over all space, contrary to the convention used in the other parts of this paper.

The transport equation for the system outlined above may be obtained by integrating Equation (4) of Chapter I over all $\underline{\Omega}$ to obtain:

$$\underline{\Omega} \cdot \nabla G(\underline{r}' \rightarrow \underline{r}, \underline{\Omega}) + \Sigma_t G(\underline{r}' \rightarrow \underline{r}, \underline{\Omega}) - \tag{6}$$

$$- \int_{\underline{\omega}} \Sigma_s (\underline{\omega} \rightarrow \underline{\Omega}) G(\underline{r}' \rightarrow \underline{r}, \underline{\omega}) \, d\underline{\omega} = \delta(\underline{r}' - \underline{r})$$

Using the same conversion as is used in Appendix I, Part 1

$$G(\underline{r}' \rightarrow \underline{r}, \underline{\Omega}) =$$

$$= \int_{\underline{r}'', \underline{\Omega}} \left[\frac{e^{-\Sigma_t |\underline{r}''-\underline{r}|}}{|\underline{r}''-\underline{r}|^2} \delta(\underline{\Omega}'' - \underline{\Omega}) \delta(\underline{\Omega} - [\underline{r} \overset{\Lambda}{-} \underline{r}'']) \right] x \tag{7}$$

$$\left[\int_{\underline{\omega}} \Sigma_s(\underline{\omega} \rightarrow \underline{\Omega}'') G(\underline{r}' \rightarrow \underline{r}, \underline{\omega}) \, d\underline{\omega} + \delta(\underline{r}' - \underline{r}'') \right] d\underline{r}'' d\underline{\Omega}''$$

$$G(\underline{r}' \rightarrow \underline{r}, \underline{\Omega}) = \int_{\underline{r}''} \frac{e^{-\Sigma_t |\underline{r}''-\underline{r}|}}{|\underline{r}''-\underline{r}|^2} \delta(\underline{\Omega} - [\underline{r} \overset{\Lambda}{-} \underline{r}'']) \quad x$$

$$\int_{\underline{\omega}} \Sigma_s(\underline{\omega} \rightarrow \underline{\Omega})\ G(\underline{r}' \rightarrow \underline{r}'',\ \underline{\omega})\ d\underline{\omega}d\underline{r}'' +$$

$$+ \frac{e^{-\Sigma_t|\underline{r}'-\underline{r}|}}{|\underline{r}'-\underline{r}|^2}\delta(\underline{\Omega} - [\underline{r} \overset{\Lambda}{-} \underline{r}'])$$

Now expand

$$G(\underline{r}' \rightarrow \underline{r},\ \underline{\Omega}) = \sum_{a,b} G_a^b\ (\underline{r}',\ \underline{r})\ Y_a^b\ (\underline{\Omega}) \tag{8}$$

Combine Equations (5), (8), and (9)

$$\sum_{a,b} G_a^b\ (\underline{r}',\ \underline{r})\ Y_a^b\ (\underline{\Omega}) = \int_{\underline{r}''} \frac{e^{-\Sigma_t|\underline{r}''-\underline{r}|}}{|\underline{r}''-\underline{r}|^2}\ \delta(\underline{\Omega} - [\underline{r} \overset{\Lambda}{-} \underline{r}''])\ \ x$$

$$\int_{\underline{\omega}} \sum_{l,m}^{l} Y_l^{*m}\ (\underline{\omega})\ Y_l^m\ (\underline{\Omega})\ \Sigma_{sl} \sum_{a,b} G_a^b\ (\underline{r}',\underline{r}'')\ Y_a^b\ (\underline{\omega})\ d\underline{\omega}d\underline{r}'' \tag{9}$$

$$+ \frac{e^{-\Sigma_t|\underline{r}'-\underline{r}|}}{|\underline{r}'-\underline{r}|^2}\ \ x\ \delta(\underline{\Omega} - [\underline{r} \overset{\Lambda}{-} \underline{r}'])$$

$$\sum_{a,b} G_a^b\ (\underline{r}',\ \underline{r})\ Y_a^b\ (\underline{\Omega}) = \int_{\underline{r}''} \frac{e^{-\Sigma_t|\underline{r}''-\underline{r}|}}{|\underline{r}''-\underline{r}|^2}\ \delta(\underline{\Omega}-[\underline{r} \overset{\Lambda}{-} \underline{r}''])$$

(10)

$$x \sum_{l,m}^{l} \Sigma_{sl}\ G_l^m\ (\underline{r}',\ \underline{r}'')\ Y_l^m\ (\underline{\Omega})\ d\underline{r}'' +$$

$$+ \frac{e^{-\Sigma_t|\underline{r}-\underline{r}'|}}{|\underline{r} - \underline{r}'|^2}\delta(\underline{\Omega} - [\underline{r} \overset{\Lambda}{-} \underline{r}'])$$

Now multiply by $\overset{*}{Y}{}^{D}_{C}(\underline{\Omega})$ and integrate over all $\underline{\Omega}$.

$$G^{D}_{C}(\underline{r}', \underline{r}) = \int_{\underline{r}''} \frac{e^{-\Sigma_t|\underline{r}-\underline{r}''|}}{|\underline{r}'' - \underline{r}|^2} \times \sum_{l,m}^{l} \Sigma_{sl} \times \tag{11}$$

$$G^{m}_{l}(\underline{r}', \underline{r}'') Y^{m}_{l}(\underline{r} \overset{\Lambda}{-} \underline{r}'') \overset{*}{Y}{}^{D}_{C}(\underline{r} \overset{\Lambda}{-} \underline{r}'') +$$

$$\frac{e^{-\Sigma_t|\underline{r}'-\underline{r}|}}{|\underline{r}'-\underline{r}|^2} \overset{*}{Y}{}^{D}_{C}(\underline{r} \overset{\Lambda}{-} \underline{r}')$$

For convenience let $\underline{r}' = 0$. Now take the Fourier transform of the above equation and define

$$G^{D}_{C}(\underline{K}) = \frac{1}{(2\pi)^{3/2}} \int_{\underline{r}} G^{D}_{C}(\underline{r})\, e^{-i\underline{K}\cdot\underline{r}}\, d\underline{r} \tag{12}$$

$$G^{D}_{C}(\underline{K}) = \frac{1}{(2\pi)^{3/2}} \int_{\underline{r}'',\underline{r}} \frac{e^{-\Sigma_t|\underline{r}''-\underline{r}|-i\underline{K}\cdot\underline{r}}}{|\underline{r}''-\underline{r}|^2} \times \sum_{l,m}^{l} \Sigma_{sl} \times \tag{13}$$

$$G^{m}_{l}(\underline{r}'') Y^{m}_{l}(\underline{r} \overset{\Lambda}{-} \underline{r}'') \overset{*}{Y}{}^{D}_{C}(\underline{r} \overset{\Lambda}{-} \underline{r})\, d\underline{r}''d\underline{r} +$$

$$+ \frac{1}{(2\pi)^{3/2}} \int_{\underline{r}} \frac{e^{-\Sigma_t r - i\underline{K}\cdot\underline{r}}}{r^2} \overset{*}{Y}{}^{D}_{C}(\overset{\Lambda}{\underline{r}})\, d\underline{r}$$

In Appendix I, Part 1 it is noted that

$$\int_{\underline{r}} \frac{e^{-\Sigma_t r - i\underline{K}\cdot\underline{r}}}{r^2} \; Y_C^{*D}\left(\hat{\underline{r}}\right) d\underline{r} = Y_C^{*D}\left(\hat{\underline{K}}\right) F_c\left(K, \Sigma_t\right) \tag{14}$$

The function $F_c\left(K, \Sigma_t\right)$ is discussed in Appendix I, Part 2.

Using Equation (13)

$$G_o^o\left(\underline{K}\right) = \frac{1}{(2\pi)^{3/2}} \int_{\underline{r}'',\underline{r}} \frac{e^{-\Sigma_t|\underline{r}''-\underline{r}| - i\underline{K}\cdot\underline{r}}}{|\underline{r}''-\underline{r}|^2} \; x \sum_{l,m}^{l}$$

$$\Sigma_{sl}\, G_l^m\left(\underline{r}''\right) Y_l^m\left(\underline{r} - \underline{r}''\right) Y_o^{*o}\left(\underline{r} - \underline{r}''\right) d\underline{r}''d\underline{r} \; - \tag{15}$$

$$+ \frac{1}{(2\pi)^{3/2}} \int_{\underline{r}} \frac{e^{-\Sigma_t r - i\underline{K}\cdot\underline{r}}}{r^2} \; Y_o^{*o}\left(\hat{\underline{r}}\right) d\underline{r}$$

Let $\underline{x} = \underline{r} - \underline{r}''$. Now examine the integral

$$\int_{\underline{r}} \frac{e^{-\Sigma_t|\underline{r}-\underline{r}''| - i\underline{K}\cdot\underline{r}}}{|\underline{r}-\underline{r}''|^2} \; Y_l^m\left(\underline{r} - \underline{r}''\right) Y_o^{*o}\left(\underline{r} - \underline{r}''\right) d\underline{r} =$$

$$e^{-i\underline{K}\cdot\underline{r}''} \int_{\underline{x}} \frac{e^{-\Sigma_t x - i\underline{K}\cdot\underline{x}}}{x^2} \; Y_l^m\left(\hat{\underline{x}}\right) \frac{1}{\sqrt{4\pi}}\, d\underline{x} = \tag{16}$$

$$e^{-i\underline{K}\cdot\underline{r}''} \; Y_l^m\left(\hat{\underline{K}}\right) F_e\left(K, \Sigma_t\right) \; x \; \frac{1}{\sqrt{4\pi}}$$

Thus

$$G_o^o(\underline{K}) = \frac{1}{(2\pi)^{3/2}} \int e^{-i\underline{K}\cdot\underline{r}''} \sum_{l,m}^{l} \Sigma_{sl} G_l^m(\underline{r}'') Y_l^m(\hat{\underline{K}}) F_l(K, \Sigma_t)\, d\underline{r}'' + \frac{1}{(2\pi)^{3/2}} Y_o^o(\hat{\underline{K}}) F_o(K, \Sigma_t) \tag{17}$$

$$G_o^d(\underline{K}) = \frac{1}{\sqrt{4\pi}} \sum_{l,m}^{l} \Sigma_{sl} G_l^m(\underline{K}) Y_l^m(\hat{\underline{K}}) F_l(K, \Sigma_t) + \frac{1}{(2\pi)^{3/2}} Y_o^o(\hat{\underline{K}}) F_o(K, \Sigma_t) \tag{18}$$

Assume that terms that make a contribution of the order of $(\Sigma_{sl})^2$ are small and may be neglected compared to terms of the order of Σ_{sl} in the calculation of $G_o^o(\underline{K})$.

Using the same procedure as was used above it can be shown that

$$G_l^m(\underline{K}) = \Sigma_{so} G_o^o(\underline{K}) \frac{1}{\sqrt{4\pi}} Y_l^{*m}(\underline{K}) F_l(K, \Sigma_t) + \frac{1}{(2\pi)^{3/2}} Y_l^{*m}(\hat{\underline{K}}) F_l(K, \Sigma_t) \tag{19}$$

Combining equations to solve for $G_o^o(\underline{K})$

$$G_o^o(\underline{K}) = \frac{1}{4\pi}\Sigma_{so} G_o^o(\underline{K}) F_o^o(K, \Sigma_t) + \tag{20}$$

$$\frac{1}{4\pi}\Sigma_{so}\Sigma_{s1} G_o^o(\underline{K}) F_1^2(K, \Sigma_t) \sum_{m=-1}^{1} Y_1^m(\hat{\underline{K}}) Y_1^{*m}(\hat{\underline{K}})$$

$$\frac{1}{(2\pi)^{3/2}} \frac{1}{\sqrt{4\pi}}\Sigma_{s1} F_1^2(K, \Sigma_t) \sum_{m=-1}^{1} Y_1^m(\hat{\underline{K}}) Y_1^{*m}(\hat{\underline{K}})$$

$$+ \frac{1}{(2\pi)^{3/2}} Y_o^o(\hat{\underline{K}}) F_o(K, \Sigma_t)$$

$$G_o^o(\underline{K}) = \frac{1}{(2\pi)^{3/2}} Y_o^o(\hat{\underline{K}}) \times \tag{21}$$

$$\frac{F_o(K, \Sigma_t) + \frac{3}{4\pi}\Sigma_{s1} F_1^2(K, \Sigma_t)}{1 - \frac{\Sigma_{so}}{4\pi} F_o(K, \Sigma_t) - \frac{3}{(4\pi)^2}\Sigma_{so}\Sigma_{s1} F_1^2(K, \Sigma_t)}$$

Now take the inverse Fourier transform.

$$G_o^o(\underline{r}) = \int_{\underline{K}} \frac{1}{(2\pi)^{3/2}} Y_o^o(\hat{\underline{K}}) e^{-i\underline{K}\cdot\underline{r}} \times \tag{22}$$

$$\frac{F_o(K, \Sigma_t) + \frac{3}{4\pi}\Sigma_{s1} F_1^2(K, \Sigma_t)}{1 - \frac{\Sigma_{so}}{4\pi} F_o(K, \Sigma_t) - \frac{3}{(4\pi)^2}\Sigma_{so}\Sigma_{s1} F_1^2(K, \Sigma_t)} d\underline{K}$$

Now use the results of Appendix I, Part 4.

$$G_o^o(\underline{r}) = \frac{1}{(2\pi)^3} \int_{K=0}^{\infty} \tag{23}$$

$$\frac{\left[F_o(K, \Sigma_t) + \frac{3}{4\pi}\Sigma_{s1} F_1^2(K, \Sigma_t)\right] K^2}{1 - \frac{\Sigma_{so}}{4\pi} F_o(K, \Sigma_t) - \frac{3}{(4\pi)^2}\Sigma_{so}\Sigma_{s1} F_1^2(K, \Sigma_t)} \; x$$

$$\int_{\underline{\Lambda}K} Y_o^o(\underline{\Lambda}K) \sum_{l,m} 4\pi (i)^l Y_l^{*m}(\underline{\Lambda}K) Y_l^m(\underline{\Lambda}r) \; x$$

$$j_l(Kr)\, d\underline{\Lambda}K dK$$

$$G_o^o(\underline{r}) = \frac{2}{(2\pi)^2} Y_o^o(\underline{\Lambda}r) \; x \int_{K=0}^{\infty} \tag{24}$$

$$\frac{\left[F_o(K, \Sigma_t) + \frac{3}{4\pi}\Sigma_{s1} F_1^2(K, \Sigma_t)\right] K^2 j_o(Kr)}{1 - \frac{\Sigma_{so}}{4\pi} F_o(K, \Sigma_t) - \frac{3}{(4\pi)^2}\Sigma_{so}\Sigma_{s1} F_1^2(K, \Sigma_t)} \, dK$$

To regain the $\underline{r}'$ dependance set $\underline{r} = \underline{r} - \underline{r}'$.

$$G_o^o(\underline{r} - \underline{r}') = \frac{2}{(2\pi)^2} Y_o^o(\underline{r} - \underline{\Lambda}\underline{r}') \int_{K=0}^{\infty} j_o(K|\underline{r} - \underline{r}'|) K^2 \; x \tag{25}$$

$$\frac{F_o(K, \Sigma_t) + \frac{3}{4\pi} \Sigma_{s1} F_1^2(K, \Sigma_t)}{1 - \frac{\Sigma_{so}}{4\pi} F_o(K, \Sigma_t) - \frac{3}{(4\pi)^2} \Sigma_{so} \Sigma_{s1} F_1^2(K, \Sigma_t)} \, dK$$

APPENDIX III

CONVERGENCE

Consider two elements $\Psi_n(\underline{r}, \underline{\Omega})$ and $\Psi_m(\underline{r}, \underline{\Omega})$ of the series generated by successive application of Equation (6) Chapter I

$$\Psi_n(\underline{r}, \underline{\Omega}) = (\Sigma_t^D - \Sigma_t) \int_{\underline{r}', \underline{\Omega}'} \Phi(\underline{r}, \underline{\Omega})\, G(\underline{r}', \underline{\Omega}' \to \underline{\Omega})\, d\underline{r}' d\underline{\Omega}'' \qquad (1)$$

$$+ \frac{(\Sigma_s - \Sigma_s^D)}{4\pi} \int_{\underline{r}', \underline{\Omega}'} G(\underline{r}', \underline{\Omega}' \to \underline{r}, \underline{\Omega}) \int_{\underline{\omega}} \Phi(\underline{r}', \underline{\omega})\, d\underline{\omega} d\underline{r}' d\underline{\Omega}' +$$

$$+ \int_{\underline{r}', \underline{\Omega}'} \left[S(\underline{r}', \underline{\Omega}') - S^D(\underline{r}', \underline{\Omega}'') \right] G(\underline{r}', \underline{\Omega}' \to \underline{r}, \underline{\Omega})\, d\underline{r}' d\underline{\Omega}' +$$

$$(\Sigma_t - \Sigma_t^D) \int_{\underline{r}', \underline{\Omega}'} \Psi_{n-1}(\underline{r}', \underline{\Omega}'')\, G(\underline{r}', \underline{\Omega}' \to \underline{r}, \underline{\Omega})\, d\underline{r}' d\underline{\Omega}' -$$

$$- \frac{\Sigma_s - \Sigma_s^D}{4\pi} \int_{\underline{r}', \underline{\Omega}'} G(\underline{r}', \underline{\Omega}' \to \underline{r}, \underline{\Omega}) \int_{\underline{\omega}} \Psi_{n-1}(\underline{r}', \underline{\omega})\, d\underline{\omega} d\underline{r}' d\underline{\Omega}'$$

By changing the n's to m's in Equation (1) an equation in $\Psi_m(\underline{r}, \underline{\Omega})$ is obtained. Now subtracting the equation for $\Psi_m(\underline{r}, \underline{\Omega})$ from the equation for $\Psi_n(\underline{r}, \underline{\Omega})$ one obtains:

$$\Psi_n(\underline{r}, \underline{\Omega}) - \Psi_m(\underline{r}, \underline{\Omega}) = (\Sigma_t - \Sigma_t^D) \quad x \qquad (2)$$

$$\int_{\underline{r}',\underline{\Omega}'} (\Psi_{n-1}(\underline{r}', \underline{\Omega}') - \Psi_{m-1}(\underline{r}', \underline{\Omega}')\ G(\underline{r}', \underline{\Omega}' \rightarrow \underline{r}, \underline{\Omega})\ d\underline{r}'d\underline{\Omega}' -$$

$$- \frac{\Sigma_s - \Sigma_s^D}{4\pi} \int_{\underline{r}',\underline{\Omega}'} G(\underline{r}', \underline{\Omega}' \rightarrow \underline{r}, \underline{\Omega}) \int_{\underline{\omega}} (\Psi_{n-1}(\underline{r}', \underline{\omega}) - \Psi_{m-1}(\underline{r}', \underline{\omega}))d\underline{\omega}d\underline{r}'d\underline{\Omega}'$$

Define $\| A(\underline{r}, \underline{\Omega}) \| = \underset{\text{Max. any } \underline{\Omega}}{\text{Max. any } \underline{r}}$ of $| A(\underline{r}, \underline{\Omega}) |$ (3)

$$\| \Psi_n(\underline{r}, \underline{\Omega}) - \Psi_m(\underline{r}, \underline{\Omega}) \| = \| (\Sigma_t - \Sigma_t^D)\ x \tag{4}$$

$$\int_{\underline{r}',\underline{\Omega}'} (\Psi_{n-1}(\underline{r}', \underline{\Omega}') - \Psi_{m-1}(\underline{r}', \underline{\Omega}'))\ G(\underline{r}', \underline{\Omega}' \rightarrow \underline{r}, \underline{\Omega})\ d\underline{r}'d\underline{\Omega}' -$$

$$- \frac{\Sigma_s - \Sigma_s^D}{4\pi} \int_{\underline{r}',\underline{\Omega}'} G(\underline{r}', \underline{\Omega}' \rightarrow \underline{r}, \underline{\Omega}) \int_{\underline{\omega}} (\Psi_{n-1}(\underline{r}', \underline{\omega}) - \Psi_{m-1}(\underline{r}', \underline{\omega}))d\underline{\omega}d\underline{r}'d\underline{\Omega}' \|$$

$$< \| \Psi_{n-1}(\underline{r}, \underline{\Omega}) - \Psi_{m-1}(\underline{r}, \underline{\Omega}) \| \times |(\Sigma_t - \Sigma_t^D) - \Sigma_s + \Sigma_s^D| \times$$

$$\| \int_{\underline{r}',\underline{\Omega}'} G(\underline{r}', \underline{\Omega}' \rightarrow \underline{r}, \underline{\Omega})\ d\underline{r}'d\underline{\Omega}' \|$$

So the mapping of elements (or functions) $\Psi_{n-1}(\underline{r}, \underline{\Omega})$ into elements $\Psi_n(\underline{r}, \underline{\Omega})$ which Equation (1) defines will be a contraction mapping if:

$$| \Sigma_a - \Sigma_a^D | \times \| \int_{\underline{r}',\underline{\Omega}'} G(\underline{r}', \underline{\Omega}' \rightarrow \underline{r}, \underline{\Omega})\ d\underline{r}'d\underline{\Omega}' \| < 1 \tag{5}$$

or if:

$$\| \int_{\underline{r}',\underline{\Omega}'} G(\underline{r}', \underline{\Omega}' \rightarrow \underline{r}, \underline{\Omega})\, d\underline{r}' d\underline{\Omega}' \| < \frac{1}{|\Sigma_a - \Sigma_a^D|} \tag{6}$$

Using the reciprocity theorem

$$\Sigma_a \int_{\underline{r}'} G(\underline{r}' \rightarrow \underline{r}, \underline{\Omega})\, d\underline{r}' = \Sigma_a \int_{\underline{r}'} G(\underline{r}, -\underline{\Omega} \rightarrow \underline{r}')\, d\underline{r}' = \tag{7}$$

the integral over the detector volume of the rate of capture of neutrons by the moderator due to a source of neutrons at point $\underline{r}$ emitting one neutron per second in direction $-\underline{\Omega}'$.

Clearly the integral over a finite volume of the capture rate is less than one for a source emitting one neutron per second. Thus

$$\int_{\underline{r}'} G(\underline{r}' \rightarrow \underline{r}, \underline{\Omega})\, d\underline{r}' < \frac{1}{\Sigma_a} \tag{8}$$

and Equation (8) holds for all detector sizes and compositions, thus

$$\int_{\underline{r}'} G(\underline{r}' \rightarrow \underline{r}, \underline{\Omega})\, d\underline{r}' < \frac{1}{\Sigma_a} < \frac{1}{|\Sigma_a - \Sigma_a^D|} \tag{9}$$

Next consider two elements $\psi_n(\underline{r})$ and $\psi_m(\underline{r})$ of the series generated by successive application of Equation (15) Chapter I

$$\psi_n(\underline{r}) = \frac{\Sigma_a^D}{4\pi} \varphi \int_{\underline{r}'} G(\underline{r}' \to \underline{r})\, d\underline{r}' - \tag{10}$$

$$- \frac{(\Sigma_a^D - \Sigma_a)}{4\pi} \int_{\underline{r}'} \psi_{n-1}(\underline{r}')\, G(\underline{r}' \to \underline{r})\, d\underline{r}'$$

and

$$\psi_m(\underline{r}) = \frac{\Sigma_a^D}{4\pi} \varphi \int_{\underline{r}'} G(\underline{r}' \to \underline{r})\, d\underline{r}' - \tag{11}$$

$$- \frac{(\Sigma_a^D - \Sigma_a)}{4\pi} \int_{\underline{r}'} \psi_{m-1}(\underline{r}')\, G(\underline{r}' \to \underline{r})\, d\underline{r}'$$

Subtracting Equation (11) from (10)

$$\psi_n(\underline{r}) - \psi_m(\underline{r}) = (\Sigma_a - \Sigma_a^D) \times \frac{1}{4\pi} \tag{12}$$

$$\int_{\underline{r}'} (\psi_{n-1}(\underline{r}') - \psi_{m-1}(\underline{r}'))\, G(\underline{r}' \to \underline{r})\, d\underline{r}'$$

$$\| \psi_n(\underline{r}) - \psi_m(\underline{r}) \| = |\Sigma_a - \Sigma_a^D| \times \frac{1}{4\pi} \tag{13}$$

$$\| \int_{\underline{r}'} (\psi_{n-1}(\underline{r}') - \psi_{m-1}(\underline{r}'))\, G(\underline{r}' \to \underline{r})\, d\underline{r}' \| < \tag{14}$$

$$\frac{|\Sigma_a - \Sigma_a^D|}{4\pi} \times \| \psi_{n-1}(\underline{r}) - \psi_{m-1}(\underline{r}) \| \times \| \int_{\underline{r}'} G(\underline{r}' \to \underline{r})\, d\underline{r}' \|$$

Thus Equation (10) will define a contraction mapping if

$$\frac{|\Sigma_a - \Sigma_a^D|}{4\pi} \int_{\underline{r}'} G(\underline{r}' \to \underline{r})\, d\underline{r}' < 1 \tag{15}$$

Using the reciprocity theorem

$$\frac{1}{4\pi} \Sigma_a \int_{\underline{r}'} G(\underline{r}' \to \underline{r})\, d\underline{r}' = \frac{\Sigma_a}{4\pi} \int_{\underline{r}'} G(\underline{r} \to \underline{r}')\, d\underline{r}' = \tag{16}$$

the integral over the detector volume of the rate of capture of neutrons by the surrounding medium due to a source of neutrons at point $\underline{r}$ emitting isotropically one neutron per second at any point $\underline{r}$ in the surrounding medium.

Clearly the integral over a finite volume of the capture rate is less than one. Thus

$$\frac{1}{4\pi} \int_{\underline{r}'} G(\underline{r}' \to \underline{r})\, d\underline{r}' \leqslant \frac{1}{\Sigma_a} \tag{17}$$

$$\text{and } \frac{1}{4\pi} \int_{\underline{r}'} G(\underline{r}' \to \underline{r})\, d\underline{r}' \leqslant \frac{1}{|\Sigma_a - \Sigma_a^D|} \text{ for all} \tag{18}$$

detector sizes and compositions.

Both Equation (1) and (10) are of the form:

$$f(x) = Pf(x) \text{ where P is an operator.} \tag{19}$$

The iterative equation is:

$$f_n(x) = P\, f_{n-1}(x) \tag{20}$$

Define $\| f_n(x) \| = \text{Max. any } x \text{ of } | f_n(x) |$ (21)

Subtracting Equation (19) from (20) and taking norms one obtains:

$$\| f_n(x) - f(x) \| = \| P(f_{n-1}(x)\, f(x)) \| \quad \text{further} \tag{22}$$

$$\| f_n(x) - f_m(x) \| = \| P(f_{n-1}(x) - f_{m-1}(x) \| \tag{23}$$

$$\| P \| = K < 1 \tag{24}$$

It has been shown that for the operators P used here:

$$\| f_n(x) - f(x) \| \leqslant K \| f_{n-1}(x) - f(x) \| \tag{25}$$

for all detector sizes and compositions where K is some number less than one. With successive applications of equation one finds:

$$\| f_n(x) - f(x) \| \leqslant K^n \| f_o(x) - f(x) \| \tag{26}$$

Where $f_o(x)$ is some arbitrary initial guess at the solution to Equation (20) and $f(x)$ is the solution to Equation (19) .

Clearly as n goes to infinity Equation (26) requires that the quantity $\| f_n(x) - f(x) \|$ go to zero. Thus as n goes to infinity the solution of the iterative equation, Equation (20), approaches the solution $f(x)$ of the original Equation (19) .

Thus it has been demonstrated that the series generated by Equation (1) and (10) converge, and that they converge respectively to the solutions of Equations (5) and (13) in Chapter I .

APPENDIX IV

GEOMETRY AND GRID POINT NETWORK

The basic shape of the detector will be a right circular cylinder with radius $R\theta$ and height 2 x ZE

Cylinderical grid surfaces will be located around the central axis and will be spaced a distance $\Delta R\theta$ from one another. Plane grid surfaces will be located perpendicular to the central axis and will be spaces at distances ΔZE from one another.

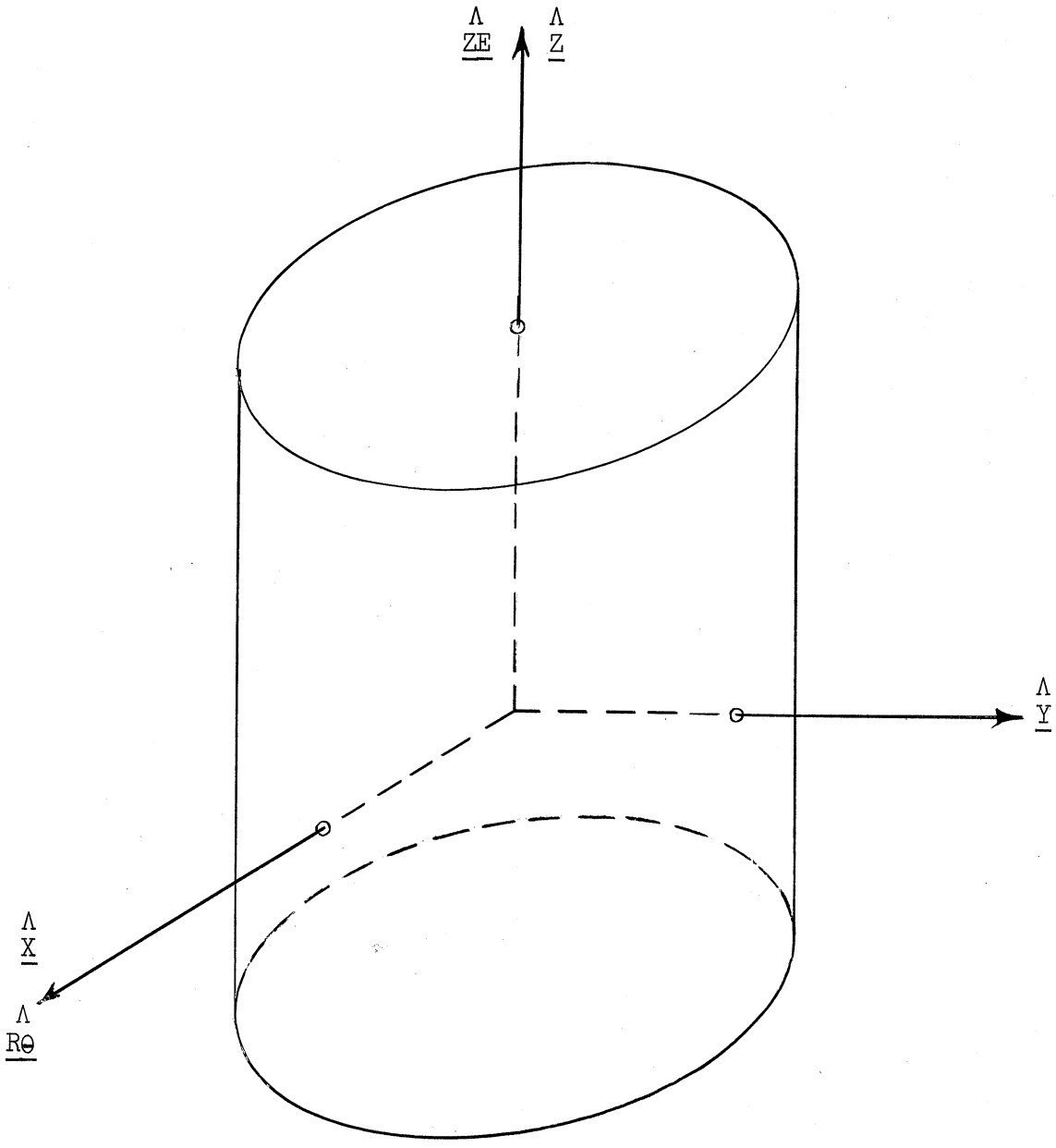

Figure 49. Location of the Coordinate Axies.

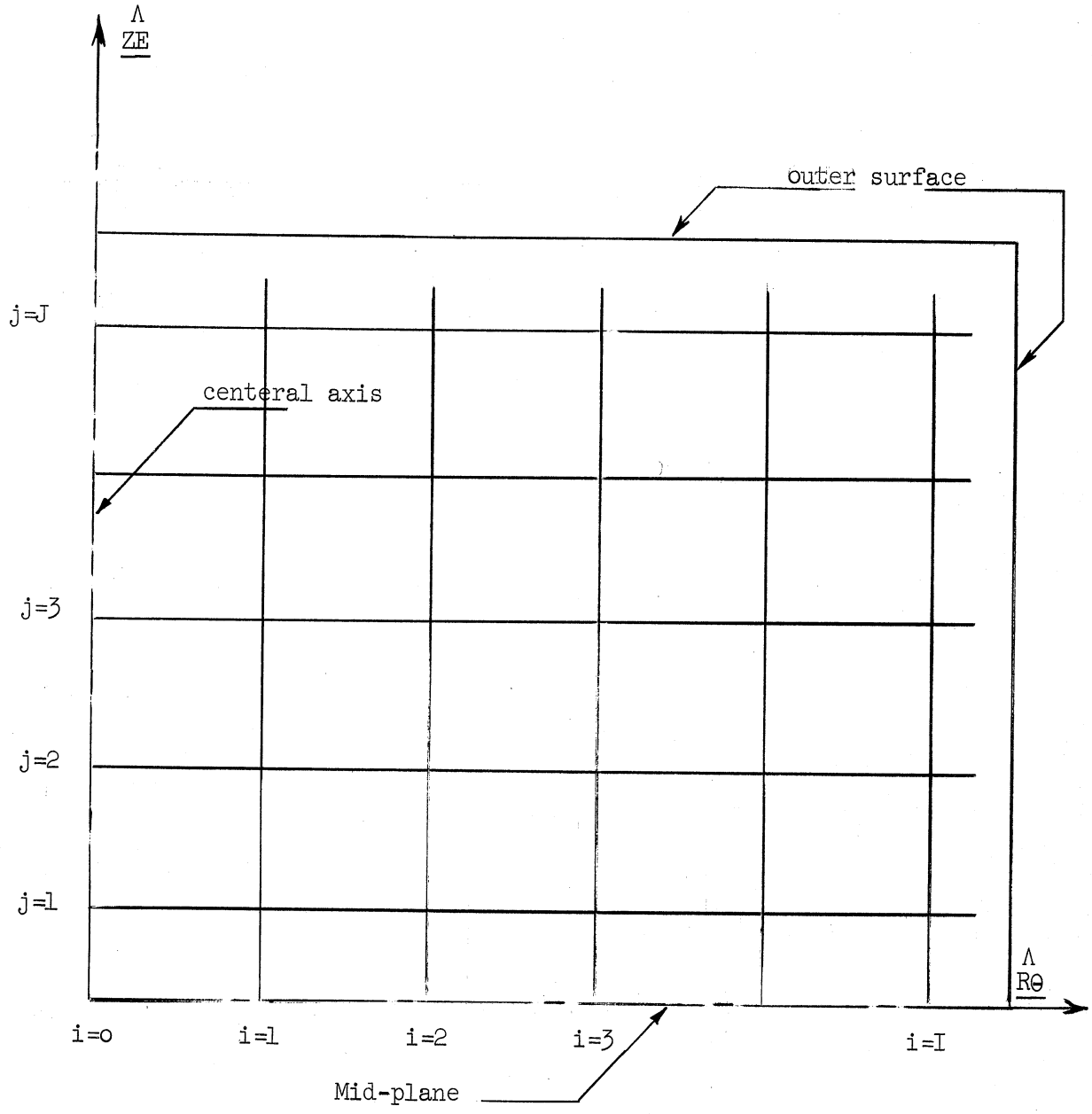

Figure 50. Location of the Grid Points.

Note that a half interval is placed at the outer surface so that a full unit volume may be associated with those points next to the outer surface. No points are located on the mid-plane so that reflection across the mid-plane can be carried out without regard to points on the mid-plane.

The circle defined by the intersection of cylinder i with plane j will be called circle (i,j) . The point where this circle (i,j) cuts the $\hat{ZE}$ - $\hat{R\theta}$ plane will be called point (i,j,0) .

i = 0,1,2,3....I where I = the number of points along the $R\theta$ axis excluding the point on the centeral axis.

j = 1,2,3,4....J where J = the number of points along the ZE axis.

Coordinates of the point (i,j,0) are

$$X = i \times \Delta R\theta$$

$$Y = 0$$

$$Z = (j - \tfrac{1}{2}) \times \Delta ZE$$

The circle (i,j) will be divided by a series of equally spaced points. The circumferential spacing between points will be equal and as near as possible to $\Delta R\theta$ in length. The number of points on circle (i,j) = 6xI . The angular spacing between points on the circle (i,j) will be

$$2\pi/6i$$

The points spaced around the circle (i,j) will be denoted point (i,j,k), k = 0 . The volume associated with point (i,j,k) = $\pi (\Delta R\theta)^2 \Delta ZE$ $((i + \frac{1}{2})^2 - (i - \frac{1}{2})^2)/ 6i$ except where $i-\frac{1}{2}$ is negative, then the volume around point (i,j,k) = $\pi (\Delta R\theta/2)^2 \Delta ZE$

Coordinates of the point (i,j,k) are

$$X = i\Delta R\theta \times \text{Cos } (2\pi K/6i)$$

$$Y = i\Delta R\theta \times \text{Sin } (2\pi K/6i)$$

$$Z = j\Delta ZE$$

Due to the cylindrical symmetry and the symmetry across the mid-plane it is necessary to calculate unit volumes and fluxes only for points in the RΘ - ZE plane. Associated with each of these points (i,j,0) in the RΘ - ZE plane there will be several other points having the same flux and unit volumes:

1. The point (i, -j,0)
2. The points around the circle (i,k) excluding the point (i,j,0)
3. The points around the circle (i, -j) excluding the point (i, -j,0)

APPENDIX V

NUMERICAL INTEGRATIONS

In order to solve Equation (15) of Chapter I one must evaluate

$$\int_{\underline{r}'} \psi_{n-1}(\underline{r}')\, \bar{G}_o(|\underline{r} - \underline{r}'|)\, d\underline{r}' \tag{1}$$

and

$$\int_{\underline{r}'} \bar{G}_o(|\underline{r} - \underline{r}'|)\, d\underline{r}' \tag{2}$$

Where $\psi_{n-1}(\underline{r})$ is known function.

Let the detector volume be divided into a series of small volumes v_i surrounding a series of points $\underline{r}_i$. Thus:

$$\int_{\underline{r}'} \psi_{n-1}(\underline{r}')\, \bar{G}_o(|\underline{r} - \underline{r}'|)\, d\underline{r}' \simeq \tag{3}$$

$$\sum_i \psi_{n-1}(\underline{r}_i)\, \bar{G}_o(|\underline{r} - \underline{r}_i|)\, v_i$$

$$\int_{\underline{r}'} \bar{G}_o(|\underline{r} - \underline{r}'|)\, d\underline{r}' \simeq \sum_i \bar{G}_o(|\underline{r} - \underline{r}_i|)\, v_i \tag{4}$$

Examination of the numerical results shows that to a good approximation

$$\bar{G}_a\left(|\underline{r} - \underline{r}'|\right) = \frac{1 + C_a \times |\underline{r} - \underline{r}'|}{|\underline{r} - \underline{r}'|^2} \quad \text{for} \quad |\underline{r} - \underline{r}'| < \tfrac{1}{4} \text{ cm.} \tag{5}$$

$$C_a = \frac{d}{d|\underline{r} - \underline{r}'|}\left[|\underline{r} - \underline{r}'|^2 \ \bar{G}_a\left(|\underline{r} - \underline{r}'|\right)\right] \tag{6}$$

Due to the $1/|\underline{r} - \underline{r}'|^2$ dependence of $G_a\left(|\underline{r} - \underline{r}'|\right)$ difficulty will occur in the summation process when $\underline{r} = \underline{r}_i$.

Further difficulty will occur in the case of a coin shaped detector.

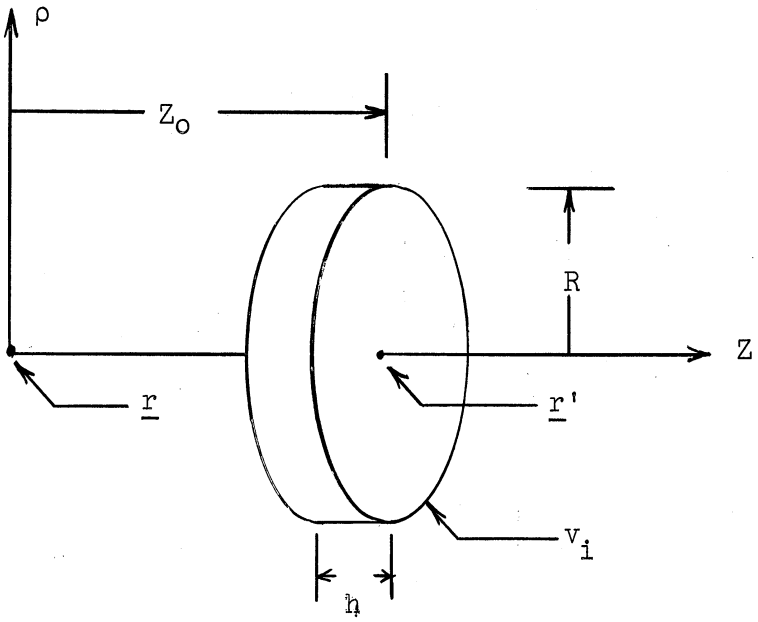

R >> h

Figure 51. Point on the Same Z Axis Outside of Volume Element.

For a point $\underline{r}$ located at the origin in the above figure

$$\int_{v_i} \bar{G}_a\left(|\underline{r} - \underline{r}'|\right) d\underline{r}' \neq \bar{G}_a\left(|\underline{r} - \underline{r}_i|\right) v_i \tag{7}$$

when $R \gg h$ and $R \gg Z_o$.

For a coin shaped detector it will be necessary to evaluate the integral

$$\int_{v_i} \bar{G}_a \left(|\underline{r} - \underline{r}_i|\right) d\underline{r}_i \tag{8}$$

analytically when the points $\underline{r}$ and $\underline{r}'$ have the same x and y coordinates.

In the case of a wire detector a similar difficulty will occur.

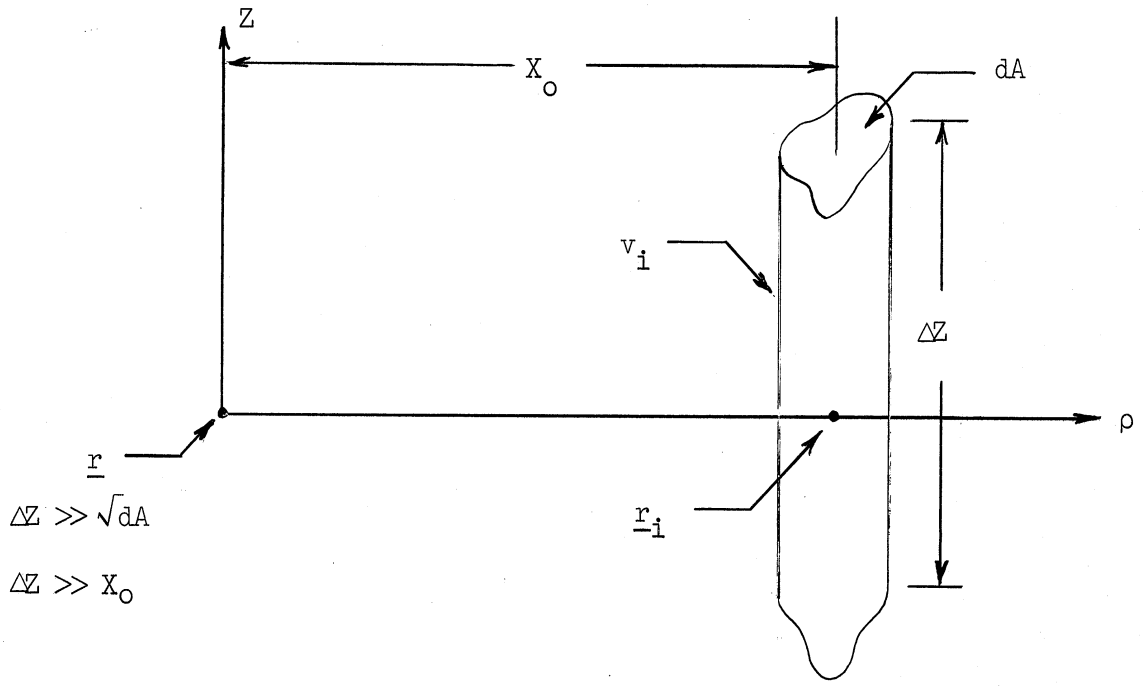

Figure 52. Point in the Same Z Plane Outside of a Volume Element.

$$\int_{\underline{r}_i} \bar{G}_a \left(|\underline{r} - \underline{r}_i|\right) d\underline{r}_i = \bar{G}_a \left(|\underline{r} - \underline{r}_i|\right) v_i \tag{9}$$

when $\Delta Z \gg \sqrt{dA}$ and $\Delta Z \gg X$.

For a wire shaped detector it will be necessary to evaluate the integral

Here again $$\int \bar{G}_a \left(|\underline{r} - \underline{r}_i|\right) d\underline{r}_i \tag{10}$$

analytically for the case where the points $\underline{r}$ and $\underline{r}_i$ have the same Z coordinate.

If the point $\underline{r}$ is inside the volume v_i

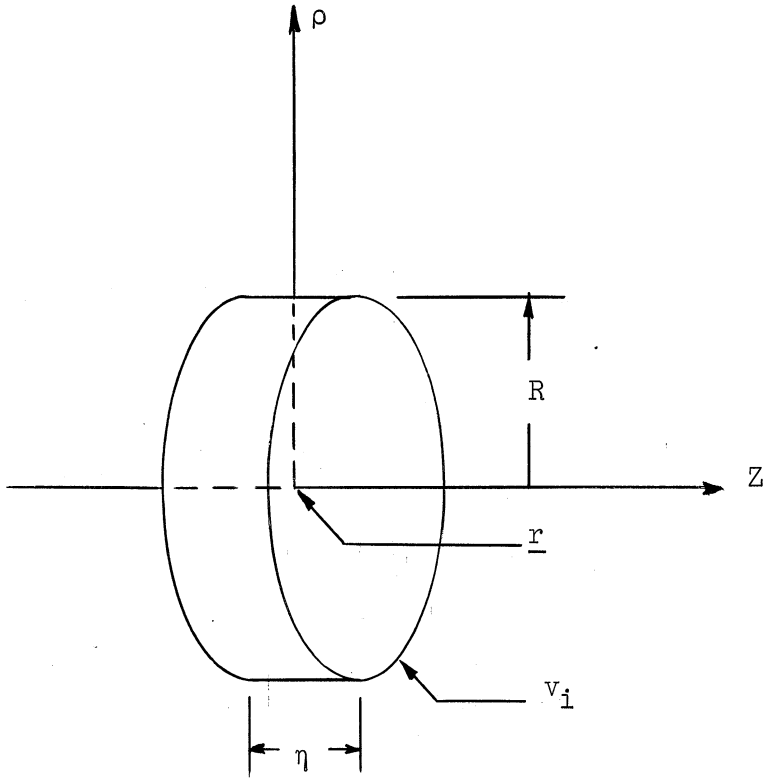

Figure 53. Point Inside a Volume Element.

then:

$$\int_{v_i} \bar{G}_a \left(|\underline{r} - \underline{r}'|\right) d\underline{r}' = \tag{11}$$

$$4\pi R \tan^{-1} \frac{h}{2R} + \pi h \ln \left(1 + \left(\frac{2R}{h}\right)^2\right)$$

$$+ 2\pi C_a \left[\frac{h}{2}\sqrt{\left(\frac{h}{2}\right)^2 + R^2} + R^2 \ln \left(\frac{h}{2} + \sqrt{\left(\frac{h}{2}\right)^2 + R^2}\right)\right.$$

$$- R^2 \ln (R) - (\tfrac{h}{2})^2 \Big]$$

If the point $\underline{r}$ is outside the volume v_i but $\underline{r}$ and $\underline{r}'$ have the same x and y coordinates as in Figure 51 then

$$\int_{v_i} \bar{G}_a \left(|\underline{r} - \underline{r}'|\right) d\underline{r}' = \tag{12}$$

$$2\pi \left[(Z_o + \tfrac{h}{2}) \ln \left(\frac{R}{Z_o + \frac{h}{2}}\right) - (Z_o - \tfrac{h}{2}) \ln \left(\frac{R}{Z_o - \frac{h}{2}}\right) + h \right]$$

$$+ \pi C_a \left[(Z_o + \tfrac{h}{2}) \sqrt{R^2 + (Z_o + \tfrac{h}{2})^2} + R^2 \ln \left(Z_o + \tfrac{h}{2} + \sqrt{R^2 + (Z_o + \tfrac{h}{2})^2}\right) \right.$$

$$- (Z_o - \tfrac{h}{2}) \sqrt{R^2 + (Z_o - \tfrac{h}{2})^2} - R^2 \ln \left(Z_o - \tfrac{h}{2} + \sqrt{R^2 + (Z_o - \tfrac{h}{2})^2}\right)$$

$$\left. - (Z_o + \tfrac{h}{2})^2 + (Z_o - \tfrac{h}{2})^2 \right]$$

If $\underline{r}$ is outside the volume v_i but $\underline{r}$ and $\underline{r}$ have the same Z coordinate as Figure 52 then

$$\int_{v_i} \bar{G}_a \left(|\underline{r} - \underline{r}'|\right) d\underline{r}' = \frac{2dA}{x_o} \tan^{-1} \left(\frac{\Delta Z}{2x_o}\right) + \tag{13}$$

$$2\, d\, A\, C_a\, n \left(\frac{\Delta Z}{2x_o} + \sqrt{1 + \left(\frac{\Delta Z}{2x_o}\right)^2}\right)$$

From this point on in this appendix a convention will be observed.

$\sum_i \bar{G}_a (|\underline{r} - \underline{r}_i|) \times f(\underline{r}_i) v_i$ will be understood to mean

the sum for all points except $\underline{r} = \underline{r}_i$. In the case of a coin shaped detector all points for which the x and y coordinated of $(\underline{r} - \underline{r}_i) = 0$ will also be excluded from the sum. In the case of a wire detector all points for which the Z coordinate of $(\underline{r} - \underline{r}_i) = 0$ will be excluded from the sum.

For all of the points excluded from the summation the analytical calculation of the integral $\int_{v_i} \bar{G}_a (|\underline{r} - \underline{r}'|) d\underline{r}'$

will be carried out as outlined above.

Thus:

$$\int_{\underline{r}'} \psi_{n-1}(\underline{r}') \bar{G}_o (|\underline{r} - \underline{r}'|) d\underline{r}' \simeq \sum_i \psi_{n-1}(\underline{r}_i) \bar{G}_o (|\underline{r} - \underline{r}_i|) v_i \qquad (14)$$

and

$$\int_{\underline{r}'} \bar{G}_o (|\underline{r} - \underline{r}'|) d\underline{r}' \cong \sum_i \bar{G}_o (|\underline{r} - \underline{r}_i|) v_i \qquad (15)$$

In the limit as v_i goes to zero the integral will be exactly equal to the summation. In the numerical problem it will not be practical to let v_i go to zero. But the same detector will be calculated using several different sub-division sizes in order to see the effect of sub-division size upon $\psi(\underline{r})$.

Next consider the integral

$$\int_{\underline{r}'',\underline{r}',\underline{\Omega}',\underline{r}} \psi(\underline{r}'')\, G(\underline{r}'' \to \underline{r}',\, \underline{\Omega}')\, G(\underline{r}',\, \underline{\Omega}' \to \underline{r})\, d\underline{r}''d\underline{r}'d\underline{\Omega}'d\underline{r} \tag{16}$$

where $\psi(\underline{r})$ is a known function. Using the spherical harmonic expansion for $G(\underline{r}',\, \underline{\Omega}' \to \underline{r})$ the integral becomes, after integration over $\underline{\Omega}'$

$$\int_{\underline{r}'',\underline{r}',\underline{r}} \psi(\underline{r}'') \sum_{a,b} Y_a^{*b}(\underline{r}' - \underline{r}'')\, \bar{G}_a(|\underline{r}' - \underline{r}''|)\, x \tag{17}$$

$$Y_a^b(\underline{r} - \underline{r}')\, \bar{G}_a(|\underline{r} - \underline{r}'|)\, d\underline{r}''d\underline{r}'d\underline{r}$$

Denote the real part $Y_a^b(\underline{\Omega})$ as $RY_a^b(\underline{\Omega})$ and the imaginary part as $\mathfrak{I} Y_a^b(\underline{\Omega})$

Next consider two terms, for $b = b'$ and $b = -b'$, in the above summation. $\underline{\varphi} = \underline{r}' - \underline{r}''$, $\underline{\theta} = \underline{r} - \underline{r}'$

$$\overset{*}{Y}_a^{b'}(\underline{\hat{\varphi}})\,\bar{G}_a(\varphi) \times Y_a^{b'}(\underline{\hat{\theta}})\,\bar{G}_a(\theta) + \tag{18}$$

$$\overset{*}{Y}_a^{-b'}(\underline{\hat{\varphi}})\,\bar{G}_a(\varphi) \times Y_a^{-b'}(\underline{\hat{\theta}})\,\bar{G}_a(\theta) =$$

$$= \bar{G}_a(\varphi)\,\bar{G}_a(\theta)\Big[\, RY_a^{*b'}(\underline{\hat{\varphi}})\, RY_a^{b'}(\underline{\hat{\theta}}) +$$

$$i^2 \mathcal{J}\, \overset{*}{Y}_a^{b'}(\underline{\hat{\varphi}})\, \mathcal{J}\, Y_a^{b'}(\underline{\hat{\theta}}) + i\, RY_a^{*b'}(\underline{\hat{\varphi}})\, \mathcal{J}\, Y_a^{b'}(\underline{\hat{\theta}}) +$$

$$i\, \mathcal{J}\, \overset{*}{Y}_a^{b'}(\underline{\hat{\varphi}})\, RY_a^{b'}(\underline{\hat{\theta}}) + RY_a^{*-b'}(\underline{\hat{\varphi}})\, RY_a^{*-b'}(\underline{\hat{\varphi}})\, RY^{-b'}(\underline{\hat{\theta}}) +$$

$$i^2 \mathcal{J}\, \overset{*}{Y}_a^{-b'}(\underline{\hat{\varphi}})\, \mathcal{J}\, Y_a^{-b}(\underline{\hat{\theta}}) + i\, RY_a^{*-b'}(\underline{\hat{\varphi}})\, \mathcal{J}\, Y_a^{-b'}(\underline{\hat{\theta}}) +$$

$$i\, \mathcal{J}\, \overset{*}{Y}_a^{-b'}(\underline{\hat{\varphi}})\, RY_a^{-b'}(\underline{\hat{\theta}}) \,\Big]$$

Note that

$$RY_a^{b}(\underline{\Omega}) = RY_a^{-b}(\underline{\Omega}) \tag{19}$$

$$\mathcal{J}\, Y_a^{b}(\underline{\Omega}) = -\,\mathcal{J}\, Y_a^{-b}(\underline{\Omega}) \tag{20}$$

Thus

$$\overset{*}{Y}_a^{b'}(\underline{\hat{\varphi}})\,\bar{G}_a(\varphi)\, Y_a^{b'}(\underline{\hat{\theta}})\, G_a(\theta) + \tag{21}$$

$$Y_a^{-b'}(\underline{\hat{\varphi}})\,\bar{G}_a(\varphi)\, Y_a^{-b'}(\underline{\hat{\theta}})\, G_a(\theta) =$$

$$= \bar{G}_a(\varphi)\,\bar{G}_a(\theta) \times \epsilon_{b'} \times \Big[\, RY_a^{*b'}(\underline{\hat{\varphi}})\, RY_a^{b'}(\theta) -$$

$$- \mathcal{I} Y_a^{*b'}(\underline{\hat{\varphi}}) \mathcal{I} Y_a^{b'}(\Theta) \Big]$$

$$\text{Where } \epsilon_{b'} = \begin{cases} 1 \text{ if } b' = 0 \\ 2 \text{ if } b' \neq 0 \end{cases} \tag{22}$$

So the summations $\sum_{\substack{a=0 \\ b=-a}}^{\substack{a=\infty \\ b=a}}$ can now be replaced with $\sum_{\substack{a=0 \\ b=0}}^{\substack{a=\infty \\ b=a}} \epsilon_b$.

Thus

$$\int_{\underline{r}'',\underline{r}',\underline{\Omega}',\underline{r}} \psi(\underline{r}'') G(\underline{r}'' \to \underline{r}', \underline{\Omega}') G(\underline{r}', \underline{\Omega}' \to \underline{r}) \, d\underline{r}'' d\underline{r}' d\underline{\Omega}' d\underline{r} = \tag{23}$$

$$= \int_{\underline{r}'',\underline{r}',\underline{r}} \psi(\underline{r}'') \sum_{a,b} \epsilon_b Y_a^{*b}(\underline{r}' \overset{\Lambda}{-} \underline{r}'') \bar{G}_a(|\underline{r}' - \underline{r}''|) \, x$$

$$Y_a^b(\underline{r} \overset{\Lambda}{-} \underline{r}') \bar{G}_a(|\underline{r} - \underline{r}'|) \, d\underline{r}'' d\underline{r}' d\underline{r}$$

Next consider

$$\int_{\underline{r}''} \psi(\underline{r}'') \bar{G}_a(|\underline{r}' - \underline{r}''|) \, d\underline{r}'' \simeq RF_a^b(\underline{r}') + i \mathcal{I} F_a^b(\underline{r}') \tag{24}$$

Where

$$RF_a^b(\underline{r}') = \sum_i \sqrt{\epsilon_b} \, \psi(\underline{r}_i) \bar{G}_a(|\underline{r}' - \underline{r}_i|) \, x \tag{25}$$

$$RY_a^{*b}(\underline{r}' \overset{\Lambda}{-} \underline{r}_i) \, v_i$$

$$\mathcal{I} F_a^b(\underline{r}') = \sum_i \sqrt{\epsilon_b} \, \psi(\underline{r}_i) \bar{G}_a(|\underline{r}' - \underline{r}_i|) \, x \tag{26}$$

$$Y_a^{*b}(\underline{r}' \hat{-} \underline{r}_i)\, v_i$$

Next consider

$$\int_{\underline{r}} \bar{G}_a(|\underline{r} - \underline{r}'|)\, Y_a^b(\underline{r} \hat{-} \underline{r}')\, d\underline{r} \simeq RE_a^b(\underline{r}') + i\mathcal{J} E_a^b(\underline{r}') \quad (27)$$

Where

$$RE_a^b(\underline{r}') = \sum \sqrt{\epsilon_b}\, \bar{G}_a(|\underline{r}_i - \underline{r}'|)\, RY_a^b(\underline{r}_i \hat{-} \underline{r}')\, v_i \quad (28)$$

$$\mathcal{J} E_a^b(\underline{r}') = \sum \sqrt{\epsilon_b}\, \bar{G}_a(|\underline{r}_i - \underline{r}'|)\, \mathcal{J} Y_a^b(\underline{r}_i \hat{-} \underline{r}')\, v_i \quad (29)$$

Thus

$$\int_{\underline{r}'',\underline{r}',\underline{r}} \psi(\underline{r}'')\, \bar{G}_a(|\underline{r}' - \underline{r}''|)\, Y_a^{*b}(\underline{r}' \hat{-} \underline{r}'')\, \bar{G}_a(|\underline{r} - \underline{r}'|)\, x \quad (30)$$

$$Y_a^b(\underline{r} \hat{-} \underline{r}')\, d\underline{r}''d\underline{r}'d\underline{r} =$$

$$\int_{\underline{r}'} \left[RF_a^b(\underline{r}')\, RE_a^b(\underline{r}') - \mathcal{J} F_a^b(\underline{r}')\, \mathcal{J} E_a^b(\underline{r}')\right] d\underline{r}' \simeq$$

$$\sum_k \left[RF_a^b(\underline{r}_k)\, RE_a^b(\underline{r}_k) - \mathcal{J} F_a^b(\underline{r}_k)\, \mathcal{J} E_a^b(\underline{r}_k)\right] v_k$$

Finally

$$\int_{\underline{r}'',\underline{r}',\underline{\Omega}',\underline{r}} \psi(\underline{r}'')\, G(\underline{r}'' \to \underline{r}', \underline{\Omega}'')\, G(\underline{r}', \underline{\Omega}' \to \underline{r})\, d\underline{r}''d\underline{r}'d\underline{\Omega}'d\underline{r} = \quad (31)$$

$$\sum_{a,b}\Big[\sum_k \Big\{ RF_a^b(\underline{r}_k)\, RE_a^b(\underline{r}_k) -$$

$$\mathcal{J} F_a^b(\underline{r}_k)\, \mathcal{J} E_a^b(\underline{r}_k) \Big\}\, v_k \Big]$$

Now consider the integral

$$\int_{\underline{r}'',\underline{r}',\underline{\Omega}',\underline{r}} G(\underline{r}'' \to \underline{r}', \underline{\Omega}')\, G(\underline{r}', \underline{\Omega}' \to \underline{r})\, d\underline{r}''d\underline{r}'d\underline{\Omega}'d\underline{r} = \tag{32}$$

$$= \int_{\underline{r}'',\underline{r}',\underline{r}} \sum_{a,b} Y_a^{*b}(\underline{r}' \overset{\Lambda}{-} \underline{r}'')\, \bar{G}_a(|\underline{r}' - \underline{r}''|)\, Y_a^b(\underline{r} \overset{\Lambda}{-} \underline{r}')\, x$$

$$\bar{G}_a(|\underline{r} - \underline{r}'|)\, d\underline{r}''d\underline{r}'d\underline{r}$$

Consider

$$\int_{\underline{r}''} Y_a^{*b}(\underline{r}' \overset{\Lambda}{-} \underline{r}'')\, \bar{G}_a(|\underline{r}' - \underline{r}''|)\, d\underline{r}'' = RH_a^b(\underline{r}') + i\mathcal{J} H_a^b(\underline{r}') \tag{33}$$

$$RH_a^b(\underline{r}') = \sum_i \sqrt{\epsilon_b}\, RY_a^{*b}(\underline{r}' \overset{\Lambda}{-} \underline{r}_i)\, \bar{G}_a(|\underline{r}' - \underline{r}''|)\, v_i \tag{34}$$

$$H_a^b(\underline{r}') = \sum_i \sqrt{\epsilon_b}\, \mathcal{J} Y_a^{*b}(\underline{r}' \overset{\Lambda}{-} \underline{r})\, \bar{G}_a(|\underline{r}' - \underline{r}''|)\, v_i \tag{35}$$

Thus

$$RH_a^b(\underline{r}'_i) = (-1)^a\, RE_a^b(\underline{r}_i) \tag{36}$$

$$\mathcal{J} H_a^b(\underline{r}') = (-1)^a\, \mathcal{J} E_a^{*b}(\underline{r}_i) = (-1)^a\,(-1)\mathcal{J} E_a^b(\underline{r}_i) \tag{37}$$

Thus

$$\int_{\underline{r}'',\underline{r}',\underline{\Omega}',\underline{r}} G(\underline{r}'' \to \underline{r}', \underline{\Omega}')\, G(\underline{r}', \underline{\Omega}' \to \underline{r})\, d\underline{r}''d\underline{r}'d\underline{\Omega}'d\underline{r} = \tag{38}$$

$$= \sum_{a,b} \int_{\underline{r}'} (-1)^a \left[\left\{ RE_a^b (\underline{r}') \right\}^2 - \left\{ E_a^b (\underline{r}') \right\}^2 \right] d\underline{r}' =$$

$$\sum_{a,b} \left[\sum_{K} (-1)^a \left[\left\{ RE_a^b (\underline{r}_k) \right\}^2 - \left\{ E_a^b (\underline{r}_k) \right\}^2 \right] \right]$$

APPENDIX VI

NUCLEAR CONSTANTS

The nuclear constants used are all taken from the Tables of Neutron Cross-Sections in BNL - 325[6] . In the energy range which the room temperature thermal neutron distribution the cross sections are either constant or have a 1/v dependence.

For the case of a constant cross-section the average of the cross-section over a thermal neutron distribution presents no problem. For the 1/v cross-section it is well known that the cross-section averaged over a thermal neutron distribution satisfies the equation:

$$\bar{\sigma} = \frac{\sqrt{\pi}}{2}\,\sigma(2200\ \tfrac{m}{s})$$

For water

$$\bar{\sigma}_t = \frac{\sqrt{\pi}}{2} \times 106\ \text{b/molecule} = 94.0\ \text{b/mol.}$$

Since the absorption cross-section for oxygen is very small compared to hydrogen

$$\bar{\sigma}_a \text{ for } H_2O = 2 \times \frac{\sqrt{\pi}}{2} \times .332 = .588\ \text{b/mol.}$$

$$\sum_t = \frac{94.0 \times .6023 \times .997}{18} = 3.14\ \text{cm}^{-1}$$

$$\sum_a = \frac{.588 \times .6023 \times .997}{18} = .0196\ \text{cm}^{-1}$$

For $\bar{\mu}$ the classic value of 2/3A is not valid for bound hydrogen. Radkowsky[10] has suggested the prescription

$$\bar{\mu}(E) = \frac{2}{3} \frac{1 - \left(\frac{\sigma_s(E)}{80}\right)^{\frac{1}{2}}}{\left(\frac{\sigma_s(E)}{80}\right)^{\frac{1}{2}}}$$

This formula gives values of $\bar{\mu}$ of .2 to .4 for energy around thermal. A value of $\bar{\mu} = 0.3$ was selected.

For graphite

$$\sum_s = \frac{4.8 \times .6023 \times 1.6}{12.01} = .385 \text{ cm}^{-1}$$

$$\sum_a = \frac{\sqrt{\pi}}{2} \frac{.0033 \times .6023 \times 1.6}{12.01} = .000235 \text{ cm}^{-1}$$

$$\sum_t = .385235 \text{ cm}^{-1}$$

For gold

$$\sum_a = \frac{\sqrt{\pi}}{2} \frac{98.8 \times .6023 \times 19.32}{197.2} = 5.17 \text{ cm}^{-1}$$

$$\sum_s = \frac{9.3 \times .6023 \times 19.32}{197.2} = .549 \text{ cm}^{-1}$$

$$\sum_t = 5.719 \text{ cm}^{-1}$$

For indium

$$\sum_a = \frac{\sqrt{\pi}}{2} \frac{196. \times .6023 \times 7.28}{114.76} = 6.64 \text{ cm}^{-1}$$

$$\sum_s = \frac{2.2 \times .6023 \times 7.28}{114.76} = .0842 \text{ cm}^{-1}$$

$$\sum_t = 6.7242 \text{ cm}^{-1}$$

BIBLIOGRAPHY

1. Bengston, Joel, Neutron Self-Shielding of A Plane Absorbing Foil, Oak Ridge National Laboratory, OF-56-3-170, Microdard, United States Government Printing Office, Washington 25, D. C., 1956.

2. Case, K. M., F. de Hoffman and G. Placzek, Introduction To The Theory of Neutron Diffusion, Volume 1, United States Government Printing Office, Washington 25, D. C., 1953.

3. Davison, B. and J. B. Sykes, Neutron Transport Theory, Oxford University Press, Oxford England: 1957.

4. Fitch, S. H. and J. E. Drummond, Neutron Detector Perturbations, Livermore Research Laboratory, LRL-95, United States Government Printing Office, Washington 25, D. C., 1954.

5. Gallagher, Tom L., "Flux Depression Factors for Indium Disk Detectors," Nuclear Science and Engineering (January 1958), 3:110-112.

6. Hughes, Donald J. and Robert B. Schwartz, Neutron Cross Sections, Brookhaven National Laboratory, BNL-325, Second Edition, United States Government Printing Office, Washington 25, D. C., 1958.

7. Jahnke, Eugene and Fritz Emde, "Tables of Functions", Dover Publications, New York, New York, 1945.

8. Klema, E. D. and R. H. Ritchie, "Thermal Neutron Flux Measurements In Graphite Using Gold and Indium Foils," Physical Review (July 1952), 87:167.

9. Morse, Philip M. and Herman Feshbach, Methods of Theoretical Physics, McGraw Hill, New York, New York, 1953.

10. Petrie, C. D., M. L. Storm and P. F. Zweifel, "Calculation of Thermal Group Constants for Mixtures Containing Hydrogen," Nuclear Science and Engineering (November 1957), 2:728-744.

11. Skyrme, T. H. R., Reduction In Neutron Density Caused By An Absorbing Disc, British Atomic Energy Research Establishment, M. S. 91.

12. Thompson, M. W. "Some Effects of The Self-Absorption of Neutron Detecting Foils," Journal of Nuclear Engineering (British Journal, 1955), 2:286-290.

13. Zobel, W., "Determination of Experimental Flux Depression and Other Corrections for Gold Foils Exposed In Water," Section 8.8 in Neutron Physics Division Annual Progress Report, Oak Ridge National Laboratory, ORNL 2842, pp. 202-203, United States Government Printing Office, Washington 25, D. C., 1959.